Changes in the timing of the seasonal cycle of streamflow in Europe

Master's Thesis

Faculty of Science

University of Bern

presented by

Päivi van Wijnkoop

2015

Supervisor:

Prof. Stefan Brönnimann
GIUB and Oeschger Centre for Climate Change Research

Co-Supervisor:

Prof. Sonia Seneviratne
IAC, ETH Zurich

Advisor:

Lukas Gudmundsson
IAC, ETH Zurich

Abstract

The aim of this thesis is to provide information about changes in the seasonality of streamflow in near-natural catchments across Europe. To achieve this, a statistical analysis of a data set of 657 gauging stations was conducted over the period 1970 - 2005.

The first part of the thesis investigates trends in the timing of the annual cycle of streamflow. A trend test was conducted for six measures of the timing of the annual cycle of streamflow. The results show that there are no detectable trends in timing of the annual cycle of streamflow which are field significant at a 5% significance level.

The second part of the thesis focuses on the influence of large-scale controls on streamflow seasonality through teleconnection patterns over the North Atlantic using a correlation analysis. The results of this analysis show that the timing of the annual cycle of streamflow is influenced by the teleconnection patterns. The strengths of the correlations range from -0.6 to 0.6. These results are field significant at a global 5% significance level. The most influencing pattern is the Scandinavian Pattern. The second most influencing pattern is the North Atlantic Oscillation. The patterns are known to influence climatic variables, such as precipitation, across Europe, which in turn influences streamflow amounts. The results of the present thesis show that this also affects the timing of the annual cycle of streamflow. The influence of atmospheric patterns differs, however, for the different timing measures. In addition, distinct regional differences are found.

Contents

1. Introduction **8**
- 1.1. Motivation . . . 8
- 1.2. Previous research . . . 9
  - 1.2.1. Local controls on streamflow seasonality . . . 9
  - 1.2.2. Large-scale controls on seasonal streamflow . . . 12

2. Data **14**
- 2.1. Streamflow from near natural catchments . . . 14
- 2.2. Time series of northern teleconnection patterns . . . 15
- 2.3. Precipitation and temperature observations . . . 16

3. Methods **17**
- 3.1. Definition of timing measures . . . 17
  - 3.1.1. Date of maximum and minimum annual streamflow . . . 17
  - 3.1.2. Center timing . . . 19
- 3.2. Correlation between the six timing measures . . . 22
- 3.3. Trend Analysis . . . 22
  - 3.3.1. Trends . . . 22
  - 3.3.2. Field significance . . . 22
- 3.4. Correlation of northern teleconnection patterns . . . 23
  - 3.4.1. Correlation coefficients . . . 23
  - 3.4.2. Field significance . . . 23
  - 3.4.3. Correlation between the teleconnection patterns, precipitation and temperature . . . 24

4. Results **25**
- 4.1. Correlation between the timing measures . . . 25
- 4.2. Climatology of the timing measures . . . 25
- 4.3. Trend analysis . . . 27
- 4.4. Correlation with northern teleconnection patterns . . . 30

5. Discussion **41**
- 5.1. Definition of the timing measures . . . 41
- 5.2. Local controls on streamflow seasonality . . . 41
- 5.3. Trends in streamflow seasonality . . . 42
- 5.4. Large-scale controls on seasonal streamflow . . . 44

6. Conclusions **52**

A. Appendix **60**

A.1. Monthly correlations between the timing measures and teleconnection patterns 60

List of Figures

1.1. Streamflow regime types and their spatial distribution 10
1.2. Regime type 1: shift of snowmelt streamflow peak 12
1.3. Hypothesis: Shift of the minimum annual streamflow towards later in the season due to longer lasting drought periods. 12

2.1. analysed streamflow gauging stations 14

3.1. Max and Min timing measures 18
3.2. Max91: occurrence date 19
3.3. Max91: deviations from the mean 20
3.4. CT timing measure 20
3.5. Max, Min and CT timing measures 21

4.1. Climatologies of the six timing measures 26
4.2. Trend analysis: critical values 28
4.3. Results of the trend analysis 29
4.4. Correlations (r^2) for CT1 - northern teleconnection patterns 31
4.5. Correlations (r^2) CT2 - northern teleconnection patterns 32
4.6. Correlations (r^2) Max91 - northern teleconnection patterns 33
4.7. Correlations (r^2) Max181 - northern teleconnection patterns 34
4.8. Correlations (r^2) Min91 - northern teleconnection patterns 35
4.9. Correlations (r^2) Min181 - northern teleconnection patterns 36
4.10. Correlation analysis: critical values 37
4.11. Spatial patterns of the correlation analysis 39
4.12. Monthly correlations CT1 - SCA 40

5.1. Regime type 1: possible changes 43
5.2. Possible change of the RC2: longer drought periods in summer time, without changes in the timing of the minimum annual streamflow. 43
5.3. Scandinavian Pattern correlations with precipitation, temperature, and CT1/CT2 46
5.4. Scandinavian Pattern correlations with precipitation, temperature, and Max91 47
5.5. North Atlantic Oscillation index correlations with precipitation, temperature, and Max181 48
5.6. Scandinavian Pattern correlations with precipitation, temperature, and Min91 49

5.7. East Atlantic/Western Russia index correlations with precipitation, temperature, and Min181 51

A.1. Monthly correlations CT1 - East Atlantic 61
A.2. Monthly correlations CT1 - East Atlantic/Western Russia 62
A.3. Monthly correlations CT1 - North Atlantic Oscillation 63
A.4. Monthly correlations CT1 - Polar/Eurasia 64
A.5. Monthly correlations CT1 - Tropical/Northern Hemisphere 65
A.6. Monthly correlations CT2 - East Atlantic 66
A.7. Monthly correlations CT2 - East Atlantic/Western Russia 67
A.8. Monthly correlations CT2 - North Atlantic Oscillation 68
A.9. Monthly correlations CT2 - Polar/Eurasia 69
A.10. Monthly correlations CT2 - Scandinavian Pattern 70
A.11. Monthly correlations CT2 - Tropical/Northern Hemisphere 71
A.12. Monthly correlations Max91 - East Atlantic 72
A.13. Monthly correlations Max91 - East Atlantic/Western Russia 73
A.14. Monthly correlations Max91 - North Atlantic Oscillation 74
A.15. Monthly correlations Max91 - Polar/Eurasia 75
A.16. Monthly correlations Max91 - Scandinavian Pattern 76
A.17. Monthly correlations Max91 - Tropical/Northern Hemisphere 77
A.18. Monthly correlations Max181 - East Atlantic 78
A.19. Monthly correlations Max181 - East Atlantic/Western Russia 79
A.20. Monthly correlations Max181 - North Atlantic Oscillation 80
A.21. Monthly correlations Max181 - Polar/Eurasia 81
A.22. Monthly correlations Max181 - Scandinavian Pattern 82
A.23. Monthly correlations Max181 - Tropical/Northern Hemisphere 83
A.24. Monthly correlations Min91 - East Atlantic 84
A.25. Monthly correlations Min91 - East Atlantic/Western Russia 85
A.26. Monthly correlations Min91 - North Atlantic Oscillation 86
A.27. Monthly correlations Min91 - Polar/Eurasia 87
A.28. Monthly correlations Min91 - Scandinavian Pattern 88
A.29. Monthly correlations Min91 - Tropical/Northern Hemisphere 89
A.30. Monthly correlations Min181 - East Atlantic 90
A.31. Monthly correlations Min181 - East Atlantic/Western Russia 91
A.32. Monthly correlations Min181 - North Atlantic Oscillation 92
A.33. Monthly correlations Min181 - Polar/Eurasia 93
A.34. Monthly correlations Min181 - Scandinavian Pattern 94
A.35. Monthly correlations Min181 - Tropical/Northern Hemisphere 95

List of Tables

4.1. Correlation coefficients between the six timing measures 25
4.2. Results: trend analysis 27
4.3. Results: correlation analysis 30

1. Introduction

1.1. Motivation

Freshwater availability is an essential resource for the development of a region and is strongly linked to the climate system. Streamflow as part of the water cycle is therefore of great interest not only to various research disciplines, but also to industry, policy makers and governments. The distribution of water throughout the year plays a substantial role. Poff et al. (1997) shows that modifications in the timing of streamflow can lead to widespread adverse impacts. For example, many plant species and aquatic animals are highly adapted to seasonal streamflows (Poff et al., 1997). Streamflow reflects the sum of all streamflow generating processes and characteristics in a catchment (Poff et al., 1997). The three main processes influencing streamflow are: precipitation, storage of water (in soils and aquifers such as snow and ice), and evapotranspiration (Freeze, 1974). These processes are further linked to other variables.
Recent studies have observed changes in the seasonality of variables that are linked to the water cycle. Stine et al. (2009) investigated changes in the phase of the annual cycle of surface temperatures over ocean and land in mid and high latitudes. They found that the phase of the annual cycle over extratropical land shifted towards earlier seasons by 1.7 days between 1954 and 2007, implying an earlier onset of summer. Many studies have investigated changes of the annual cycle in biological systems: Studer et al. (2005) and Schleip et al. (2008) showed an earlier onset of the phenological spring season in the Swiss alpine region and central Europe. Sparks and Menzel (2002) provides an overview over changes in seasons, covering the response of several animals and plants to a changing climate. One of their findings is that the life cycle of insects changes, which can lead to further impacts on agriculture and land use. Myneni et al. (1997) showed that changes in temperatures and vegetation have effects on the terrestrial surface carbon uptake and thus on the CO_2 in the atmosphere. CO_2 in the atmosphere is linked to the water cycle through evapotranspiration by plants (Ramirez and Finnerty, 1996). According to the latest report of the Intergovernmental Panel on Climate Change (IPCC), there is evidence of changes in the water cycle and streamflow (Stocker et al., 2013). Stahl et al. (2010) have shown that this is true for the amount of streamflow in Europe, with positive and negative trends in different regions in different seasons. A study conducted by Renner and Bernhofer (2011) assessed the trends in seasonality of annual streamflow on a local scale in Saxony, Germany. They found a change in seasonality of annual streamflow towards earlier dates in the year. Stewart et al. (2005) found changes toward earlier streamflow timing in snow-dominated catchments across western North America. Cunderlik and Ouarda (2009) found negative trends in the timing and amount

of spring snowmelt floods across Canada. Such changes may have widespread impacts on ecosystems and the handling and management of streamflows.

As far as we know, no study has yet investigated the change in the timing of the seasonal cycle of streamflow on a European scale. The aim of this master thesis is, therefore, to assess changes in the phasing of the seasonal cycle of streamflow in Europe. The first objective is to investigate whether there are detectable changes in the timing of the annual cycle. The second objective is to investigate large-scale controls through teleconnections on the timing of the annual cycle.

These questions are approached empirically through a statistical analysis of streamflow observations from small catchments across Europe. Changes in the timing are investigated for six different measures of the timing of the annual cycle, which were derived from pursuing two different approaches. These changes are assessed by conducting a trend analysis. In addition to that, the timing measures were related to six different northern teleconnection patterns in order to assess the influence of these teleconnection patterns on the timing of the annual cycle.

The following sections describe controls on the seasonality of streamflow. In chapter 2, the considered data is introduced. Chapter 3 describes the methods applied in the study. In chapter 4 the results are presented. In chapter 5 the results are discussed, and chapter 6 consists of the conclusions of the study and a short outlook.

1.2. Previous research

1.2.1. Local controls on streamflow seasonality

This thesis distinguishes two different streamflow regime types according to the classification by Gudmundsson et al. (2011). The two regime types and their spatial distribution across Europe are shown in figure 1.1. The regime type one (RC1) is influenced by snow, with a streamflow minimum in winter due to the storage of water as snow, and a streamflow maximum in summer. The regime type two (RC2) is less influenced by snow, with a streamflow maximum in winter due to winter storms and a streamflow minimum in summer.

Various studies on trends in the volume and the timing of streamflow, and their spatial patterns have been conducted in the USA and Canada (e.g. Cunderlik and Ouarda, 2009; Burn, 2008; Regonda et al., 2005; Hidalgo et al., 2009; Barnett et al., 2008). Burn (2008) explored the trend behaviour of nine different measures of the timing of streamflow for three subwatersheds of the Mackenzie River Basin in northern Canada. He found the strongest trend signal for the spring freshet date (the date at which the first flood of the river from melted snow occurs). The spring freshet date was also the measure with the largest percentage of catchments with a locally significant trend. It was observed

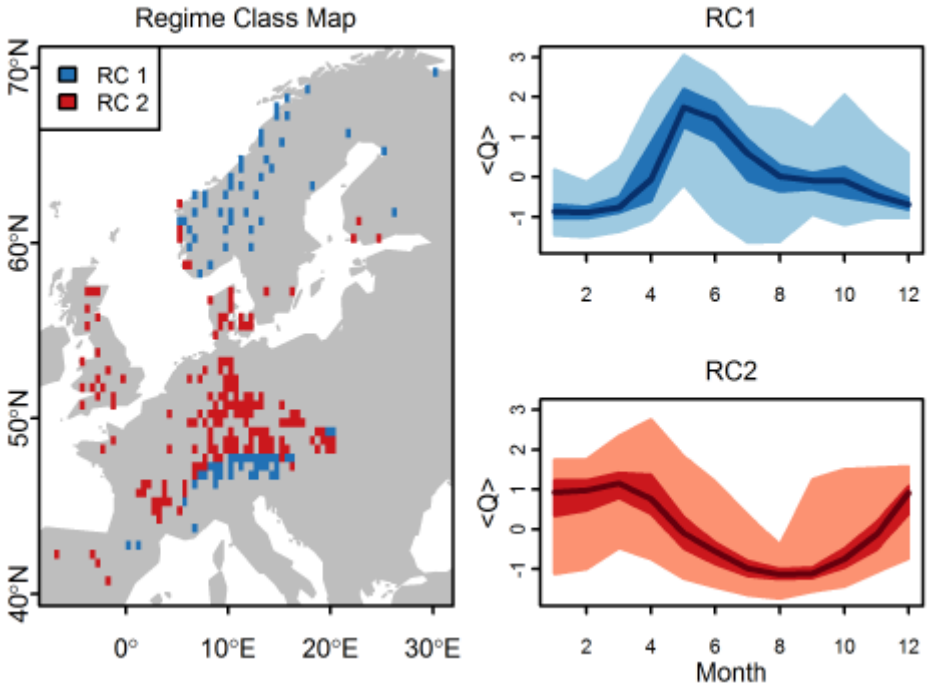

Figure 1.1.: Streamflow regime types and their spatial distribution (Gudmundsson 2011).

to be occurring earlier in the year. Regonda et al. (2005) investigated the seasonal cycle shifts in hydroclimatology over the western United States. One of their findings is that the observed increasing temperatures lead to a smaller extent of snow cover during winter and an earlier onset of snowmelt in spring in high-elevation catchments. This has further effects on soil moisture and streamflow of river catchments. Hidalgo et al. (2009) and Barnett et al. (2008) investigated changes in the hydrological cycle in three major hydrological regions of the western United States over the second half of the 20th century. They found that the observed shift towards earlier streamflow (center timing) cannot be explained solely by natural variability, but also by human-induced climate changes (e.g. changes in the composition of the atmosphere, land use changes). In particular, Barnett et al. (2008) states that observed changes in center timing goes along with increasing temperatures. The temperature increase changes precipitation in winter (from snow to rain) and leads to a shift in center timing towards earlier dates.

In Europe, a large number of studies on streamflow have been carried out in recent times on national or regional scales (e.g. Renner and Bernhofer, 2011; Köplin et al., 2014; Fiala, 2008; Parajka et al., 2010; Birsan et al., 2012). Fiala (2008) investigated the characteristics and trends of mean annual and monthly streamflows of Czech rivers. Birsan et al. (2012) investigated trends in streamflow in Romania. Both studies focussed on the amount of discharge, and found that trends differed in different months.

Parajka et al. (2010) investigated the main flood-producing processes across the Alpine-Carpathian range. The paper presents a classification with eight groups of catchments

which show differences in flood-producing processes. In general, they found that small flood events can be produced by a range of mechanisms including short and long storms, effects of snow melt on antecedent soil moisture, rain on snow, and various atmospheric circulation patterns.

In Switzerland, a considerable amount of investigations have been undertaken to assess changes in streamflow regimes (e.g. Köplin et al., 2014; CH2014-Impacts, 2014; Volken, 2012; SGHL and CHy, 2011). These studies, however, use very detailed regime type definitions that are most appropriate for local scale investigations. In general, they conclude that in alpine catchments, runoff regimes are projected to shift from snow controlled to more rain controlled conditions. Streamflow in winter increases because more precipitation falls down as rain due to increasing temperatures. Streamflow in summer and autumn decreases due to a smaller contribution of snowmelt. This results in a change in seasonality, but only a small change in the annual sum of streamflow. Köplin et al. (2014) modeled trends in the seasonality of floods across Switzerland. They project changes due to changes in flood-generating processes such as precipitation and temperature.

According to Stahl et al. (2010), information on streamflow patterns on a larger than river-basin or national scale enables the identification and attribution of change in flow regimes, which are influenced by large-scale processes such as climate change. Therefore, they conducted a statistical analysis on observed streamflow data across Europe. They found positive and negative trends in the amount of streamflow in different months and different regions. This could be an indication for changes in the seasonality of streamflow. In general, the percentage of positive annual streamflow trends (towards wetter conditions) exceeds the percentage of negative trends (towards drier conditions). The amount of monthly streamflow exhibits positive trends for most of the stations in the winter months. Exceptions are Spain and the southern parts of France, where even in the winter season the streamflow amount exhibits negative trends. From April to August, most of the regions exhibit negative monthly streamflow amounts. In some of these months, Stahl et al. (2010) found positive monthly streamflow amounts in Scandinavia and in Central Europe. In addition to trends in streamflow amount, they investigated trends in the timing of summer low-flows. They found that the timing of the 7-day summer low flow has shifted to an earlier date (negative trend) in a majority of catchments, particularly in Germany, eastern France, Switzerland, Austria and Slovakia. Stahl et al. (2008) investigated drought conditions across Europe in summer, and discovered distinct regional differences. They found that drought severity (e.g. longer duration of droughts) has increased over the period 1962 - 2004 in Spain, France, Britain, Slovakia, central and northern Germany, eastern Austria and most of Norway.

Considering results from recent studies which investigated streamflow in snow-dominated catchments, one could expect a change in the timing of the annual cycle for the regime type one, due to increasing temperatures. The peak from the snowmelt streamflow is expected to occur earlier in spring. This hypothesis is illustrated in figure 1.2. For the timing measures defined in the present thesis, this means that one could expect a negative trend for the two Maximum and the two CT timing measures.

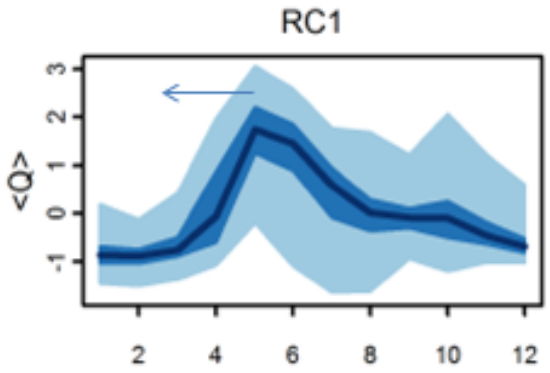

Figure 1.2.: Hypothesis: Shift of the snowmelt peak towards earlier in the season due to warmer temperatures.

Considering results from Stahl et al. (2008) on droughts, one could expect that low streamflows in summer exhibit a longer duration in some regions, resulting in a shift in the timing of the minimum annual streamflow towards later in the season. This hypothesis is illustrated in figure 1.3 by the red arrow.

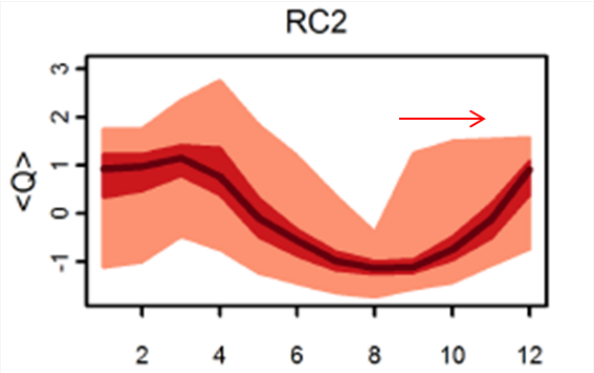

Figure 1.3.: Hypothesis: Shift of the minimum annual streamflow towards later in the season due to longer lasting drought periods.

1.2.2. Large-scale controls on seasonal streamflow

Variability of atmospheric circulation is thought to be the most important factor causing variability of fresh water fluxes from the continents (Bouwer et al., 2008). In particular, decadal changes in temperature and precipitation are related to changes in wintertime atmospheric circulation over the ocean basins of the Northern Hemisphere (Hurrell and van Loon, 1997). Barnston and Livezey (1987) investigated and defined low-frequency atmospheric circulation patterns in the northern hemisphere. These patterns influence air mass transport, climate and weather conditions in vast parts of the northern hemisphere. The relationship between teleconnection patterns and important climatic variables have

been studied by various researchers (e.g. Hurrell and van Loon, 1997; Blackburn and Hoskins, 2002; Trigo et al., 2004; Bueh and Nakamura, 2007; Lopez Moreno and Vicente Serrano, 2008). Burn (2008) did a partial correlation analysis to attribute some observed trends in measures of the timing of streamflow in Canada to trends in meteorological variables. Based on this, he was able to show that the timing of streamflow in Canada is affected by the Pacific Decadal Oscillation (PDO), the North Atlantic Oscillation (NAO), the North Pacific (NP) index and the Atlantic Multidecadal Oscillation (AMO), but not by the El Niño Southern Oscillation (ENSO) or the Arctic Oscillation (AO). Bouwer et al. (2006) investigated relationships between winter atmospheric circulation and winter discharges (December-February) of eleven large river basins that drain northwest Europe. They correlated river discharges to the frequency of west circulation (FWC) in winter (indicated by the Grosswetterlagen classification system) and to the NAO index. They found that the frequency of west circulation over Europe is a better indicator of climate variability and climate change impacts on river discharges in northwest Europe. Bouwer et al. (2008) investigated how regional sensitivities of mean and peak river discharge correspond to climate variability in Europe. They correlated mean and annual winter discharges to four different atmospheric indices. The four indices are: the North Atlantic Oscillation (NAO) index, the Arctic Oscillation (AO) index, the frequency of west circulation (FWC), and the north to south sea level pressure difference across the European continent (SLPD). In general, they found that the influence of atmospheric circulation is stronger on annual maximum discharges than on mean discharges. Discharge in Iberia and Scandinavia are generally more sensitive than those in central and northwest Europe. Similar to Bouwer et al. (2006), they found that FWC and SLPD are of greater use than NAO and AO for analysing climate impacts on streamflow in northwest Europe. Trigo et al. (2004) investigated the influence of the North Atlantic Oscillation (NAO) on Iberian Peninsula precipitation and river flow regime. Their results show that the large inter-annual variability in the flows of the considered rivers is largely modulated by the NAO phenomenon. Bueh and Nakamura (2007) investigated possible impacts of the Scandinavian Pattern on the Eurasian climate. One of their findings is that in cold seasons, the positive phase of the pattern gives rise to decreased precipitation over northeastern Europe. Lopez Moreno and Vicente Serrano (2008) investigated the influence of the NAO on droughts for all of Europe using the standardised precipitation index (SPI). They found that the responses of droughts to the phases of the NAO vary spatially and depend on the month of the year. During the positive phases of the NAO, negative SPI values are generally recorded in southern Europe. Considering the known influences of northern teleconnection patterns it seems reasonable to investigate the correlation between teleconnection patterns and the timing of the annual cycle of streamflow.

2. Data

2.1. Streamflow from near natural catchments

A data set of mean daily streamflow observations across Europe forms the basis for the present master thesis. The records originate from the European Water Archive (EWA), which has been collected by the UNESCO's FRIEND (Flow Regime from International Experiment and Network Data) program. Stahl et al. (2010) updated the database and added some new sets of gauging stations. The update and data collection is further described in Stahl et al. (2008).

Stahl et al. (2010) mentioned diverse reasons for a lack of data from some European countries. Some countries were unable to provide data at no cost. In some countries streamflow archives are local and no central database exists for larger administrative regions. And finally, some countries were not contacted since no contact person could be identified.

For the present master thesis, stations with more than 10 percent missing values in the time period 1970 - 2005 were excluded from the analysis. After this exclusion, a data set containing 657 stations remained. The stations are shown in figure 2.1

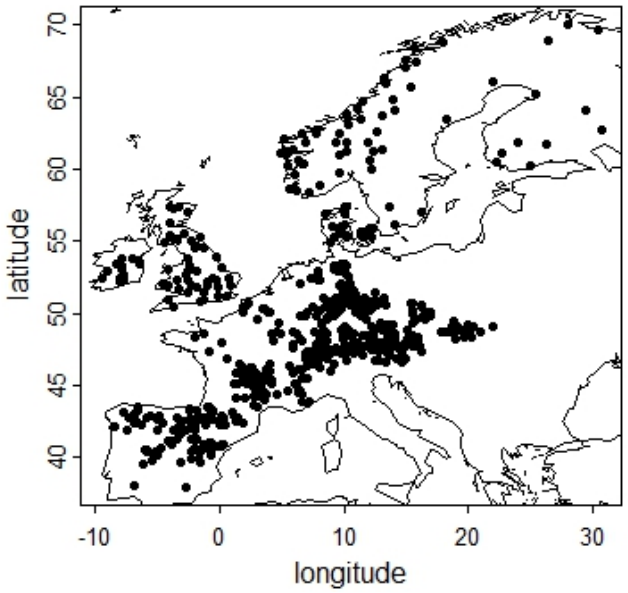

Figure 2.1.: analysed streamflow gauging stations

2.2. Time series of northern teleconnection patterns

In the present master thesis, the effect of six different northern hemisphere teleconnection patterns on the seasonality of streamflow are assessed. The teleconnection patterns considered are: North Atlantic Oscillation (NAO), Scandinavian Pattern (SCA), East Atlantic (EA), East Atlantic/Western Russia (EAWR), Polar/Eurasia (POLEUR), Tropical/Northern Hemisphere (TNH). Teleconnection patterns reflect large-scale changes in the atmospheric wave pattern, and influence temperature, rainfall, storm tracks, and jet stream location and intensity over different regions. Data sets containing monthly tabulated time series of the teleconnection indices originate from the National Weather Service (http://www.cpc.ncep.noaa.gov/data/teledoc/telecontents.shtml). The most important influences of the six northern hemisphere teleconnection patterns on climate and weather conditions in Europe are summarised as follows: The North Atlantic Oscillation is one of the most prominent teleconnection patterns in all seasons (Barnston and Livezey, 1987). When the North Atlantic Oscillation index is high, the westerly winds are stronger than normal. The moderating influence of the North Atlantic Ocean then leads to warmer than normal conditions over the Eurasian continent (Hurrell and van Loon, 1997). A high North Atlantic Oscillation index in winter is associated with drier conditions over much of central and southern Europe, and wetter than normal conditions over Iceland and Scandinavia (Greatbatch, 2000). The Scandinavian Pattern has been previously referred to as the Eurasia-1 pattern by Barnston and Livezey (1987). The positive phase of the Scandinavian Pattern is associated with below-average temperatures across central Russia and over western Europe. It is also associated with above-average precipitation across central and southern Europe, and below-average precipitation across Scandinavia (NOAA and National Weather Service, 2012). The positive phase of the East Atlantic pattern is associated with above-average surface temperatures in Europe in all months, as well as wetter than normal conditions over northern Europe and Scandinavia, and with drier than normal conditions across southern Europe (NOAA and National Weather Service, 2012). The positive phase of the East Atlantic/Western Russia pattern is associated with below-average temperatures over large portions of western Russia as well as with below-average precipitation across central Europe (NOAA and National Weather Service, 2012). The positive phase of the Polar/Eurasia index is associated with positive temperature anomalies in central Europe, and with negative precipitation anomalies in north-eastern parts of central Europe and southern parts of Scandinavia (NOAA and National Weather Service, 2012). For the Tropical/Northern Hemisphere pattern, there exists only data for the winter season December, January, and February. The Tropical/Northern Hemisphere mainly influences weather conditions in Northern America, but is also associated with below-average precipitation across much of the central North Atlantic Ocean (NOAA and National Weather Service, 2012).

2.3. Precipitation and temperature observations

The influence of the northern teleconnection patterns on the timing measures are discussed in the present thesis considering the relationship between the teleconnection patterns and precipitation and temperature. For the latter correlations, a data set of daily precipitation and daily temperature observations over the analysed time period is used. This data set originates from Haylock et al. (2008) and is provided on the webpage of the European Climate Assessment and Dataset (ECA&D) (http://www.ecad.eu).

3. Methods

3.1. Definition of timing measures

3.1.1. Date of maximum and minimum annual streamflow

Six different measures of the timing of the annual cycle of streamflow are defined by pursuing two different approaches.

The first four timing measures were obtained by defining the date of occurrence of the maximum and the minimum flow of the climatological annual cycle of streamflow. The climatological annual cycle is estimated by applying a moving average filter. This filter was also used in earlier studies to extract the annual cycle (e.g. Coopersmith et al., 2012; Bosshard et al., 2011). In the present thesis, two different averaging window widths are applied. One window width is 91 days, and the other is 181 days. The maximum and the minimum flows are then defined from the smoothed curves. This leads to the first four timing measures, to which we refer as maximum 91 (Max91), maximum 181 (Max181), minimum 91 (Min91) and minimum 181 (Min181). The definition of these timing measures is illustrated in figure 3.1. The figure shows a three year window from an original streamflow time series for one station. The red curve shows the annual cycle resulting from filtering the time series with the window width of 91 days. The blue curve shows the resulting annual cycle for the window width of 181 days.

Further steps are described in the following paragraph taking the example of Max91 and one single station. First, the date of occurrence for the timing measure is defined for every year of the analysed period. This results in a time series showing the day of year, when the timing measure occurred. The dates are given in julian dates with 1 being January 1. An example is shown in figure 3.2. Calculating the mean occurrence date for the timing measure from such a time series presents a particular problem (Bayliss and Richard, 1993). Day 1 and day 365 have adjacent values in the time series but will not be considered as such if day numbers are used (Bayliss and Richard, 1993). To get around this problem the day number is converted into angular values (expressed in radians) following previous studies (e.g. Bayliss and Richard, 1993; Köplin et al., 2014; Cunderlik and Burn, 2001).

$$Max\theta i = (Juliandate)i * ((2 * pi)/365)$$

With $Max\theta i$ as the date of occurrence of the Max91 for year i expressed in angular values. Leap years are taken into account by setting the denominator to 366. The dates can then be handled in a polar coordinate system, and the mean date for the Max91

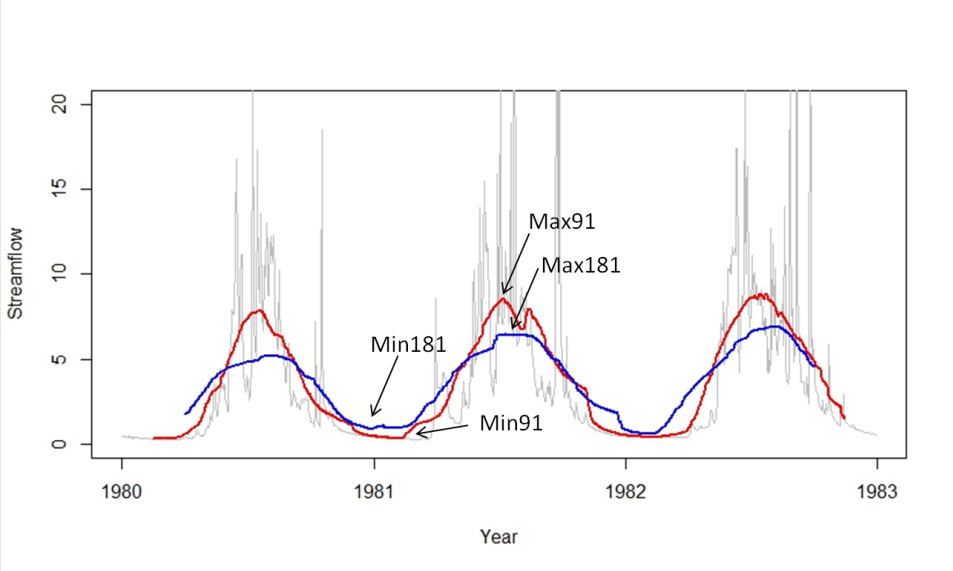

Figure 3.1.: Smoothed curves from applying a moving average filter with a 91-days window width (red) and a 181-days window width (blue). Max and Min timing measures are indicated by the arrows.

can be calculated (expressed in radians). The mean is then subtracted from each $Max\theta i$ to obtain the deviations from it in angular values, denoted here as $Maxdfm_{rad}$. These values can then be converted back into deviations from the mean expressed in days ($Maxdfm$) as

$$Max\ dfm_i = (Maxdfm_{rad})i * (365/(2 * pi))$$

These transformations result in a time series showing the deviations from the mean occurrence date expressed in days. The example of Max91 for one station is shown in 3.3. Similar time series are calculated for every station of the data set. The same procedure is performed for the timing measures Max181, Min91 and Min181.

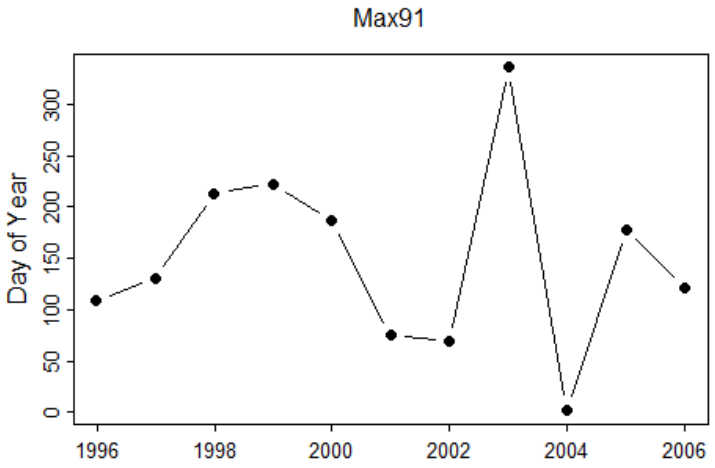

Figure 3.2.: Occurrence date for the Max91 in julian dates with 1 being January 1.

3.1.2. Center timing

Two additional timing measures are defined by calculating the center timing. The center timing is the date in the year when half of the annual streamflow amount is exceeded. The definition of center timing for one station is indicated by the red line in Figure 3.4. In general, an early date of occurrence of center timing means that considerable amounts of the annual streamflow occur in the first months of the year, whereas in the later months the flows are lower. In contrast, a late occurrence date means that major portions of the annual streamflow occurs late in the year in this particular catchment. According to Moore et al. (e.g 2007); Regonda et al. (e.g 2005) and Rauscher et al. (2008) CT1 is defined as the julian day when 50% of the annual flow is exceeded. According to Stewart et al. (2005) CT2 is defined as

$$CT2 = \sum(t_i * q_i) / \sum q_i$$

where t_i is time in days from the beginning of the year and q_i is the corresponding streamflow for day i. CT1 and CT2 are defined for each calendar year of the analysed time period. The time series of annual CT1 and CT2 were determined for each gauging station of the data set. Figure 3.5 shows the time series for all of the six defined timing measures for one station.

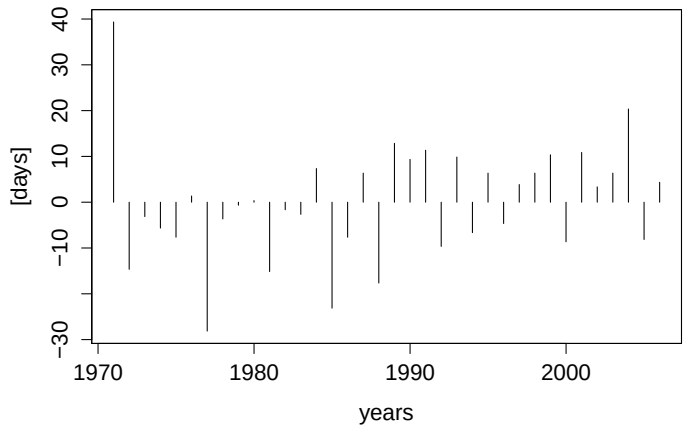

Figure 3.3.: Max91: time series for one station showing deviations from the mean in days.

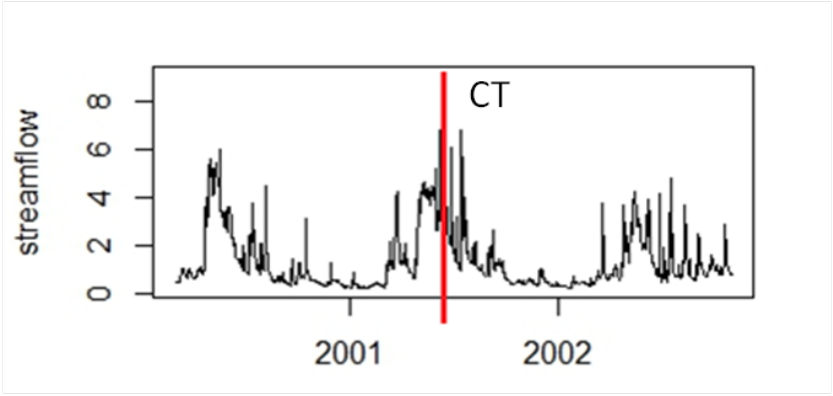

Figure 3.4.: Definition of CT (indicated by the red line).

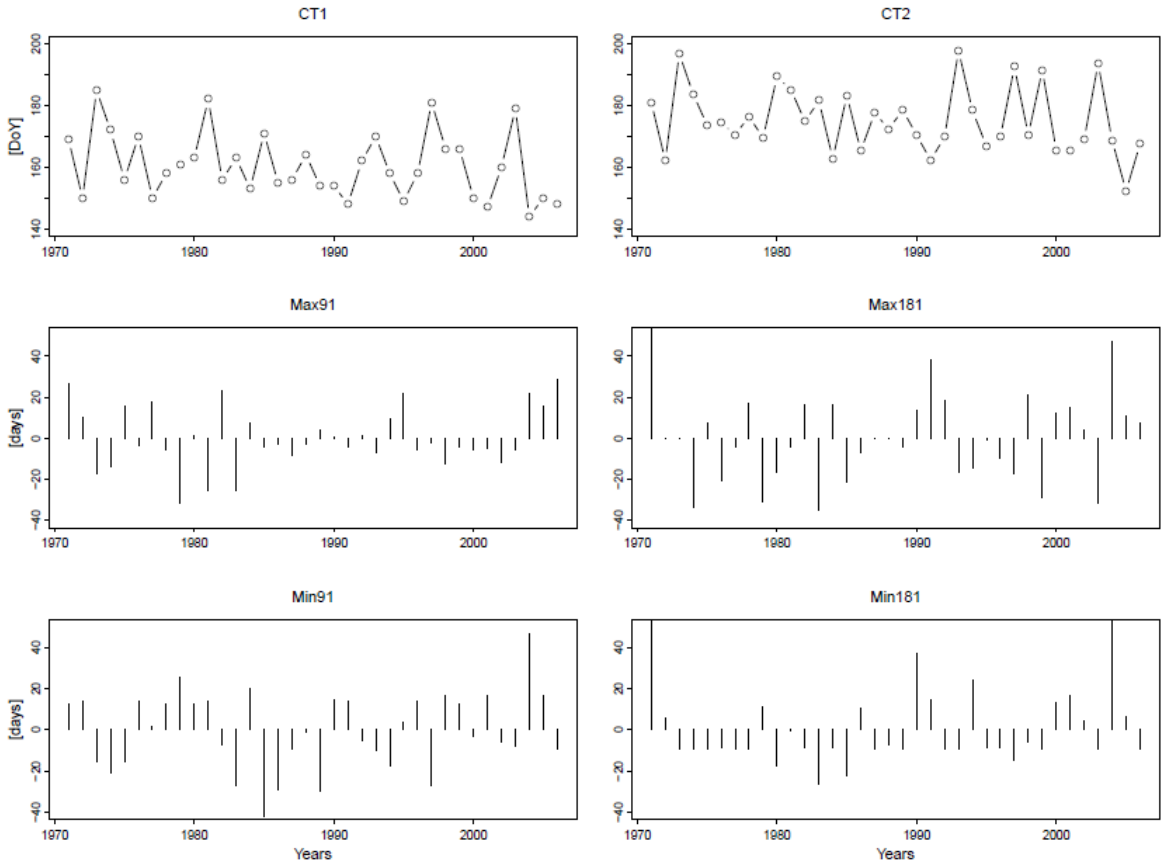

Figure 3.5.: Time series for all six defined timing measures for one station. CT1 and CT2 are given in Julian dates with 1 being January 1. The Max and Min are expressed in deviations from the mean in days.

3.2. Correlation between the six timing measures

In order to assess the relationship between the six timing measures, a correlation analysis is conducted. First, for each timing measure the time series of every station are merged together. This results in one vector for every timing measure containing the data of every station. The six vectors are then related to each other using the Pearson method in order to get the linear correlation coefficients of every timing measure pair.

3.3. Trend Analysis

3.3.1. Trends

The Mann-Kendall test is one of the most frequently used nonparametric tests for identifying trends in meteorologic variables (Mann, 1945; Kendall, 1975). It is a rank-based procedure and is especially suitable for non-normally distributed data and data containing outliers. The trend magnitude is estimated using the Sen Slope (Sen, 1968). The Mann-Kendall test and the Sen slope have also been used in many previous studies (e.g. Stahl et al., 2010, 2012; Burn, 2008). The significance of the trend test for every station is tested at the 5% significance level (p-value < 0.05). In the following this is referred to as *local* significance.

3.3.2. Field significance

Livezey and Chen (1982) emphasise the need to evaluate the collective significance of a finite set of individual significance tests. This collective significance is referred to as *field significance*. Field significance allows the determination of the percentage of tests that are expected to show a trend, at a given local significance level, purely by chance (Burn et al., 2004). In the present thesis, the question to be answered is:

> "How many stations with locally significant trend tests would be detected only by chance?"

Furthermore, when a collection of multiple tests is performed using data from spatial fields, the positive spatial correlation of the underlying data produces statistical dependence among the local tests. This leads to the fact that false rejections of the null hypothesis tend to cluster in space and can lead to the erroneous impression that a spatially coherent and physically meaningful spatial feature may exist (Wilks, 2011). One approach to assess field significance and to account for spatial correlation is to conduct a bootstrap resampling experiment (e.g. Lettenmaier et al., 1994; Douglas et al., 2000; Wilks, 2011). This approach is applied in the present master thesis, pursuing the procedure used in Burn et al. (2004).

The bootstrap approach is applied to every timing measure. Each bootstrap resampling experiment involves the following steps:

1. draw with replacement one year from the analysed time series (1970-2005)
2. enter the data value for each station for the selected year in a newly assembled data set (resampled data set)
3. repeat steps one and two until the resampled data set consists of 35 years; one year from the original time series can thereby be drawn more than once (bootstrap resampling)
4. apply the Mann-Kendall trend test on the resampled series of every station;
5. test the local significance of the trends (p-value < 0.05);
6. calculate the percentage of stations with locally significant test results;

Steps 1 - 6 are repeated 2000 times. Each time the percentage of stations with locally significant trends is saved. This results in a distribution of the percentage of significant stations that were detected only by chance. From the obtained empirical cumulative distribution function (ecdf), the value of the 95-percentile is determined. This value is taken as the critical value. The critical value is then compared to the value that was obtained from the test results with the original data set. If the critical value is higher, this means that the result is not field significant at the global significance level of 5%.

3.4. Correlation of northern teleconnection patterns

3.4.1. Correlation coefficients

A correlation analysis is conducted in order to assess the influence of the six northern teleconnection patterns mentioned in section 2.2. Correlation coefficients (r) are calculated between every timing measure and the monthly values of the teleconnection patterns. This is done for every station of the data set. The relationships are measured using the Pearson product-moment correlation coefficients. In addition, the local significance of the correlation coefficients is tested at the 5% significance level (p-value $<$ 0.05) using the t-test. The analysis is done over the same time period as the trend tests. A data set of $6 * 6 * 12 = 432$ correlation coefficients for every station is the result of this analysis ($timing\ measure * index * month$). A detailed analysis of the 432 combinations is not feasible. Therefore, the data is reduced by maintaining only the most influencing teleconnection pattern for every timing measure (monthly Index). This is achieved by choosing the six correlation pairs with the largest median r^2.

3.4.2. Field significance

The problem of field significance and spatial correlation, which is described in section 3.3.2, arises here in a similar way. Therefore, a bootstrap resampling experiment is conducted in order to account for spatial correlation and to assess field significance. The question, which has to be answered is:

> "How many stations with locally significant correlation tests would be detected only by chance?"

A bootstrap approach is applied for every correlation pair. Each bootstrap resampling experiment involves the following steps:

1. draw with replacement one year from the teleconnection pattern time series (1970-2005)
2. enter the data value for the selected year in a newly assembled data set (resampled data set)
3. repeat steps one and two until the resampled data set consists of 35 years; one year from the original time series can thereby be drawn more than once (bootstrap resampling)
4. conduct a correlation analysis: calculate the correlation coefficients r;
5. test the local significance of the correlation coefficients (p-value < 0.05) for each station;
6. calculate the percentage of stations with locally significant test results;

Similar to the procedure for the trend tests, steps 1 - 6 are repeated 2000 times. This results in a distribution of the percentage of stations with locally significant correlation coefficients. From the obtained empirical cumulative distribution function (ecdf), the value of the 95-percentile is determined. This value is taken as the critical value. The critical value is then compared to the values from the analysis with the original data set. When the critical value is larger than the original value, this means that the results are not field significant at the global 5% significance level.

3.4.3. Correlation between the teleconnection patterns, precipitation and temperature

The influence of the teleconnection patterns on precipitation and temperature across Europe is considered in the discussion of the correlations between the teleconnection patterns and the timing measures. The correlations between the teleconnection patterns and precipitation and temperature are calculated on the webpage (*http : //climexp.knmi.nl/start.cgi?id = paiviv@student.ethz.ch*; 05.02.2015) of the KNMI Climate Explorer (WMO Regional Climate Centre and KNMI, 2014). Local significance of the correlations is tested at the 10% significance level (p-value < 0.1), and field significance is assessed at the global 10% significance level.

4. Results

4.1. Correlation between the timing measures

The results of the correlation analysis between the six timing measures are shown in table 4.1. The largest correlation is that between the CT1 and the CT2 (r=0.91). The second largest correlations are those between the Max91 and the Max181, and between the Min91 and the Min181. Both pairs have a correlation coefficient of 0.5. All other correlation coefficients are rather small.

–	CT1	CT2	Max91	Max181	Min91	Min181
CT1	1	···	···	···	···	···
CT2	0.91	1	···	···	···	···
Max91	0.24	0.23	1	···	···	···
Max181	0.20	0.20	0.50	1	···	···
Min91	0.07	0.06	0.25	0.30	1	···
Min181	0.07	0.08	0.32	0.34	0.50	1

Table 4.1.: Correlation coefficients between the six timing measures

4.2. Climatology of the timing measures

This section presents the mean occurrence dates for the six timing measures. The results are shown in figure 4.1. The dates are expressed as julian dates with 1 being January 1. The CT1 mean is more or less in the middle of the year for all stations. In the catchments of the alpine region and in Scandinavia the CT1 mean is later than in the other parts of Europe. The latest mean of the CT1 is found in the south-western part of Norway. The pattern of the CT2 mean looks quite similar to that of the CT1. The Max91 occurs on average between April and June in the Pyrenees, the Alps, the Carpathian Mountains, and in Scandinavia. In most other parts of Europe, the Max91 mean is in the winter months. The spatial pattern of the Max181 looks similar to that of the Max91. However, the Max181 seems to occur slightly later than the Max91 in the summer season in the alpine region and in Scandinavia. The Min91 mean is in the winter season for stations in the Alps and in Scandinavia, and some stations in the Pyrenees and the Carpathian Mountains. In almost all other parts of Europe it occurs towards the end of the summer season. In northern parts of the UK, Ireland, and the coastal south-western part of

Norway the mean is slightly earlier in the summer season. The pattern of the Min181 looks quite similar to that of the Min91.

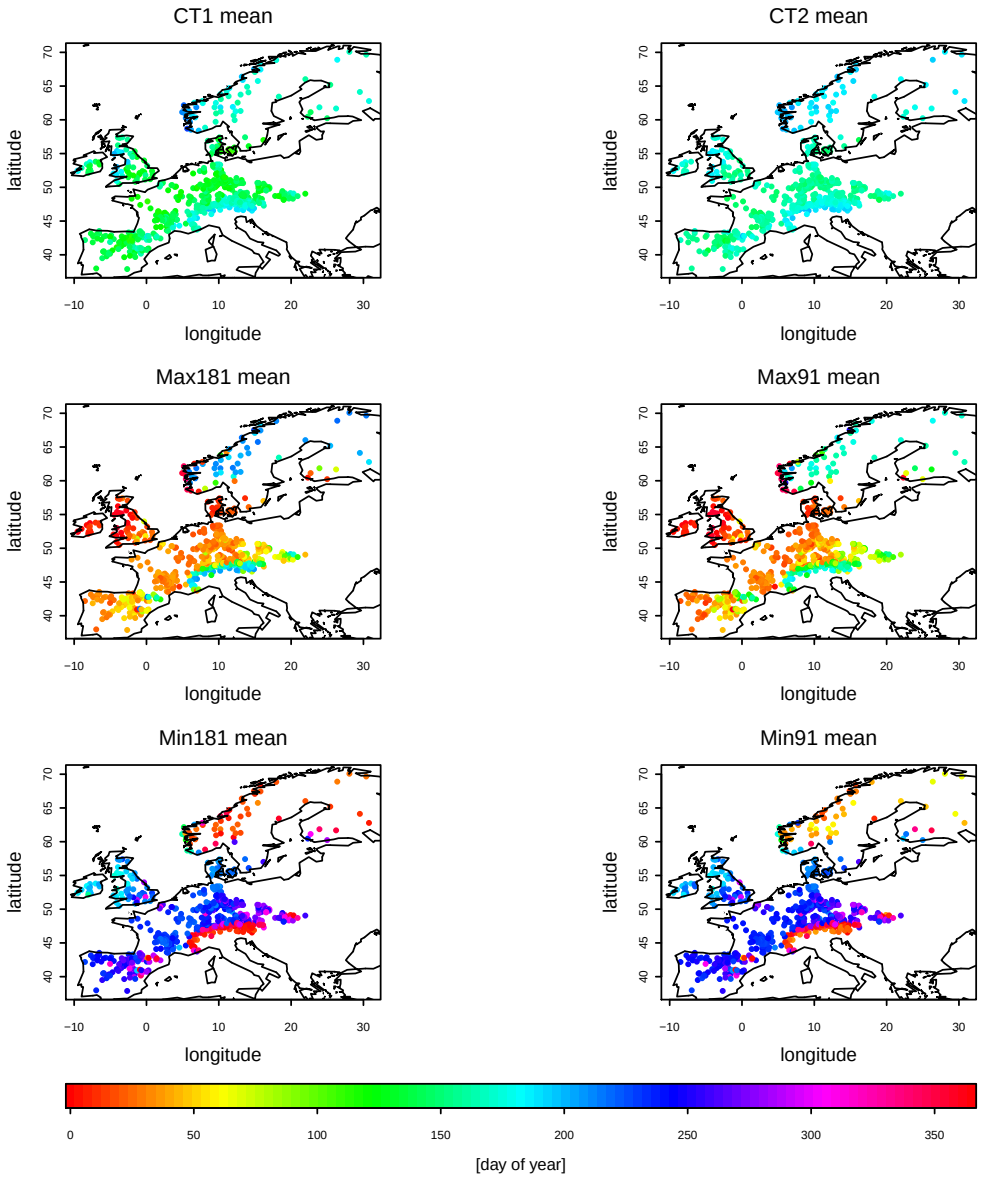

Figure 4.1.: Climatologies of the six timing measures

4.3. Trend analysis

Figure 4.2 shows the empirical cumulative distribution functions (ecdf) of the bootstrap resampling experiments of the trend assessment. The x-axes state the percentage of stations with locally significant test results. Note that the axes have different scales. The lines indicate the 95-percentile which is taken as the critical value. Exact numbers of stations with locally significant trend tests for the original data set and the bootstrap resampling experiments are shown in table 4.2. The table shows that none of the timing measures exhibit field significant trends. Even though the trends are not field significant at the global 5% significance level, the results for each timing measure are briefly summarised in the following section.

timing measures	Stations with p-value < 0.05	Stations with p-value < 0.05 [%]	Critical value [%]
CT1	68	10.4	16.3
CT2	34	5.2	17.1
Max91	65	9.9	12.5
Max181	52	7.9	13.2
Min91	63	9.6	12.2
Min181	39	5.9	13.6

Table 4.2.: Results for the trend analysis and the bootstrap resampling experiment

Figure 4.3 shows the results of the trend analysis. The trend is given in days per year. Negative trends mean that the timing measure has shifted towards earlier dates in the season. Positive trends mean that the timing measure has shifted towards later dates. The black dots mark the stations with locally significant test results (p-value < 0.05). For the CT1, most stations in central Europe and the Norwegian coast show negative trends. In Spain and the UK there are stations with positive trends. For the CT2, the spatial pattern of the trend sign is quite similar to that of the CT1. In general, the trend magnitude is smaller than that of the CT1 trends. For the Max91, most stations exhibit positive trends. This would mean that the Max91 has generally shifted towards later in the year. The Max181 exhibits rather weak overall trends. Positive trends are found for stations in Spain. Some stations with negative trends are found for stations in the western part of the domain. For the Min91, stations in central Europe exhibit positive trends. Slightly negative trends are found for stations in the UK, Ireland, Denmark, and parts of Scandinavia. For the Min181, most of the stations show rather weak or slightly positive trends. Negative trends can be seen in Ireland and some stations in the northern and the western part of Europe.

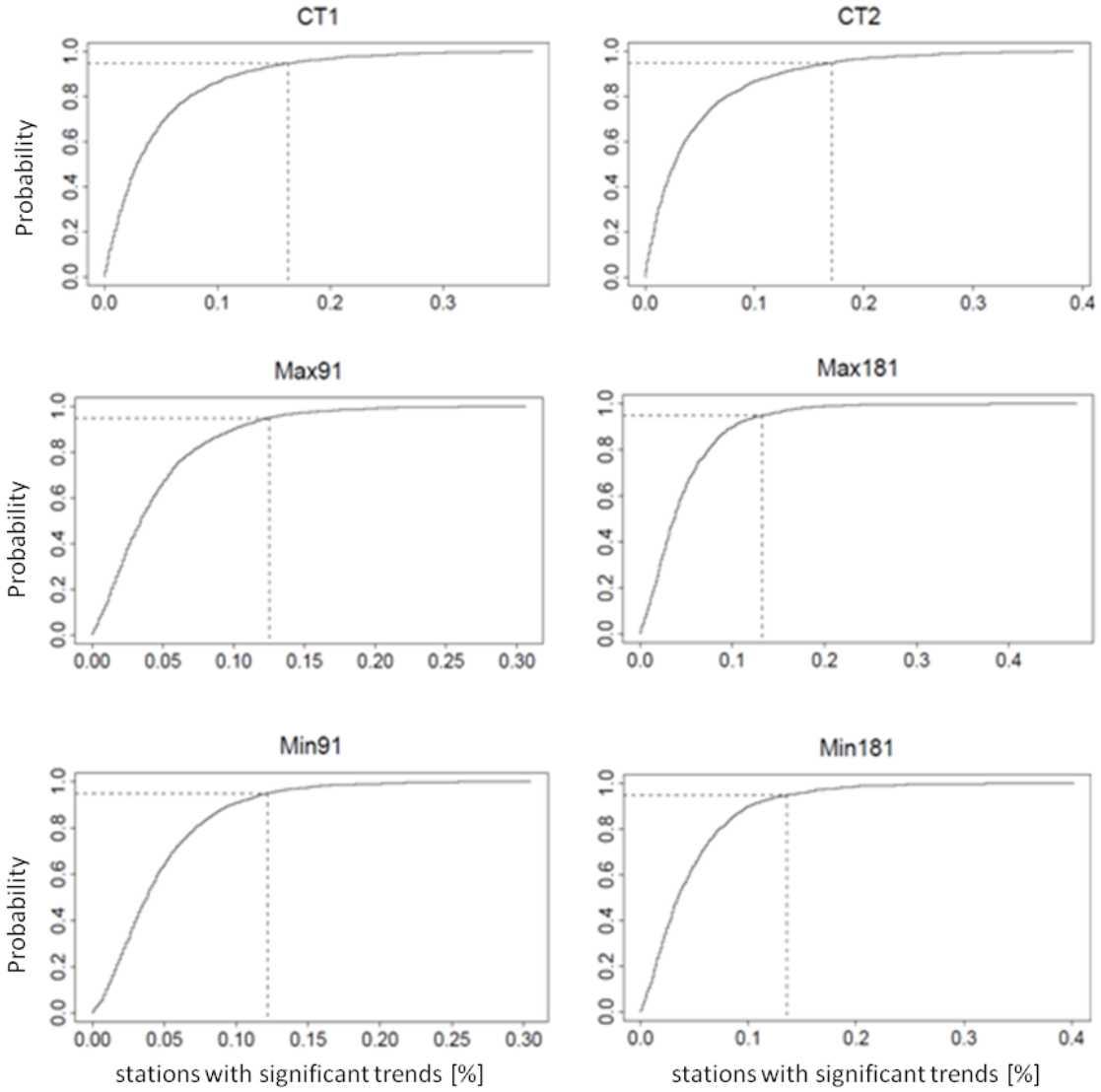

Figure 4.2.: Ecdf for every timing measure from the bootstrap resampling experiments for the trend assessment. The 95-percentile is indicated by the dashed line.

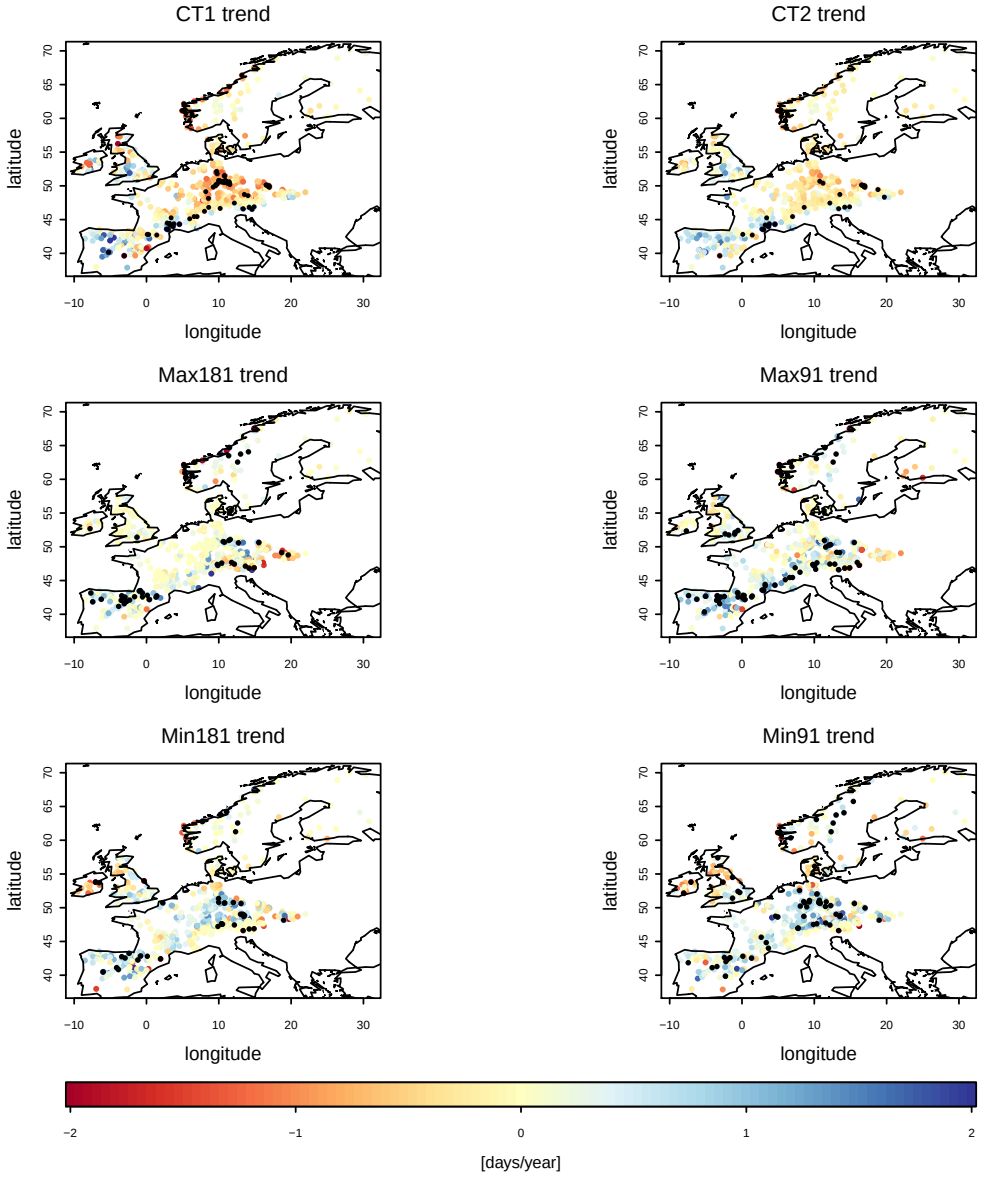

Figure 4.3.: Results of the trend analysis. Black dots mark the stations with locally significant trends (p-value < 0.05).

4.4. Correlation with northern teleconnection patterns

This section presents the results for each timing measure and its most influencing northern teleconnection pattern. As described in section 3.4.1, for each timing measure only the monthly index value with the largest median r^2 is maintained. The boxplots in figures 4.4 - 4.9 show the r^2 of the correlation analysis between one timing measure and the six northern teleconnection patterns. Note that the y-axes have different scales. The largest median r^2 is indicated by the red rectangle. The exact values of the r^2 of each selected pair, are given in table 4.3. The six pairs are:

- CT1 - Scandinavian Pattern (SCA) in January,
- CT2 - Scandinavian Pattern (SCA) in January,
- Max91 - Scandinavian Pattern (SCA) in September,
- Max181 - North Atlantic Oscillation (NAO) in October,
- Min91 - Scandinavian Pattern (SCA) in September,
- Min181 - East Atlantic/Western Russia (EAWR) in March

Figure 4.10 shows the empirical cumulative distribution functions of the bootstrap resampling experiments for the correlation analysis. The x-axes show the percentage of stations with locally significant test results. Note that the x-axes have different scales. The dashed lines indicate the 95-percentile, which is taken as the critical value. Exact numbers of stations with locally significant tests from the original data set and from the bootstrap resampling experiment are given in table 4.3. The results for all six pairs are field significant at the global 5% significance level.

timing measures	Index / month	Stations with p-value < 0.05	Stations with p-value < 0.05 [%]	Critical value [%]	Median r^2
CT1	SCA 1	288	43.84	17.19	0.0896
CT2	SCA 1	336	51.14	17.35	0.1165
Max91	SCA 9	174	26.48	11.87	0.0567
Max181	NAO 10	150	22.83	12.17	0.0472
Min91	SCA 9	136	20.70	10.04	0.0335
Min181	EAWR 3	154	23.44	13.08	0.0428

Table 4.3.: Results of the correlation analysis and the bootstrap resampling experiments

The spatial patterns of the correlations between the six pairs are shown in figure 4.11. Blue colors mean negative correlations, and red colors mean positive correlations. The black dots mark the stations with locally significant correlation coefficients. The

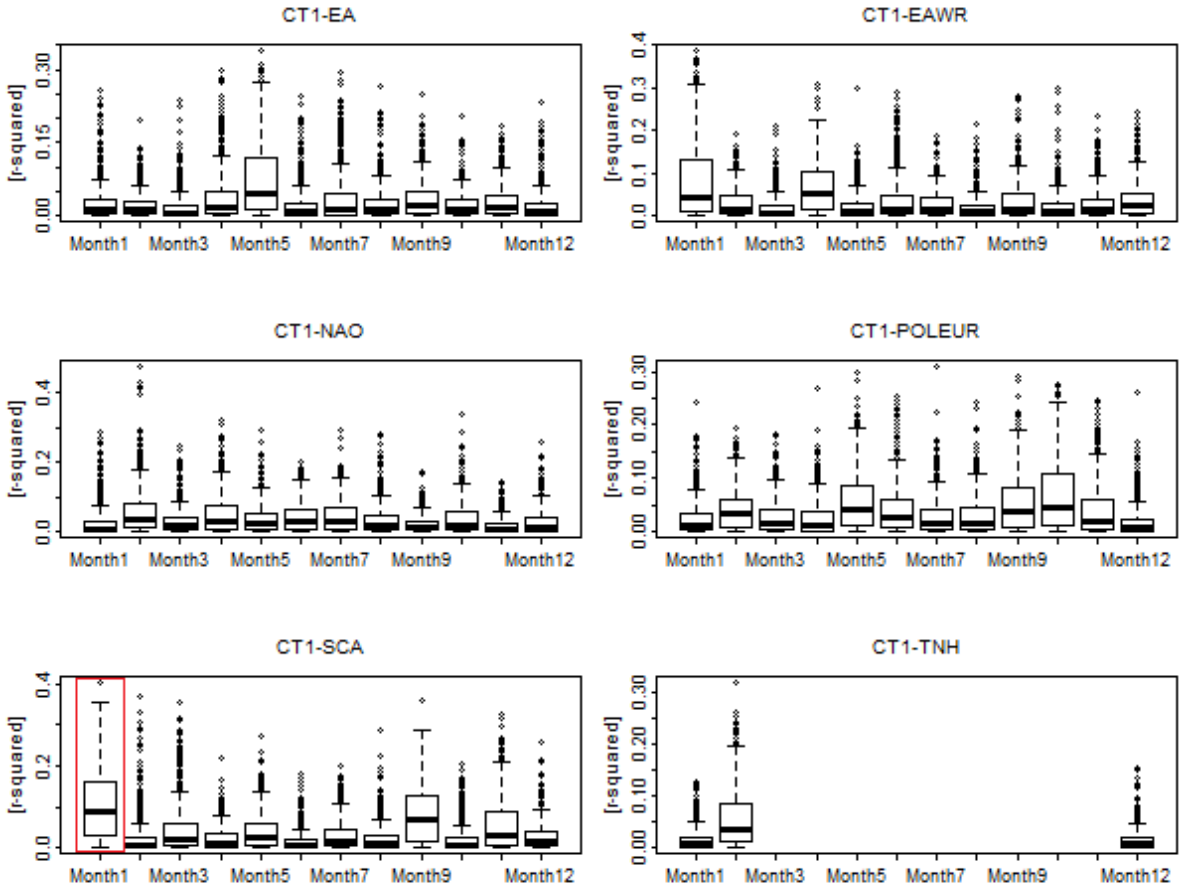

Figure 4.4.: Boxplots with the r^2 for the CT1 and the monthly indices of the six northern teleconnection patterns. The pattern with the largest median of the r-squared is indicated by the red rectangle. Note that the y-axes have different scales.

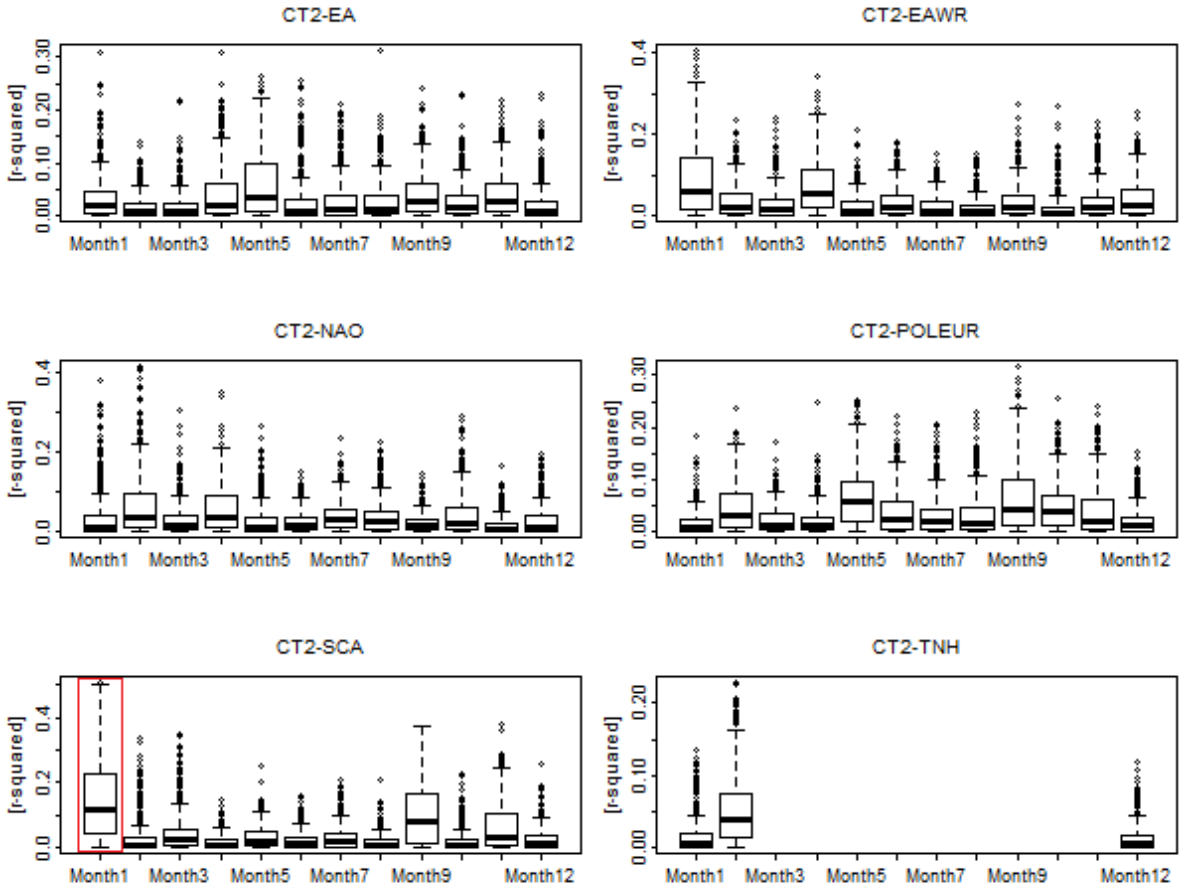

Figure 4.5.: Boxplots with the r-squared for the CT2 and the monthly indices of the six northern teleconnection patterns. The pattern with the largest median of the r^2 is indicated by the red rectangle. Note that the y-axes have different scales.

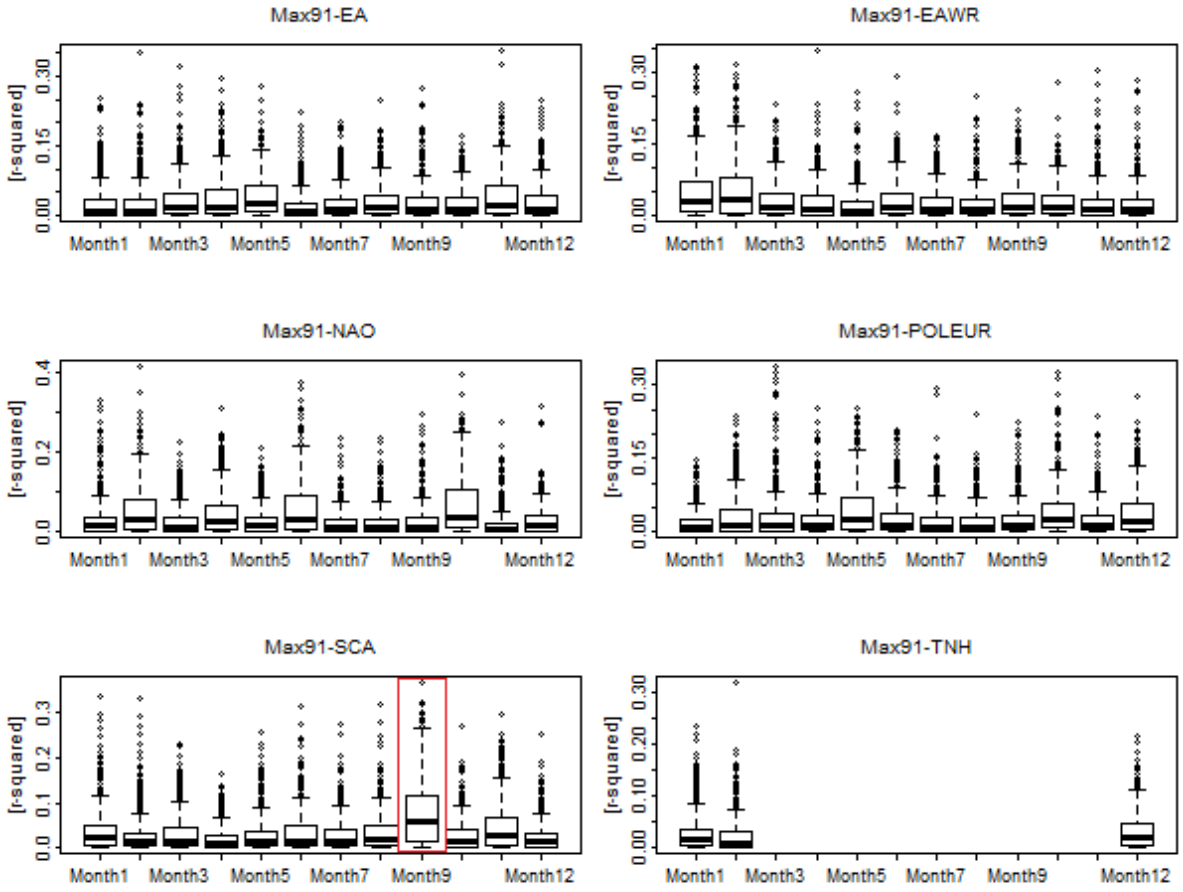

Figure 4.6.: Boxplots with the r-squared for the Max91 and the monthly indices of the six northern teleconnection patterns. The pattern with the largest median of the r^2 is indicated by the red rectangle. Note that the y-axes have different scales.

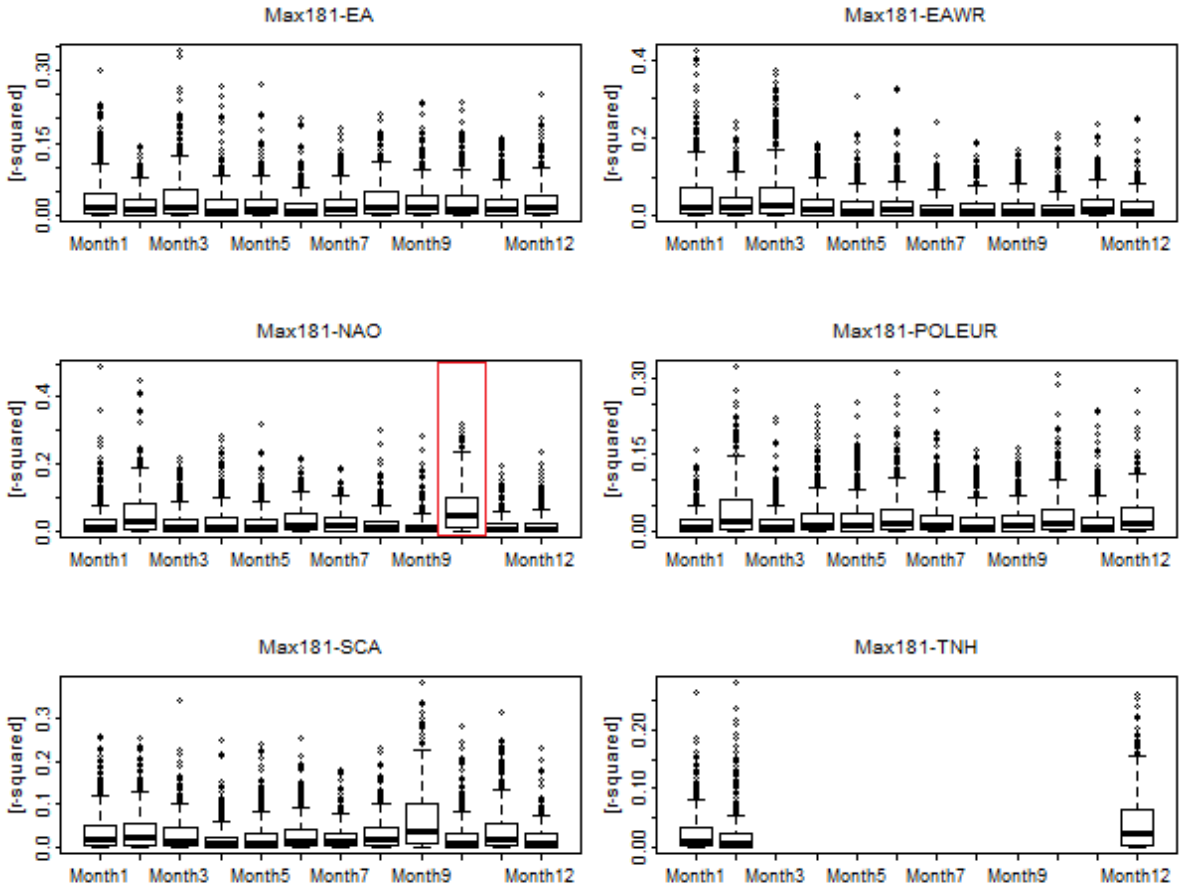

Figure 4.7.: Boxplots with the r-squared for the Max181 and the monthly indices of the six northern teleconnection patterns. The pattern with the largest median of the r^2 is indicated by the red rectangle. Note that the y-axes have different scales.

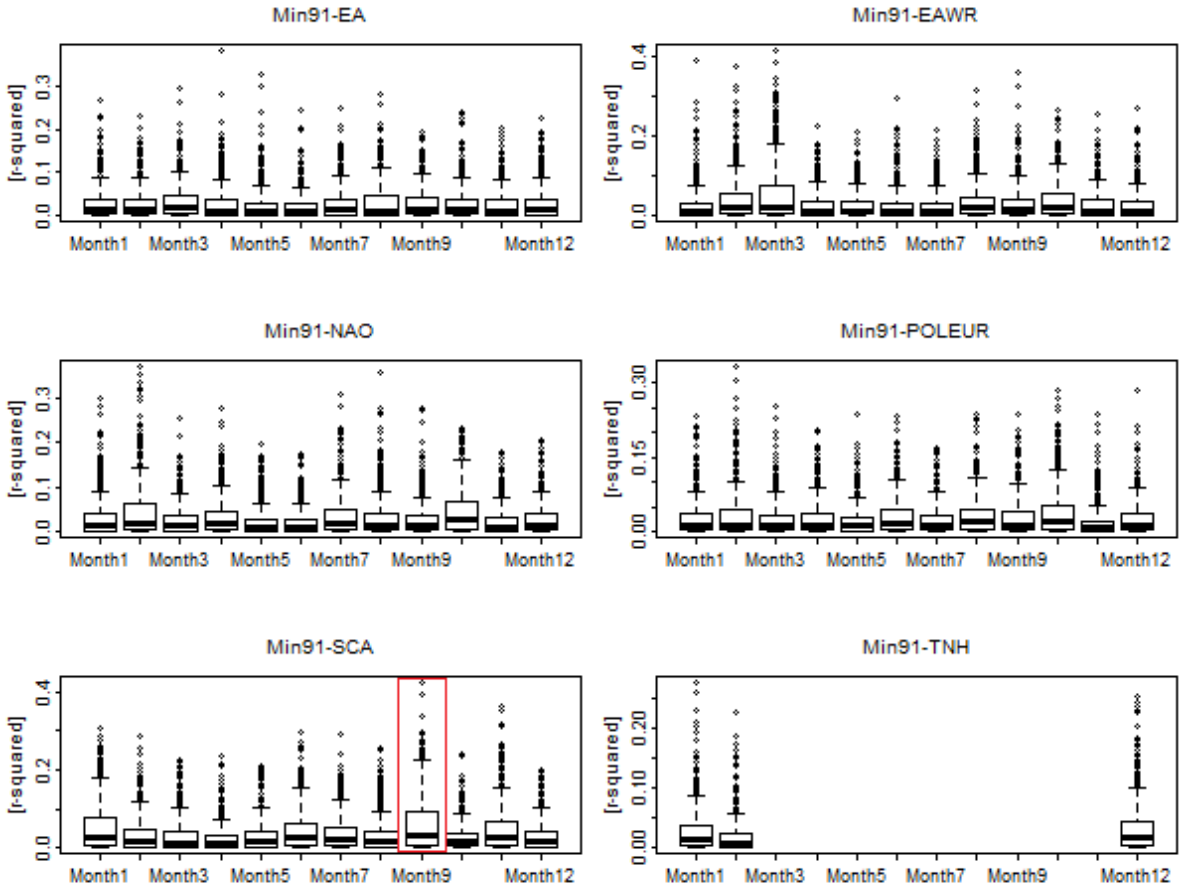

Figure 4.8.: Boxplots with the r-squared for the Min91 and the monthly indices of the six northern teleconnection patterns. The pattern with the largest median of the r^2 is indicated by the red rectangle. Note that the y-axes have different scales.

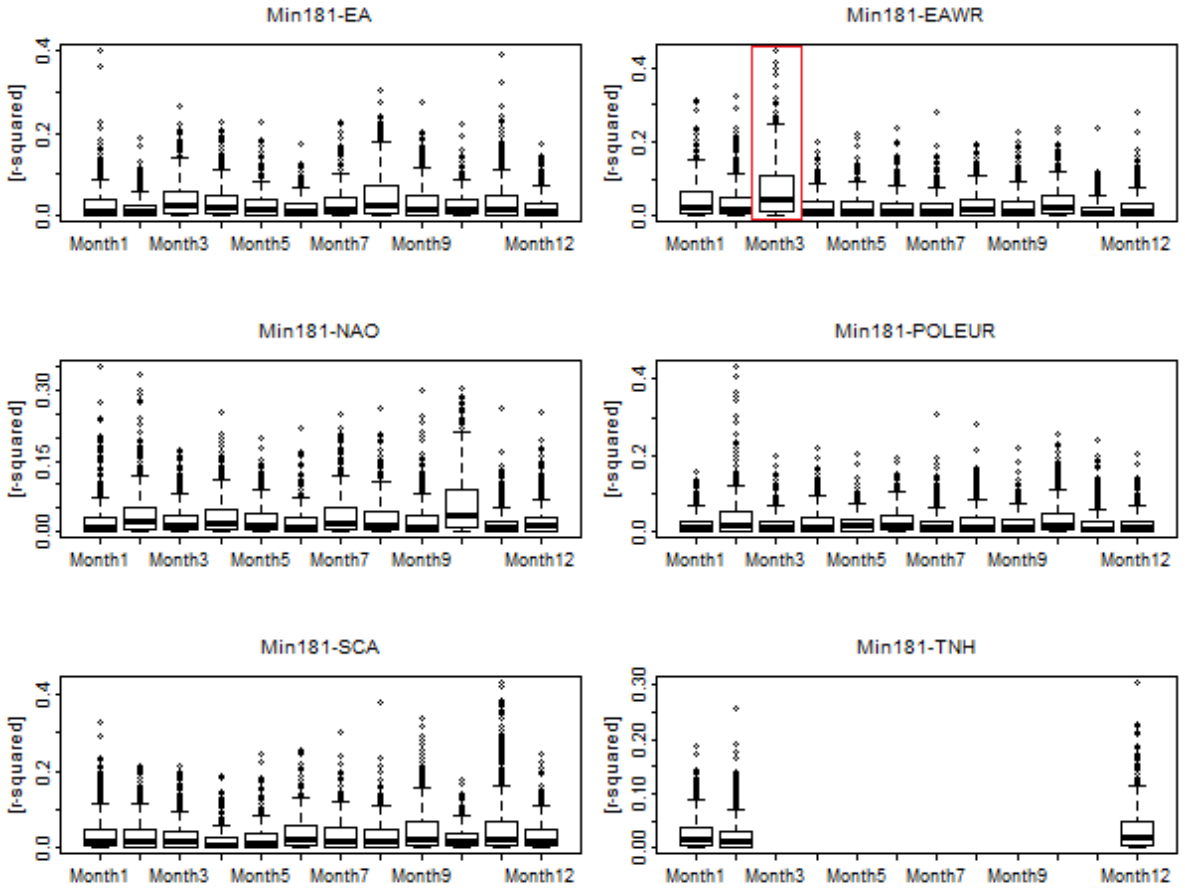

Figure 4.9.: Boxplots with the r-squared for the Min181 and the monthly indices of the six northern teleconnection patterns. The pattern with the largest median of the r^2 is indicated by the red rectangle. Note that the y-axes have different scales.

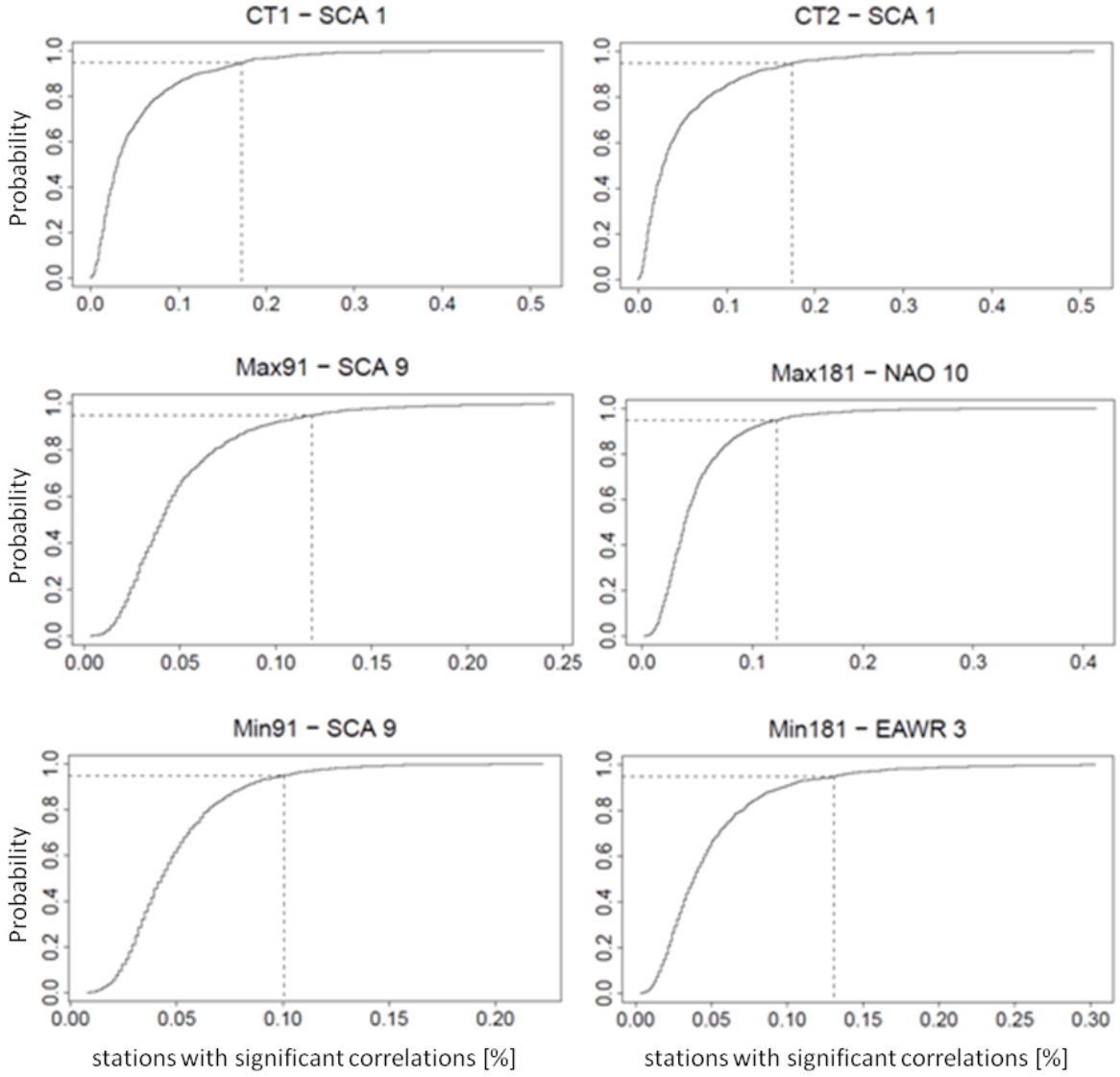

Figure 4.10.: Ecdf for each correlation pair from the bootstrap resampling experiments of the correlation analysis. The 95-percentile is indicated by the dashed line.

subsequent descriptions of the spatial patterns of the correlations are related to these stations. For the CT1 and January values of the Scandinavian Pattern, the correlation coefficients are negative for the stations in Spain, south-western parts of France and most of the stations in the UK. For most of the remaining stations, the correlation coefficients are positive. The strength of the correlations ranges from -0.60 to 0.63. For the CT2 and January values of the Scandinavian Pattern, the spatial pattern looks similar to that of the CT1. The strength of the correlations ranges from -0.62 to 0.71. For the Max91 and September values of the Scandinavian Pattern, the correlation coefficients are positive for most of the stations across Europe. Some stations with negative coefficients are found in the south-western part of Norway. The strength of the correlations ranges from -0.57 to 0.61. For the Max181 and October values of the North Atlantic Oscillation, the correlation coefficients are negative for most of the stations across Europe. The strength of the correlations ranges from -0.57 to 0.36. For the Min91 and September values of the Scandinavian Pattern, the correlation coefficients are positive for most of the stations across Europe. Some stations with negative coefficients are found in the Alps. The strength of the correlations ranges from -0.65 to 0.63. For the Min181 and March values of the East Atlantic/Western Russia pattern, the correlation coefficients in most stations are negative. Only few stations with significant correlations are found in Spain and France. The strength of the correlations ranges from -0.67 to 0.50.

In some cases, the pattern of the correlations between one timing measure and one northern teleconnection pattern varies quite strongly in different months. Figure 4.12 is presented here as an example. The figure shows the seasonal evolution of the correlations between the CT1 and the Scandinavian Pattern. The results for all the other timing measures - northern teleconnection patterns are attached in the appendix.

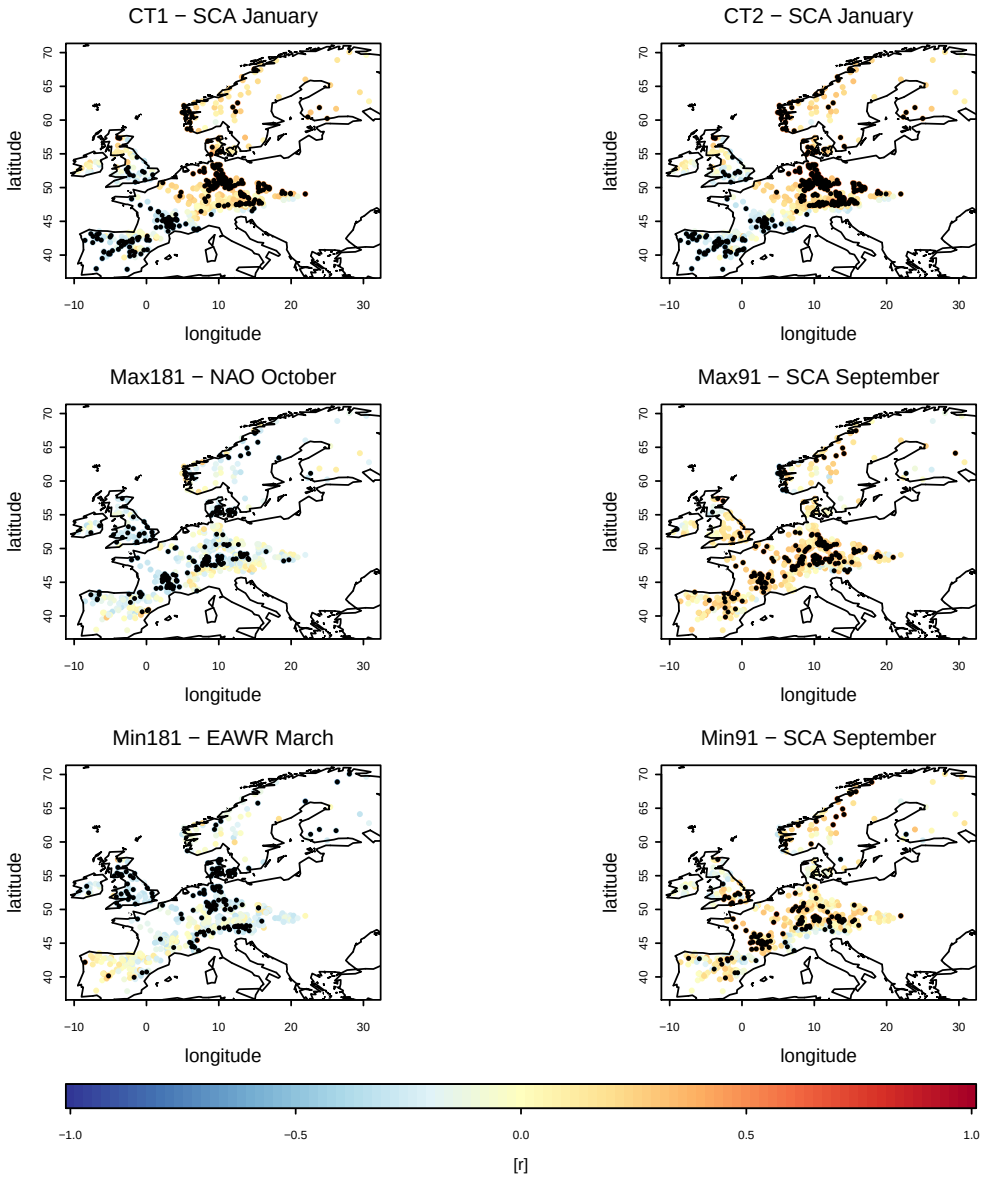

Figure 4.11.: Correlations between each timing measure and its most influencing teleconnection pattern. Black dots mark the stations with locally significant correlations (p-value < 0.05).

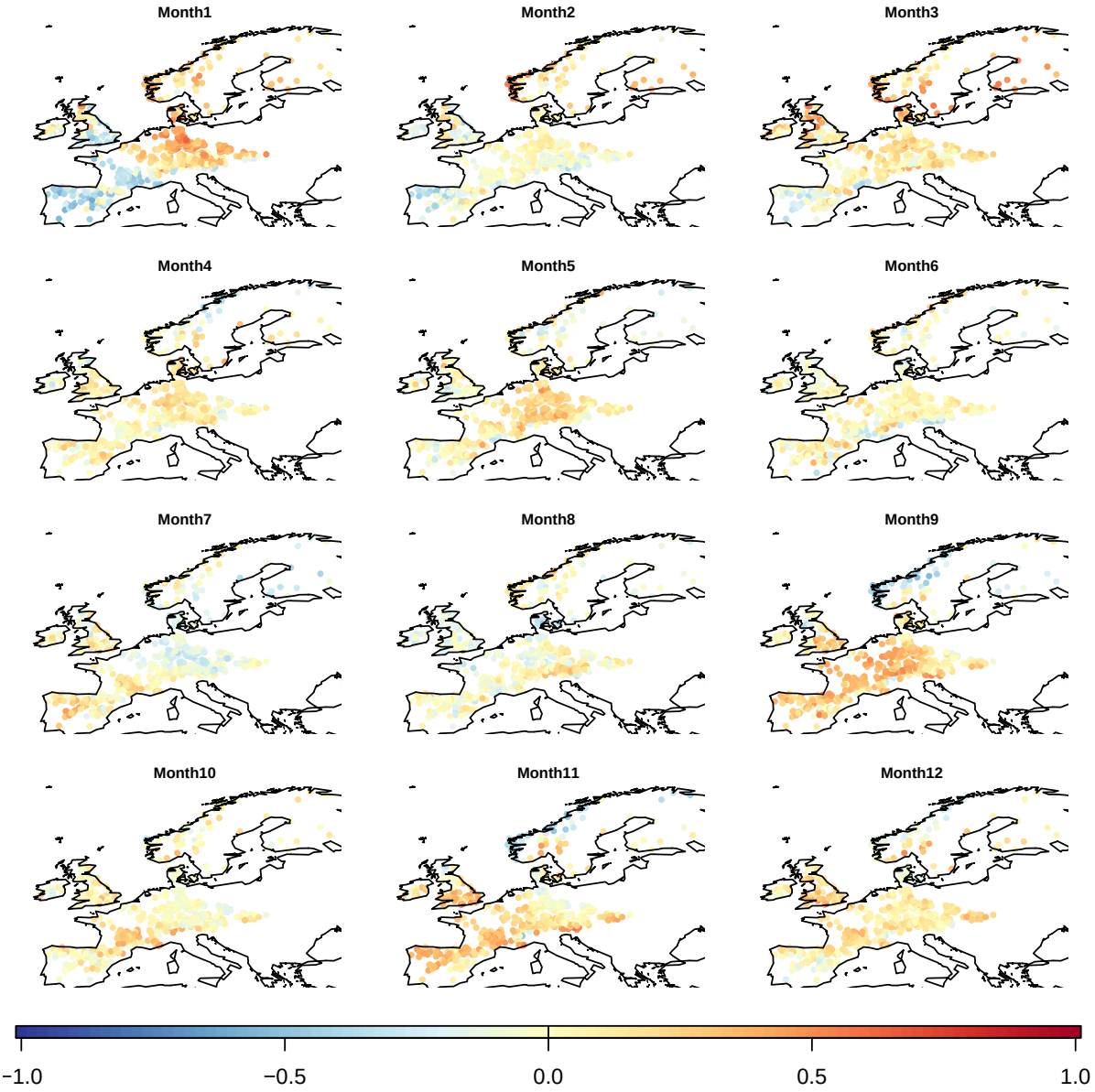

Figure 4.12.: Monthly correlations CT1 - Scandinavian Pattern

5. Discussion

5.1. Definition of the timing measures

Six different measures of the timing of the annual cycle of streamflow were considered in this thesis. No distinction was made between different seasons. The results therefore cannot be interpreted in detail regarding different factors and processes that influence streamflow, because it is known from recent studies that the influence of these factors and processes is not the same in different seasons and in different regions (e.g. Stahl et al., 2010). However, the definition of the maximum and the minimum of the annual streamflow allows a somewhat more detailed interpretation about the category of possible influencing factors and processes. This is further discussed in the next sections.

As shown in the results, the correlation coefficients between the timing measures are rather small. This shows that the different timing measures probably do not represent an identical influence of the processes on streamflow seasonality. The largest correlation coefficient is that between the CT1 and the CT2 (r=0.91). The results of the trend test and the correlation analysis with northern teleconnection patterns are similar for these two timing measures. To reduce data amount and calculation time, one could probably exclude one of these two timing measures from further investigations without losing too much information. The Max91 and the Max181, and the Min91 and Min181 have the second largest correlation coefficients (r=0.5). This shows that the choice of the moving average window width has an influence on the results. However, the two Max and the two Min timing measures are more strongly correlated to each other than to the other timing measures. This suggests that the definition of the Max91 and the Max181, and the Min91 and the Min181 is not completely arbitrary.

5.2. Local controls on streamflow seasonality

As mentioned in the section above, the presented results cannot be interpreted in detail regarding different factors and processes that influence streamflow seasonality. One can, however, make some inferences from the climatology of the timing measures about possible processes and factors influencing them. Temperature plays a role by influencing the form of precipitation, storage of water as snow and ice, and evapotranspiration. The Max91 and Max181, are probably influenced by storage of precipitation as snow, and snowmelt processes in high-elevated catchments of the Pyrenees, the Alps, the Carpathian Mountains, and catchments in most parts of Scandinavia. In these regions, temperature may play a role in the seasonality of the annual streamflow. In the other

parts of Europe the Max91 and Max181 occur during winter time. This is probably due to winter storms, which cause precipitation in the form of rain. The Min91 and Min181 show a similar spatial pattern like the Max91 and the Max181. In catchments in the mountainous regions in Europe and in catchments in most parts of Scandinavia the Min91 and the Min181 occur during winter months. This is probably due to storage of precipitation as snow and ice. In the other parts of Europe the Min91 and the Min181 occur in summer months, which could be due to high evapotranspiration and periods with little precipitation. For the CT1 and the CT2 it is even more difficult to assess different influencing processes. Both timing measures occur more or less in the middle of the year. The somewhat later occurrence in catchments of the Alps and most parts of Scandinavia could again be an effect of snowmelt processes.

5.3. Trends in streamflow seasonality

The Sen slope and the Mann-Kendall test were applied in order to investigate shifts in streamflow seasonality. As shown in the results, no trends were detected that are field significant at the global 5% significance level. According to Wilks (2011), it is important to keep in mind that the Mann-Kendall test does not prove that no changes are occurring. One can only conclude that any changes in the timing measures would be occurring too slowly over the analysed time period to be discerned from the year-to-year background variability in the data. In addition, trend results are not only dependent on the length of the time series, but also on the period of time that is analysed. This is illustrated in fig.5. in the study by Hannaford et al. (2013).

In the following section, the trend results are discussed in consideration with results from some recent studies. One hypothesis of the present thesis was that the timing of snowmelt streamflow shifted towards earlier in the season in high elevated catchments of the mountainous regions in Europe and catchments in Scandinavia. The results show, however, that none of the timing measures exhibit a detectable trend. A possible explanation could be that the annual hydrograph of the high-elevated catchments is smoothed to a greater degree with higher streamflow during winter time and a less pronounced peak in spring or summer season. At the same time, the date of the maximum (and the CT) could remain more or less the same. This is illustrated in figure 5.1. The smoothed hydrograph is represented by the red curve. This explanation would also be consistent, for example, with results from the CH2014 Impact Report, which in general found higher winter streamflow and lower summer streamflow amounts for most of the catchments in Switzerland. The explanation does not contradict the study of Stahl et al. (2010), which found positive trends in winter streamflow amount and negative trends in summer streamflow amounts (April - August) for large parts of Europe.

Longer droughts in summer season may start already earlier in the year and last longer in late summer. This does not lead to a change in the timing of the annual minimum flow. These results are consistent with Stahl et al. (e.g. 2008, 2010), who found trends towards earlier summer low flows in large parts across Europe. Figure 5.2 illustrates

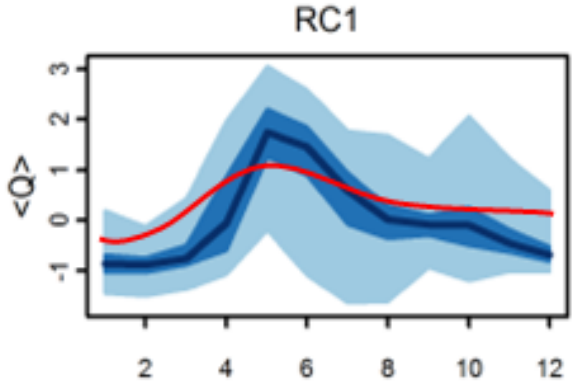

Figure 5.1.: Possible change of the RC1: smoothed annual cycle (red curve), without changes in the timing of the maximum annual streamflow.

this.

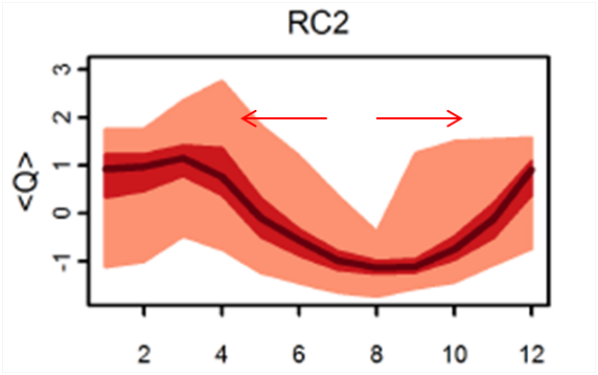

Figure 5.2.: Possible change of the RC2: longer drought periods in summer time, without changes in the timing of the minimum annual streamflow.

Burn (2008) investigated changes for different timing measures of streamflow in Canada. One was the 50-percentile date, which is similar to the definition of the CT1 timing measure. Similar to the results of the present thesis, he could not find trends in this measure that are field significant.

Barnett et al. (2008) found that the center timing in western United States is influenced by (human-induced) temperature changes. Center timing across Europe may not be exclusively influenced by temperature, but possibly by other processes like precipitation.

As mentioned above, trend detection may be dependent on the length of the analysed time period. Maurer et al. (2007) investigated CT timing shift in four (large) drainage basins in the western part of the USA over the time period 1950 - 1999. They found that trends are currently too small to be statistically significantly different from natural

climate variability. They state that it is not possible to detect significant trends in the CT on the basis of the short historical record which they analysed. In general, they state that trends over longer timescales can be more easily detected because the amplitude of noise can decline more rapidly than the magnitude of the trend signal. The length of the time period analysed in this thesis is even shorter than that which was analysed by Maurer et al. (2007). This could make the detection of trends difficult.
Stewart et al. (2005) investigated changes in CT2 dates in western USA for snow-dominated catchments over the time period 1948 - 2002. In general, they found that the CT shifted towards earlier in the season. They state that increasing temperatures advance the timing of snowmelt, while increased winter precipitation falling as snow results in an increased snowpack and generally delays the spring runoff. Such counteracting influences make the detection of trends for all the timing measures more difficult.

5.4. Large-scale controls on seasonal streamflow

A correlation analysis was conducted in order to assess the influence of northern teleconnection patterns on streamflow seasonality. The results show that the Scandinavian Pattern is the one with the largest influence. The pattern with the second largest influence is the North Atlantic Oscillation. As shown in the results, the correlations between the timing measures and the northern teleconnection patterns are field significant at the 5% significance level. In the following part, the results for each timing measure with its most influencing pattern is discussed. In addition, the correlations between the timing measures and the teleconnection patterns are compared to the correlations between the teleconnection patterns and precipitation and temperature. The monthly values of the teleconnection patterns are correlated to precipitation and temperature in the same months. Note that it is therefore only possible to assess the influence on the timing measures of precipitation and temperature conditions in these specific months. The latter correlations were calculated on the Climate Explorer webpage. The maps show the correlations which are locally significant at the 10% significance level (p-value < 0.1). All presented maps are field significant.

As presented in the results, the most influencing northern teleconnection pattern on the CT1 and the CT2 is the Scandinavian Pattern in January. Figure 5.3 shows the correlations between the Scandinavian Pattern in January and precipitation (upper left map), and temperature (upper right map) in January. The two lower maps show the results for the correlations between the Scandinavian Pattern in January and the CT1 (lower left map) and the CT2 (lower right map). The spatial pattern for the CT1 and the CT2 looks similar. The correlations are negative for the stations in Spain, south-western parts of France, some stations of the alpine region, and most of the stations in the southern part of the UK. For the remaining stations, the correlation coefficients are mostly positive. One can assume that in the regions with negative correlation coefficients the CT1 and CT2 occur earlier in the year when the Scandinavian Pattern in January is positive. From the figure, one can see that the positive Scandinavian Pattern in January

leads to wetter conditions over Spain, the southern part of France and the alpine region. It leads to drier conditions across central Europe, northern Europe and Scandinavia. The correlation pattern between the Scandinavian Pattern and precipitation looks quite similar to that between the Scandinavian Pattern and the CT1 and CT2. From these relationships, one can conclude that the two timing measures occur generally later in the year under drier weather conditions in January. Due to the fact that the CT is influenced by the Scandinavian Pattern in January, this result can even possess predictive power.

The Max91 is most strongly influenced by the Scandinavian Pattern in September. The figure 5.4 shows the correlation between the Scandinavian Pattern in September and precipitation (upper left map), and temperature (upper right map) in September. The correlation coefficients between the Max91 and the Scandinavian Pattern in September are positive for most of the stations (lower map). One can conclude that the Max91 occurs later in the year, when the Scandinavian Pattern in September is positive. The correlation between the Scandinavian Pattern and precipitation and temperature in September, however, exhibits different signs for different parts in Europe. Therefore, no direct link between the occurrence date of the Max91 and precipitation or temperature conditions in September can be made.

The Max181 is most strongly influenced by the North Atlantic Oscillation index in October. The figure 5.5 shows the correlation of the North Atlantic Oscillation index in October and precipitation (upper left map), and temperature (upper right map) in October. The correlation coefficients between the Max181 and the North Atlantic Oscillation index in October are negative for most of the stations with significant correlations (lower map). One can conclude that the Max181 occurs earlier in the year, when the North Atlantic Oscillation index in October is positive. The positive phase of the North Atlantic Oscillation index leads to drier conditions in October in large parts of Europe. This could mean that the Max181 occurs earlier in the year under drier conditions in October. From the comparison of the upper right map and the lower map, one could conclude that the temperature in October does not have a strong influence on the Max181.

The Min91 is most strongly influenced by the Scandinavian Pattern in September. Figure 5.6 again shows the correlation of the Scandinavian Pattern in September, precipitation (upper left map), and temperature (upper right map) in September. The correlation between the Min91 and the Scandinavian Pattern is positive for most of the stations with significant correlations. One can conclude that in these regions, the Min91 occurs later in the year when the Scandinavian Pattern in September is positive. Some stations with negative correlation coefficients are found in the alpine region. There, the Min91 seems to occur earlier when the Scandinavian Pattern is positive. The spatial pattern for the correlations between the Scandinavian Pattern, precipitation and temperature does not resemble that of the correlation between the Min91 and the Scandinavian Pattern. Therefore, one can conclude that precipitation and temperature in September do not have a major influence on the timing of the Min91.

The Min181 is most strongly influenced by the East Atlantic/Western Russia index in March. The figure 5.7 shows the correlation of the East Atlantic/Western Russia index in March, precipitation (upper left map), and temperature (upper right map)

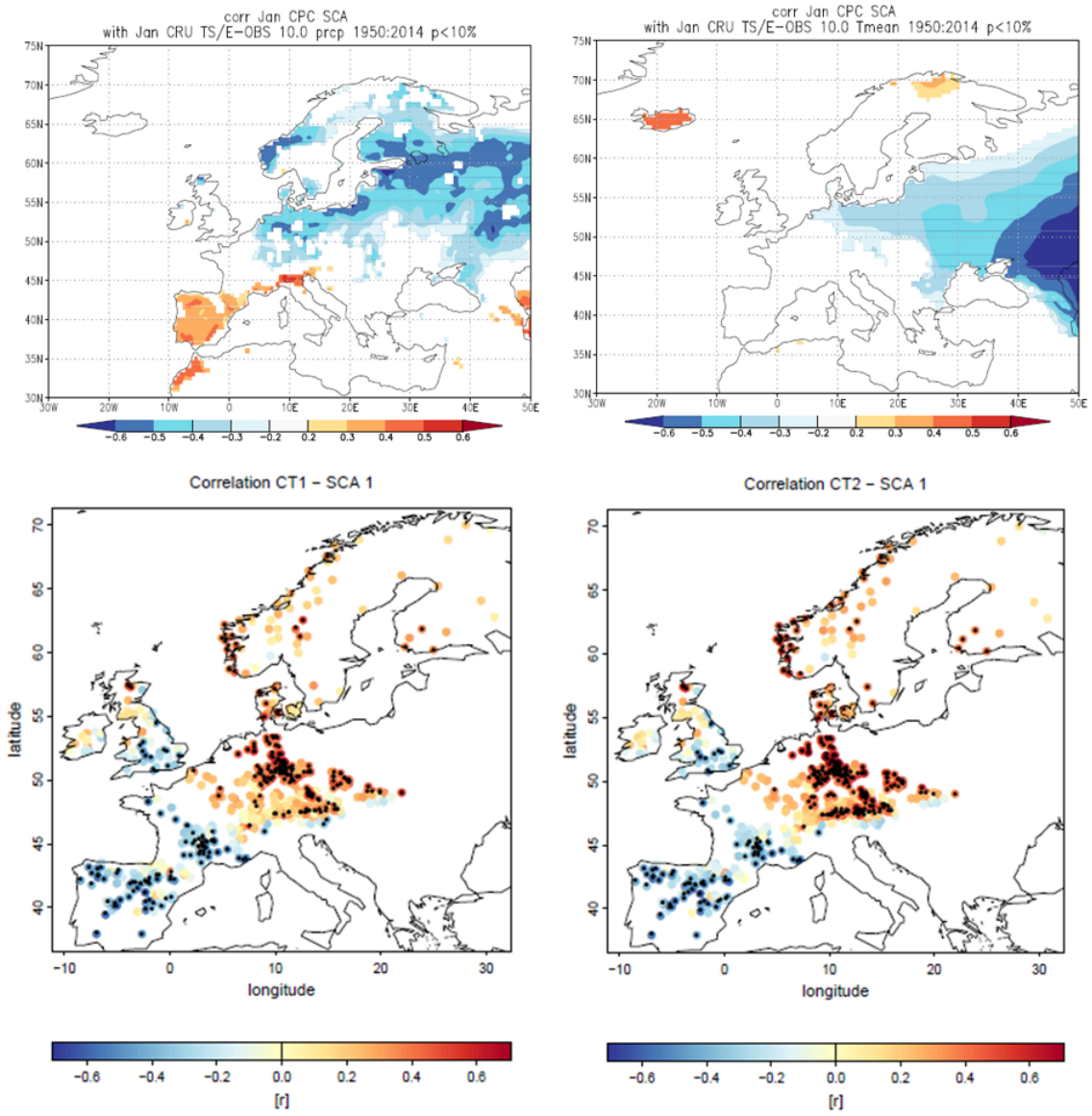

Figure 5.3.: Scandinavian Pattern in January and its correlation with precipitation (upper left map), temperature (upper right map), and the CT1 (lower left map), and the CT2 (lower right map). The upper maps present correlations with locally significant correlation coefficients ($p<0.1$). Black dots mark the stations with locally significant correlation coefficients ($p<0.05$).

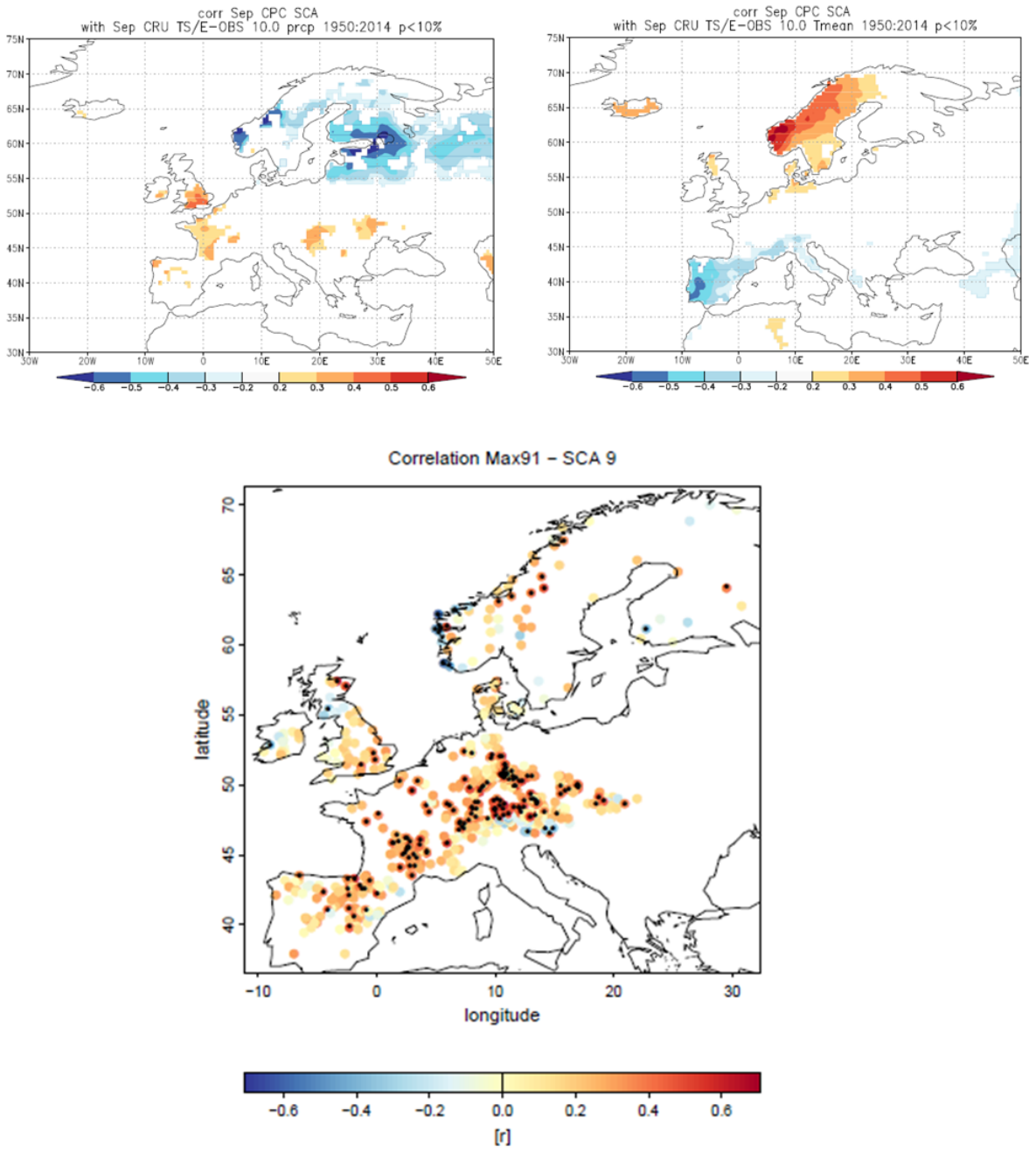

Figure 5.4.: Scandinavian Pattern in September and its correlation with precipitation (upper left map), temperature (upper right map), and the Max91 (lower map). The upper maps present correlations with locally significant correlation coefficients ($p<0.1$). Black dots mark the stations with locally significant correlation coefficients ($p<0.05$).

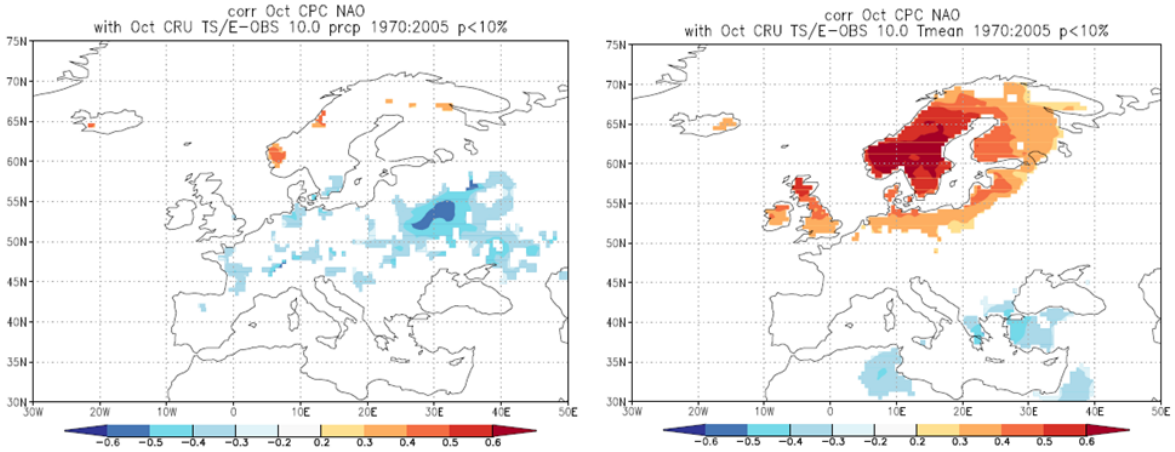

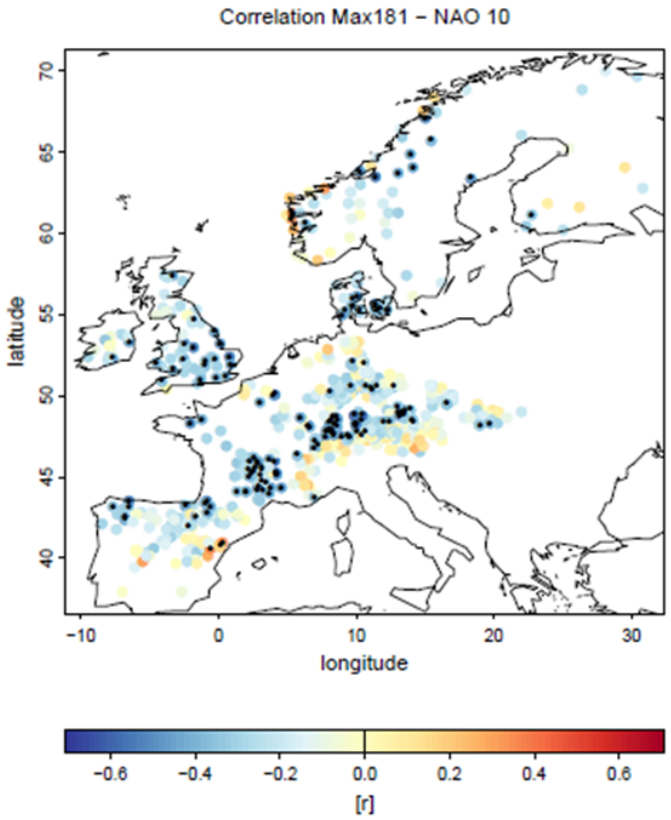

Figure 5.5.: North Atlantic Oscillation index in October and its correlation with precipitation (upper left map), temperature (upper right map), and the Max181 (lower map). The upper maps present correlations with locally significant correlation coefficients ($p<0.1$). Black dots mark the stations with locally significant correlation coefficients ($p<0.05$).

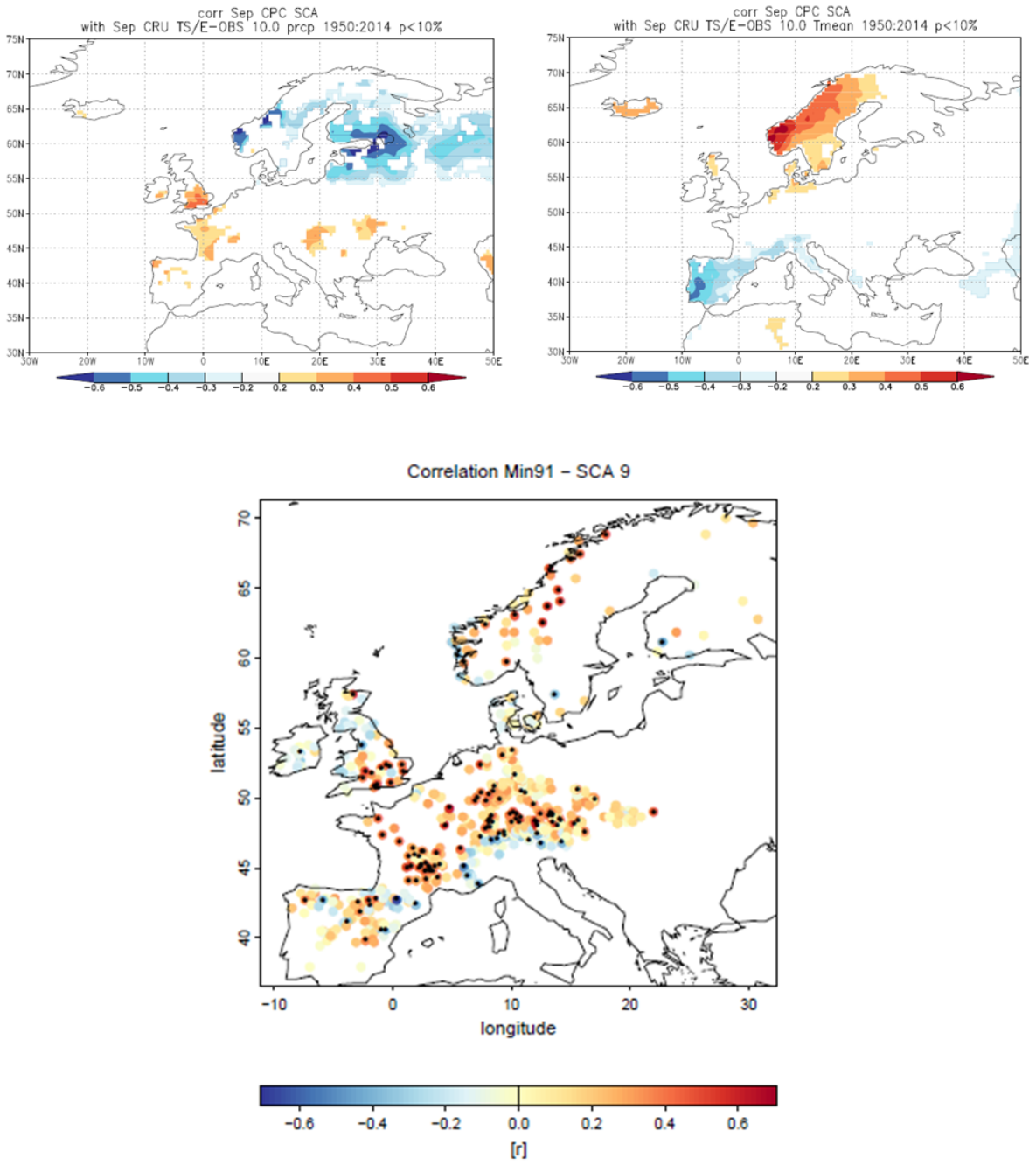

Figure 5.6.: Scandinavian Pattern in September and its correlation with precipitation (upper left map), temperature (upper right map), and the Min91 (lower map). The upper maps present correlations with locally significant correlation coefficients ($p<0.1$). Black dots mark the stations with locally significant correlation coefficients ($p<0.05$).

in March. However, there is almost no correlation between the East Atlantic/Western Russia index and precipitation. The lower map shows the correlation between the East Atlantic/Western Russia index and the Min181. The correlation coefficients for almost all stations with significant correlations are negative. One can therefore conclude that the Min181 occurs earlier in the year, when the East Atlantic/Western Russia index in March is positive. From comparing the upper right map with the lower map, one can conclude that temperature in March may influence the Min181. This is consistent with other studies which show that warmer temperatures lead to a shift in minimum streamflow towards earlier dates.

In general, one can conclude from these results that the timing measures are quite strongly influenced by northern teleconnection patterns. These relationships between the timing measures and the teleconnection patterns can be used to make predictions for the timing of the annual cycle of streamflow. The CT1 and CT2 seem to be stronger influenced by precipitation than by temperature in January. The result for the Min181 suggests that temperatures in March have an influence on streamflow timing over large parts of Europe. Even tough the Max91, the Max181 and the Min91 are most strongly correlated to teleconnection patterns in September and October, the precipitation and temperature conditions in these months do not seem to have a major influence on the timing measures.

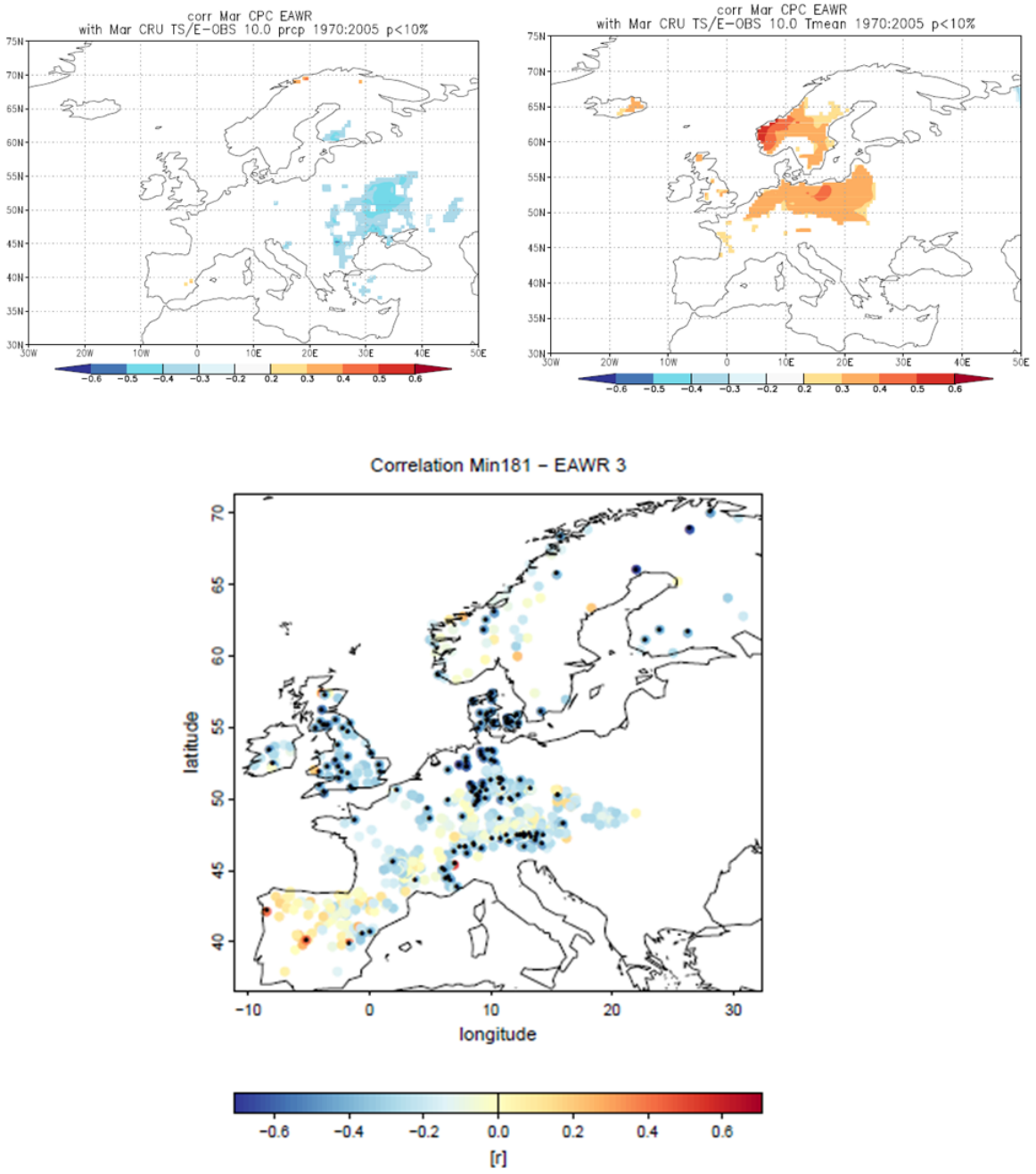

Figure 5.7.: East Atlantic/Western Russia index in March and its correlation with precipitation (upper left map), temperature (upper right map), and the Min181 (lower map). The upper maps present correlations with locally significant correlation coefficients ($p<0.1$). Black dots mark the stations with locally significant correlation coefficients ($p<0.05$).

6. Conclusions

With many hydrological studies addressing trends in the amount of streamflow or investigating seasonality of streamflow on local scales, there is not much information available about trends in the timing of the annual cycle of streamflow on a continental scale across Europe. The aim of this study was therefore to provide information that helps to close this gap. For this purpose, a European data set of streamflow from small catchments was analysed. Updated data sets will lead to an improvement of station density and data coverage, and will hence be an advantage for future studies. In spite of the fact that in the present thesis there were gaps in the spatial coverage of the data set, the study illustrates spatial patterns in streamflow seasonality and some of its influencing factors. In particular, it was found that the timing of the annual cycle of streamflow does not seem to exhibit significant trends over the time period 1970-2005. It is, however, influenced by northern teleconnection patterns. It was discovered that the patterns with the largest influence are the Scandinavian Pattern and the North Atlantic Oscillation. The knowledge of these relationships can improve our understanding of the timing of the annual cycle of streamflow. Some results of the present thesis lead to new research questions which could be addressed in future studies. Generally, one could consider to pursue another approach to extract the annual cycle. There are several possibilities: one example, used by Renner and Bernhofer (2011), would be to use Fourier form models based on harmonic functions. In terms of the trend analysis, one could consider to investigate trends over different time periods and different lengths of the time series. Another idea is first to subtract the influence of the teleconnection patterns on the timing measures, and then to conduct the trend assessment. When investigating large scale influences on the seasonality of streamflow, one could take into account additional indices describing atmospheric circulation. Two indices which are known to influence streamflow amounts across Europe, are the frequency of west circulation as described by the subjective Grosswetterlagen classification, and the north to south sea level pressure difference across the European continent (e.g. Bouwer et al., 2008). In addition to the correlation coefficients, one could also fit a linear regression model between atmospheric indices and the timing measures. This would enable the assessment of the ratio of the unit change in the timing measure (TM) per unit change of the index ($\triangle TM/\triangle index$). Yet another idea is to model the relationship between two (or more) teleconnection patterns with a linear regression model (e.g. $ScandinavianPattern = \alpha * NorthAtlanticOscillation + \beta$) and then correlate the residuals to the timing measures. This way, similar effects of the two (or more) teleconnection patterns on the timing measures would not be assessed more than once, which would reduce the amount of data. Further investigations should be conducted in order to assess the way the teleconnection patterns influence the timing of streamflow. For example, one could consider to correlate seasonal averages of the

teleconnection patterns to seasonal averages of precipitation and temperature.

Acknowledgements

I would like to thank Prof. Sonia Seneviratne for giving me the opportunity to write this master thesis within the Land-Climate Dynamics group at the ETH Zurich. I am very grateful to Prof. Stefan Brönnimann from the GIUB and the Oeschger Centre for Climate Change Research in Bern for supervising this thesis. I owe a special thanks to Lukas Gudmundsson for his dedicated support; I greatly benefited from his advice and scientific expertise. Furthermore, I want to thank Peter Schneider for reviewing this thesis and helping to improve it. Finally, I would like to thank my family for supporting me throughout my studies, and I owe special thanks to Jan for everything.

Bibliography

Barnett, T., D. Pierce, H. Hidalgo, C. Bonfils, B. Santer, T. Das, G. Bala, A. Wood, T. Nozawa, A. Mirin, D. Cayan, and M. Dettinger
2008. Human-Induced Changes in the Hydrology of the Western United States. *Science*, 319:1080–1082.

Barnston, A. and R. Livezey
1987. Classification, seasonality and persistence of low-frequency atmospheric circulation patterns. *Monthly Weather Review*, 115:1083–1126.

Bayliss, A. and C. Richard
1993. *Peaks-over-thereshold flood database: Summary statistics and seasonality.* Institute of Hydrology, Oxfordshire UK.

Birsan, M., L. Zaharia, V. Chendes, and E. Branescu
2012. Recent trends in streamflows in Romania (1976-2005). *Romanian Reports in Physics*, 64:275–280.

Blackburn, M. and B. Hoskins
2002. Atmospheric variability and extreme autumn rainfall in the UK. *EGS General Assembly Conference Abstracts*, 27:2512. Provided by the SAO/NASA Astrophysics Data System.

Bosshard, T., S. Kotlarski, T. Ewen, and C. Schär
2011. Spectral representation of the annual cycle in the climate change signal. *Hydrology and Earth System Sciences*, 15:2777–2788.

Bouwer, L., L. Vermaat, and J. Aerts
2006. Winter atmoshperic circulation and river discharge in northwest Europe. *Geophysical Research Letters*, 33:L06403.

Bouwer, L., L. Vermaat, and J. Aerts
2008. Regional sensitivities of mean and peak river discharge to climate variability in Europe. *Journal of Geophysical Research*, 113:D19103.

Bueh, C. and H. Nakamura
2007. Scandinavian pattern and its climatic impact. *Quarterly Journal of the Royal Meteorological Society*, 133:2117–2131.

Burn, D.
2008. Climatic influences on streamflow timing in the headwaters of the Mackenzie River Basin. *Journal of Hydrology*, 352:225–238.

Burn, D., J. Cunderlik, and A. Pietroniro
2004. Hydrological trends and variability in the Liard river basin. *Hydrological Science Journal*, 49:53–67.

CH2014-Impacts
2014. *Toward Quantitative Scenario of Climate Change Impacts in Switzerland*. Bern, Switzerland: OCCR, FOEN, MeteoSwiss, C2SM, Agroscope, and ProClim.

Coopersmith, E., M. Yaeger, S. Ye, L. Cheng, and M. Sivapalan
2012. Exploring the physical controls of regional patterns of flow duration curves - part 3: A catchment classification system based on regime curve indicators. *Hydrology and Earth System Sciences*, 16:4467–4482.

Cunderlik, J. and D. Burn
2001. The use of flood regime information in regional flood frequency analysis. *Hydrological Sciences Journal*, 47:77–92.

Cunderlik, J. and T. Ouarda
2009. Trends in the timing and magnitude of floods in Canada. *Journal of Hydrology*, 375:471–480.

Douglas, E., R. Vogel, and C. Kroll
2000. Trends in floods and low flows in the United States: impact of spatial correlation. *Journal of Hydrology*, 240:90–105.

Fiala, T.
2008. Statistical characteristics and trends of mean annual and monthly discharges of Czech river in the period 1961 - 2005. *J.Hydrol. Hydromech.*, 2:133–140.

Freeze, R.
1974. Streamflow generation. *Reviews of Geophysics and Space Physics*, 12(4):627–647.

Greatbatch, R.
2000. The North Atlantic Oscillation. *Stochastic Environmental Research and Risk Assessment Entretiens Jacques-Cartier, Montreal*, Pp. 1–50.

Gudmundsson, L., L. Tallaksen, K. Stahl, and A. Fleig
2011. Low-frequency variability of European runoff. *Hydrologic Earth System Science*, 15:2853–2869.

Hannaford, J., G. Buys, K. Stahl, and L. Tallaksen
2013. The influence of decadal-scale variability on trends in long European streamflow records. *Hydrol. Earth Syst. Sci.*, 17:2717–2733.

Haylock, M., N. Hofstre, A. Klein Tank, E. Klok, P. Jones, and M. New
2008. A European daily high-resolution gridded data set of surface temperature and precipitation for 1950-2006. *Journal of Geophysical Research*, 113:D20119.

Hidalgo, H., M. Das, T.and Dettinger, D. Cayan, D. Pierce, T. Barnett, G. Bala, A. Mirin, A. Wood, C. Bonfils, B. Santer, and T. Nozawa
2009. Detection and attribution of streamflow timing changes to climate change in the Western United States. *Journal of Climate*, 22:3838–3855.

Hurrell, J. and H. van Loon
1997. Decadal variations in climate associated with the North Atlantic Oscillation. *Climatic Change*, 36:301–326.

Kendall, M.
1975. *Rank Correlation Measures.* Charles Griffin, London.

Köplin, N., B. Schädler, D. Viviroli, and R. Weingartner
2014. Seasonality and magnitude of floods in Switzerland under future climate change. *Hydrological Processes*, 28:2567–2578.

Lettenmaier, D., E. Wood, and J. Wallis
1994. Hydro-climatological trends in the continental United States, 1948-88. *Journal of Climate*, 7:586–607.

Livezey, R. and W. Chen
1982. Statistical field significance and its determination by Monte Carlo techniques. *Monthly Weather Review*, 111:46–59.

Lopez Moreno, J. and S. Vicente Serrano
2008. Positive and negative phases of the wintertime North Atlantic Oscillation and drought occurrence over Europe: A multitemporal-scale approach. *Journal of Climate*, 21:1220–1243.

Mann, H.
1945. Nonparametric tests against trend. *Econometrica*, 13:245–259.

Maurer, E., I. Stewart, C. Bonfils, P. Duffy, and D. Cayan
2007. Detection, attribution, and sensitivity of trends toward earlier streamflow in the Sierra Nevada. *Journal of geophysical research*, 112:D111118.

Moore, J., J. Harper, and M. Greenwood
2007. Significance of trends toward earlier snowmelt runoff, Columbia and Missouri Basin headwaters, western United States. *Geophysical research letters*, 34:L16402.

Myneni, R., C. Keeling, C. Tucker, G. Asrar, and R. Nemani
1997. Increased plant growth in the northern high latitudes from 1981 to 1991. *Letters to Nature*, 386:698–702.

NOAA and National Weather Service
2012. Northern hemisphere teleconnection patterns. http://www.cpc.ncep.noaa.gov/data/teledoc/telecontents.shtml.

Parajka, J., S. Kohnová, G. Bálint, M. Barbuc, M. Borga, P. Claps, S. Cheval, A. Dumitrescu, E. Gaume, K. Hlavcová, R. Merz, M. Pfaundler, G. Stancalie, J. Szolgay, and G. Blöschl
2010. Seasonal characteristics of flood regimes across the Alpine-Carpathian range. *Journal of Hydrology*, 394:78–89.

Poff, N., J. Allan, M. Bain, J. Karr, K. Prestegaard, B. Richter, R. Sparks, and J. Stromberg
1997. The natural flow regime - a paradigm for river conservation and restoration. *BioScience*, 47(11):769–784.

Ramirez, J. and B. Finnerty
1996. CO2 and temperature effects on evapotranspiration and irrigated agriculture. *Journal of Irrigation and Drainage Engineering*, 122(3).

Rauscher, S., J. Pal, N. Diffenbaugh, and M. Benedetti
2008. Future changes in snowmelt-driven runoff timing over the western US. *Geophysical Research Letters*, 35:L16703.

Regonda, S., B. Rajagopalan, M. Clark, and J. Pitlick
2005. Seasonal cycle shifts in hydroclimatology over the Western United States. *Journal of Climate*, 18:272–383.

Renner, M. and C. Bernhofer
2011. Long term variability of the annual hydrological regime and sensitivity to temperature phase shifts in Saxony/Germany. *Hydrology and Earth System Sciences*, 15:1819–1833.

Schleip, C., T. Rutishauser, J. Luterbacher, and A. Menzel
2008. Time series modeling and central European temperature impact assessment of phenological records over the last 250 years. *Journal of Geophysical Research*, 113:G04026.

Sen, P.
1968. Estimates of the regression coefficient based on Kendalls's Tau. *Journal of the American Statistical Association*, 63:1379–1389.

SGHL and CHy
2011. *Auswirkungen der Klimaänderung auf die Wasserkraftnutzung - Synthesebericht. Beiträge zur Hydrologie der Schweiz*, volume Nr. 38. Schweizerische Gesellschaft für Hydrologie und Limnologie (SGHL) und Hydrologische Kommission (CHy)(Hrsg.), Bern.

Sparks, T. and A. Menzel
2002. Observed changes in seasons: An overview. *International Journal of Climatology*, 22:1715–1725.

Stahl, K., H. Hisdal, J. Hannaford, L. Tallaksen, H. van Lanen, E. Sauquet, S. Demuth, M. Fendekova, and J. Jódar
2010. Streamflow trends in Europe: evidence from a dataset of near-natural catchments. *Hydrology and Earth System Sciences*, 14:2367–2382.

Stahl, K., H. Hisdal, L. van Lanen, J. Hannaford, and E. Sauquet
2008. Trends in low flows and streamflow droughts across Europe. UNESCO Report.

Stahl, K., L. Tallaksen, J. Hannaford, and H. van Lanen
2012. Filling the white space on maps of European runoff trends: estimates from a multi-model ensemble. *Hydrology and Earth System Sciences*, 16:2035–2047.

Stewart, I., D. Cayan, and M. Dettinger
2005. Changes toward earlier streamflow timing across Western North America. *Journal of Climate*, 18:1136–1155.

Stine, A., P. Huybers, and I. Fung
2009. Changes in the phase of the annual cycle of surface temperature. *Nature*, 457:435–440.

Stocker, T., G. Plattner, M. Tignor, S. Allen, J. Boschung, A. Nauels, Y. Xia, V. Bex, and P. Midgley
2013. Climate change 2013 - the phsical science basis, working group 1 contribution to the fifth assessment report of the Intergovernmental Panel on Climate Change. summary for policymakers.

Studer, S., C. Appenzeller, and C. Defila
2005. Inter-annual variability and decadal trends in alpine spring phenology: A multivariate analysis approach. *Climatic Change*, 73:395–414.

Trigo, R., D. Pozo Vazquez, T. Osborn, Y. Castro Diez, S. Gamiz Fortis, and M. Esteban Parra
2004. North Atlantic Oscillation influence on precipitation, river flow and water resources in the Iberian Peninsula. *International Journal of Climatology*, 24:925–944.

Volken, D.
2012. *Auswirkungen der Klimaänderung auf Wasserressourcen und Gewässer. Synthesebericht zum Projekt «Klimaänderung und Hydrologie in der Schweiz» (CCHydro)*, volume 1217. Bundesamt für Umwelt (BAFU), Bern.

Wilks, D.
2011. *Statistical methods in the atmospheric sciences*, 3 edition. Elsevier Inc., USA.

WMO Regional Climate Centre and KNMI
2014. Knmi climate explorer. http://climexp.knmi.nl.

A. Appendix

A.1. Monthly correlations between the timing measures and teleconnection patterns

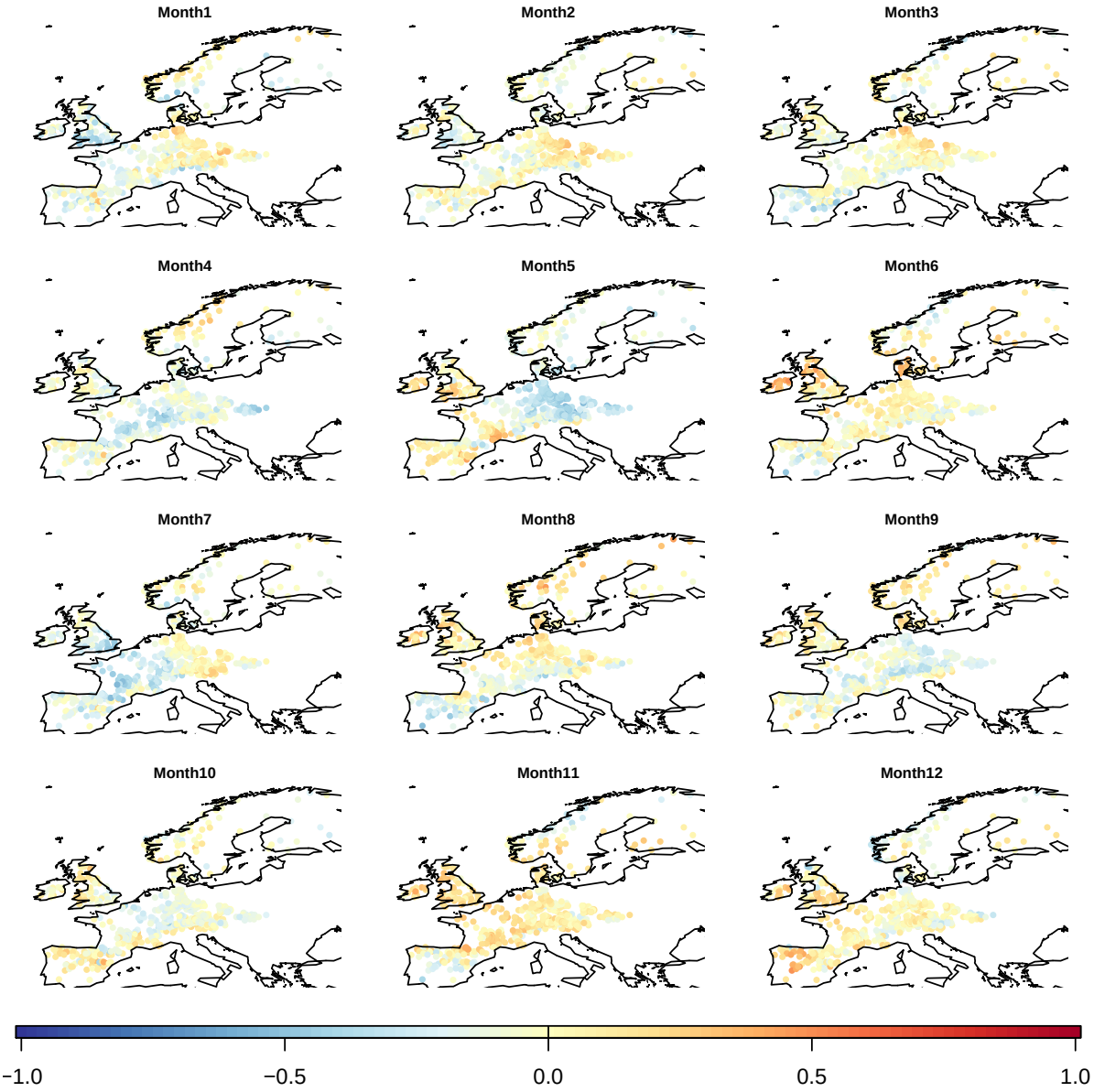

Figure A.1.: Monthly correlations CT1 - East Atlantic

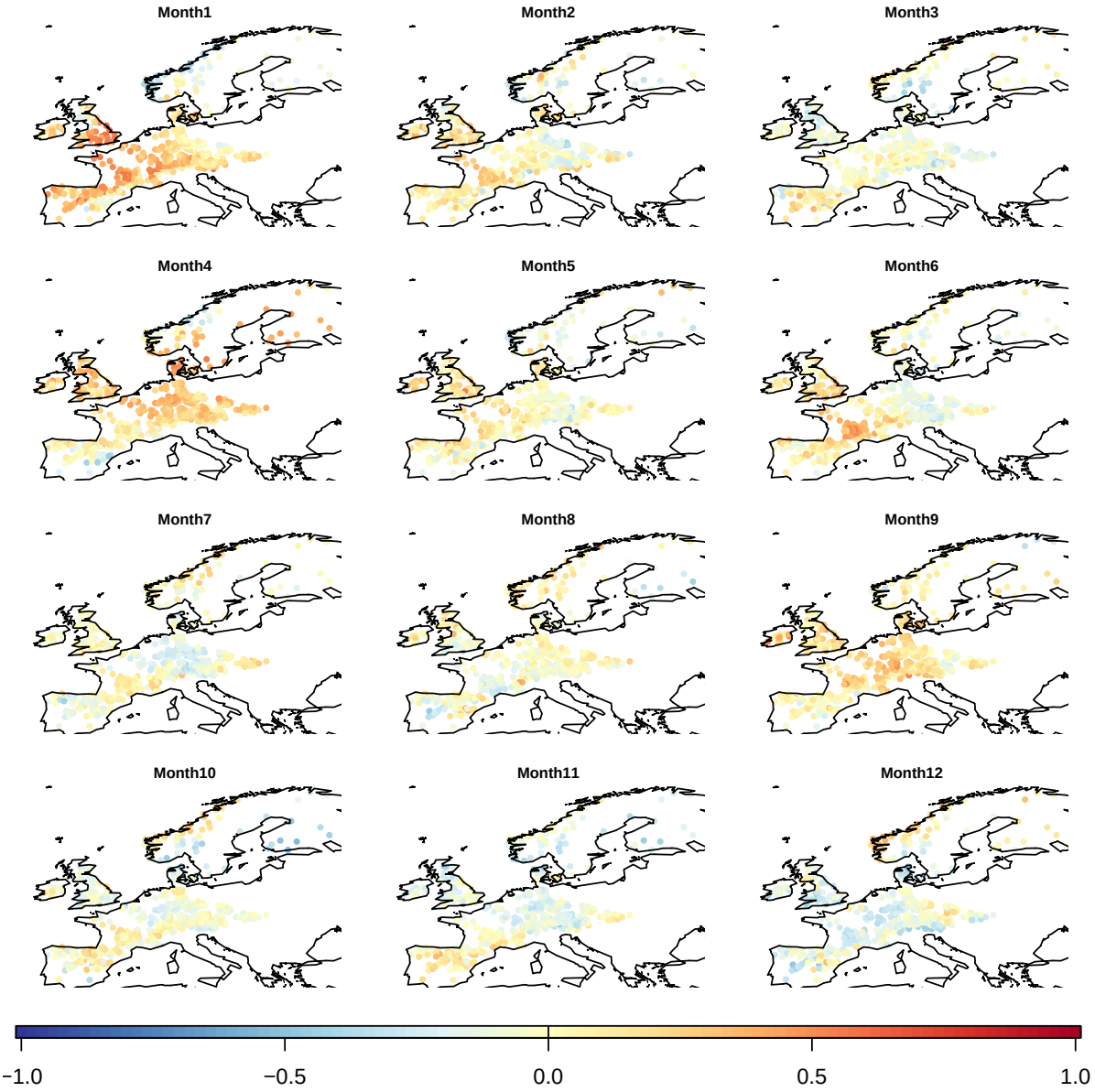

Figure A.2.: Monthly correlations CT1 - East Atlantic/Western Russia

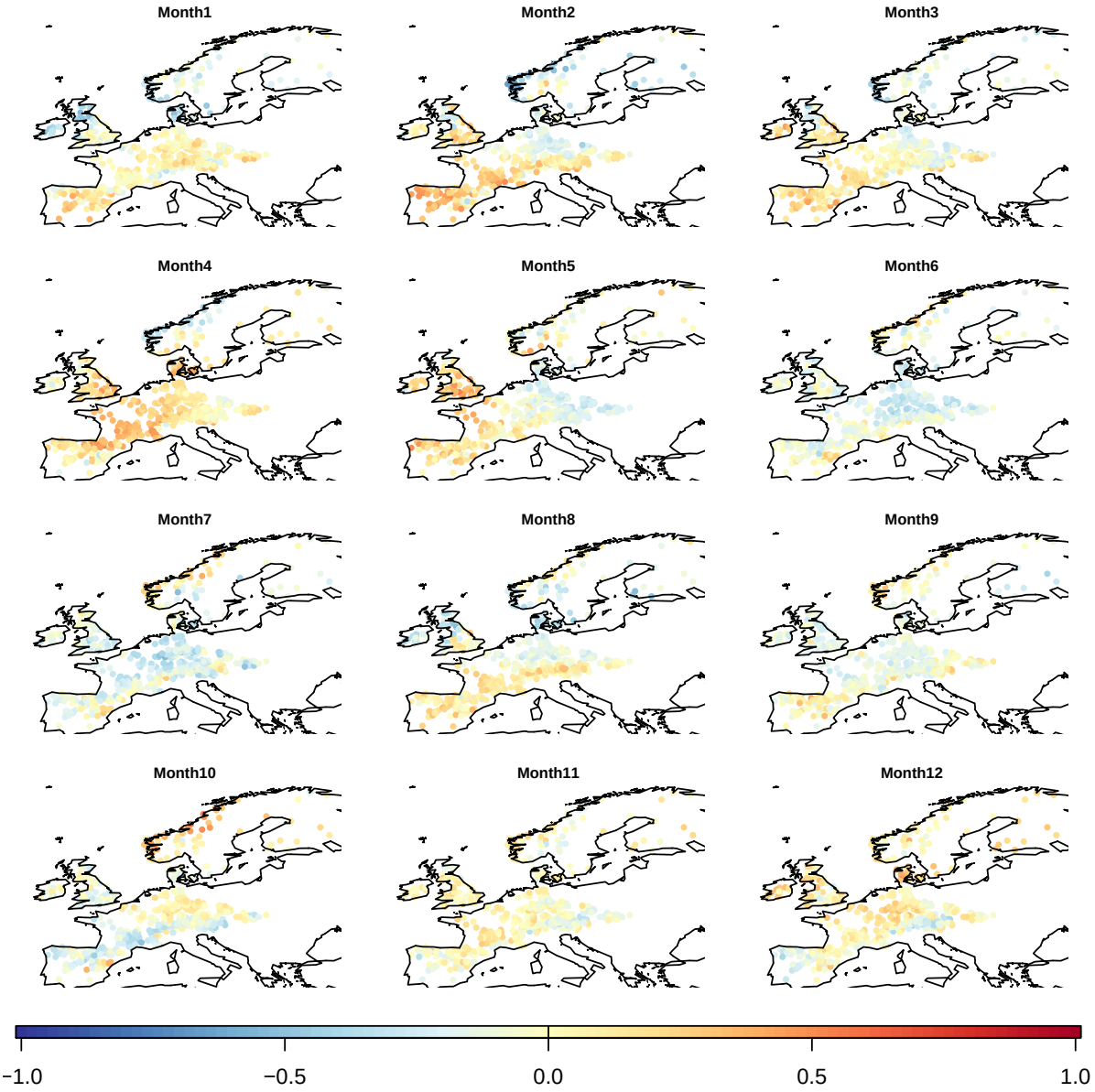

Figure A.3.: Monthly correlations CT1 - North Atlantic Oscillation

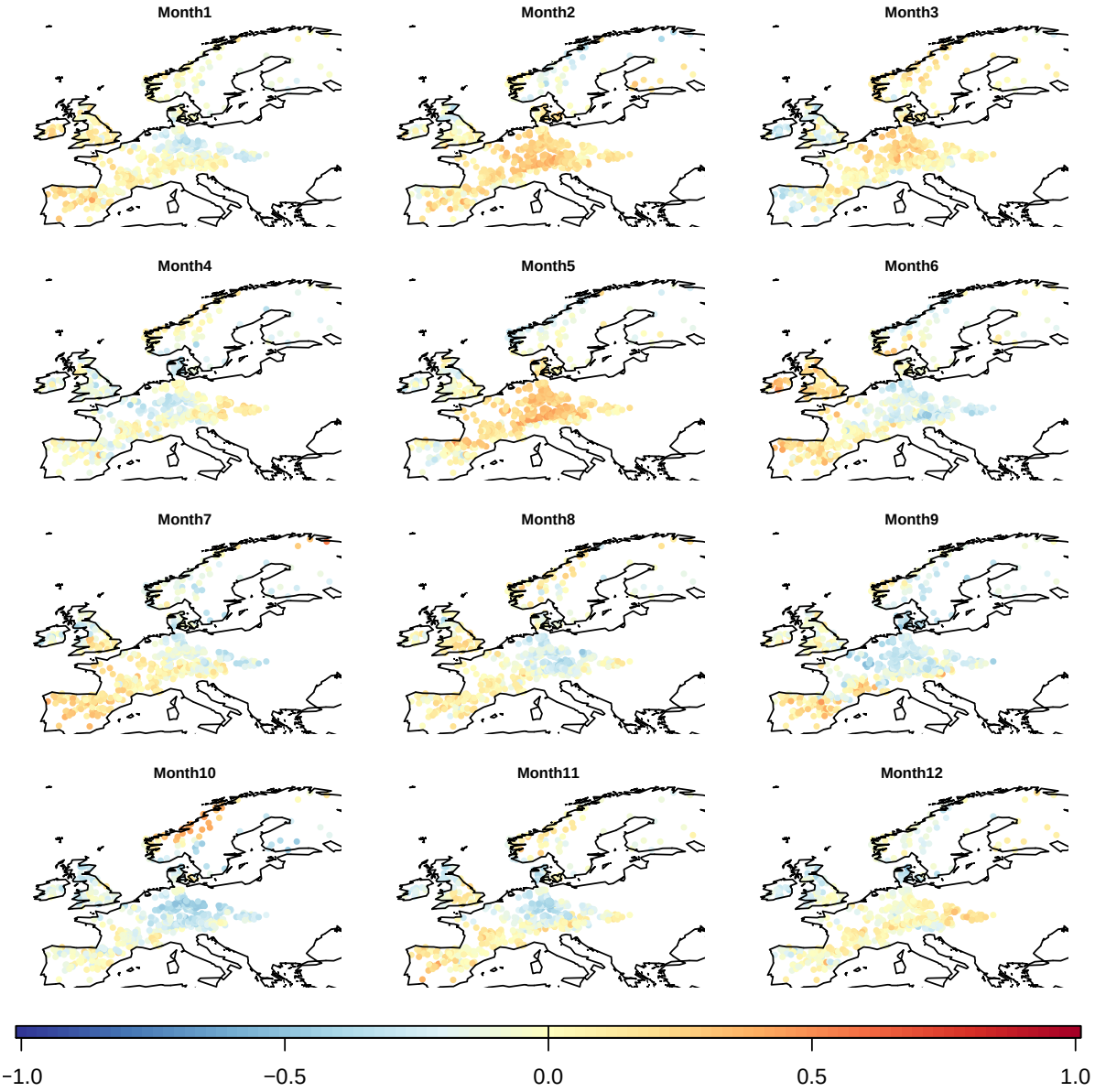

Figure A.4.: Monthly correlations CT1 - Polar/Eurasia

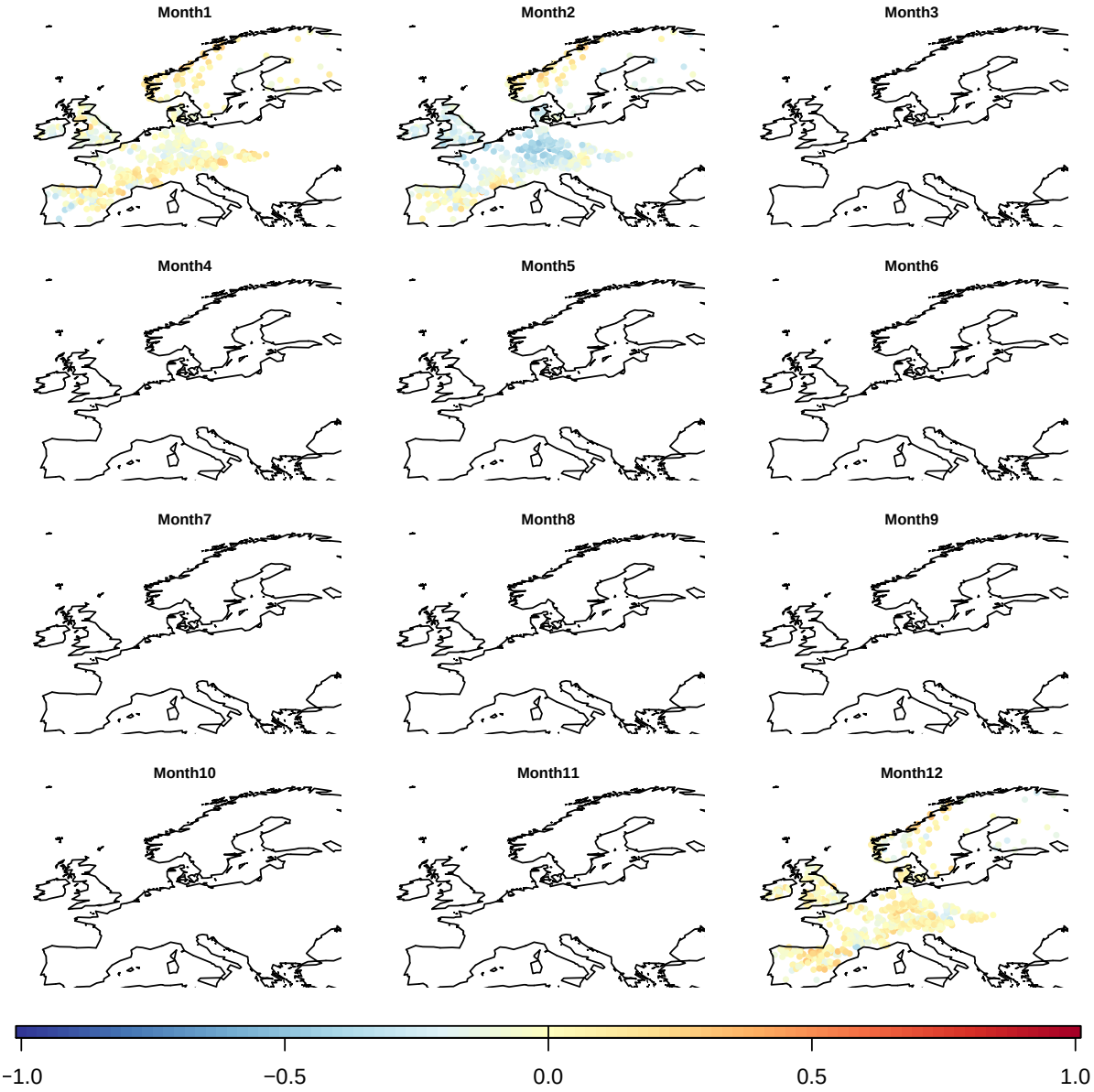

Figure A.5.: Monthly correlations CT1 - Tropical/Northern Hemisphere

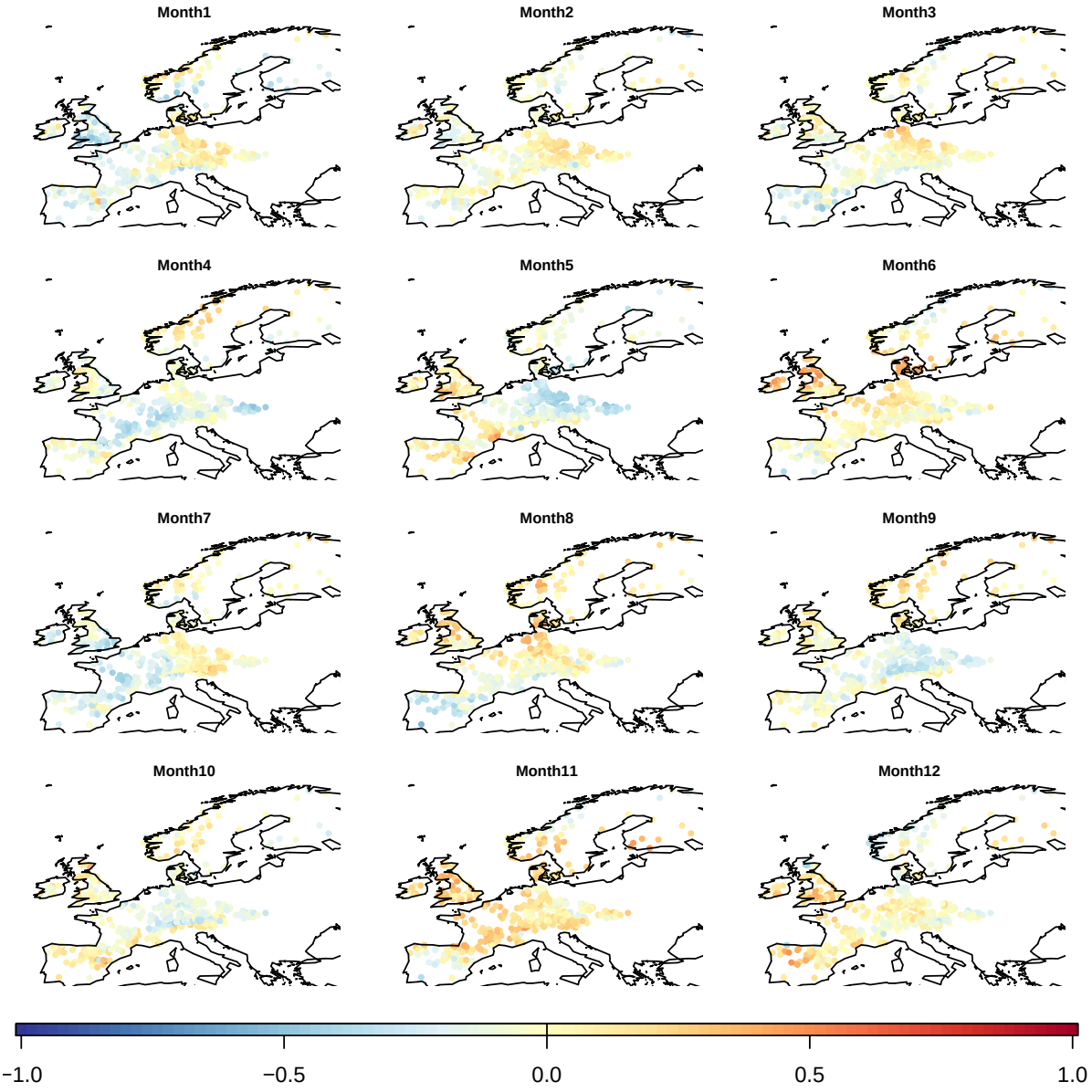

Figure A.6.: Monthly correlations CT2 - East Atlantic

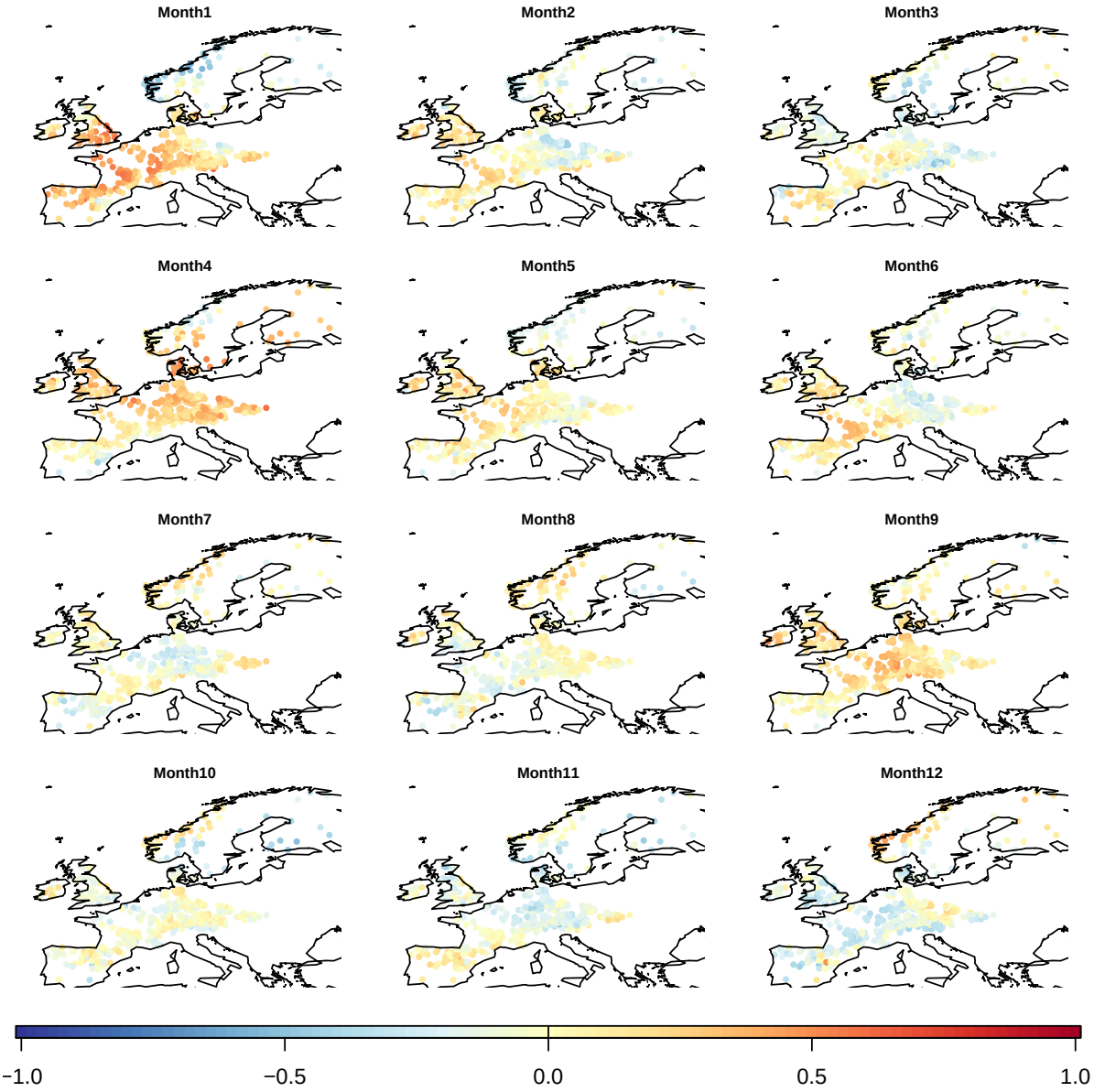

Figure A.7.: Monthly correlations CT2 - East Atlantic/Western Russia

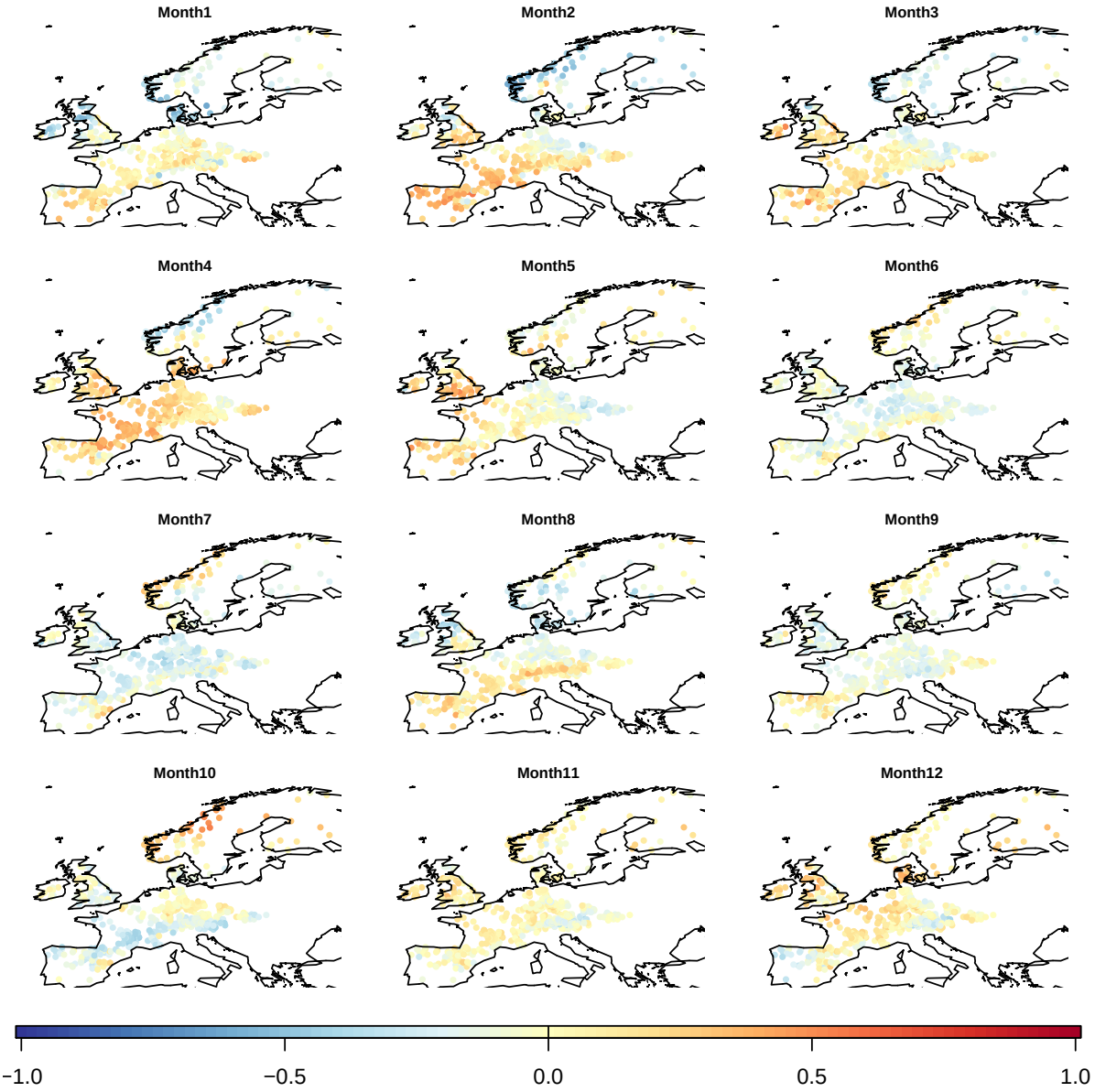

Figure A.8.: Monthly correlations CT2 - North Atlantic Oscillation

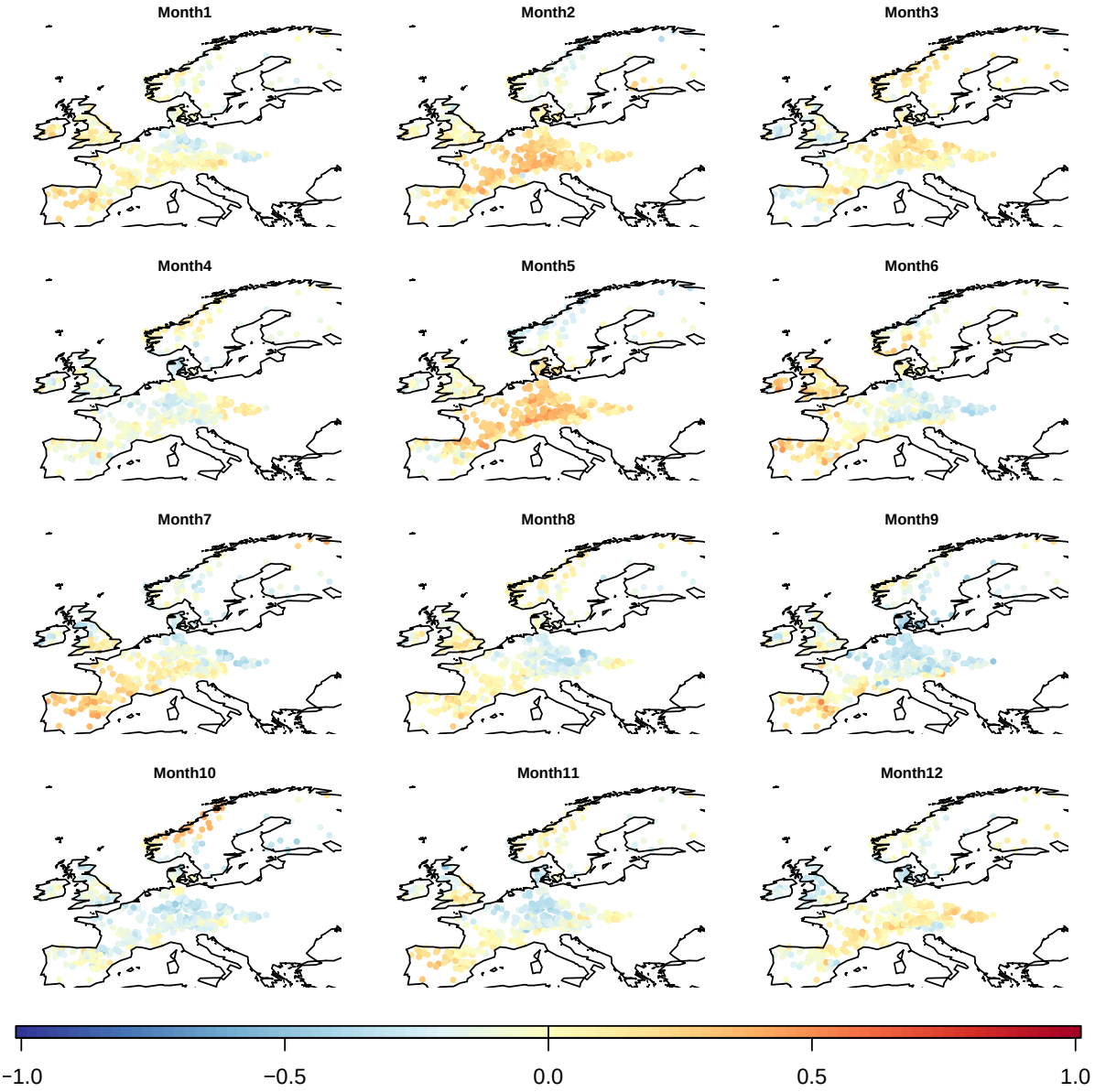

Figure A.9.: Monthly correlations CT2 - Polar/Eurasia

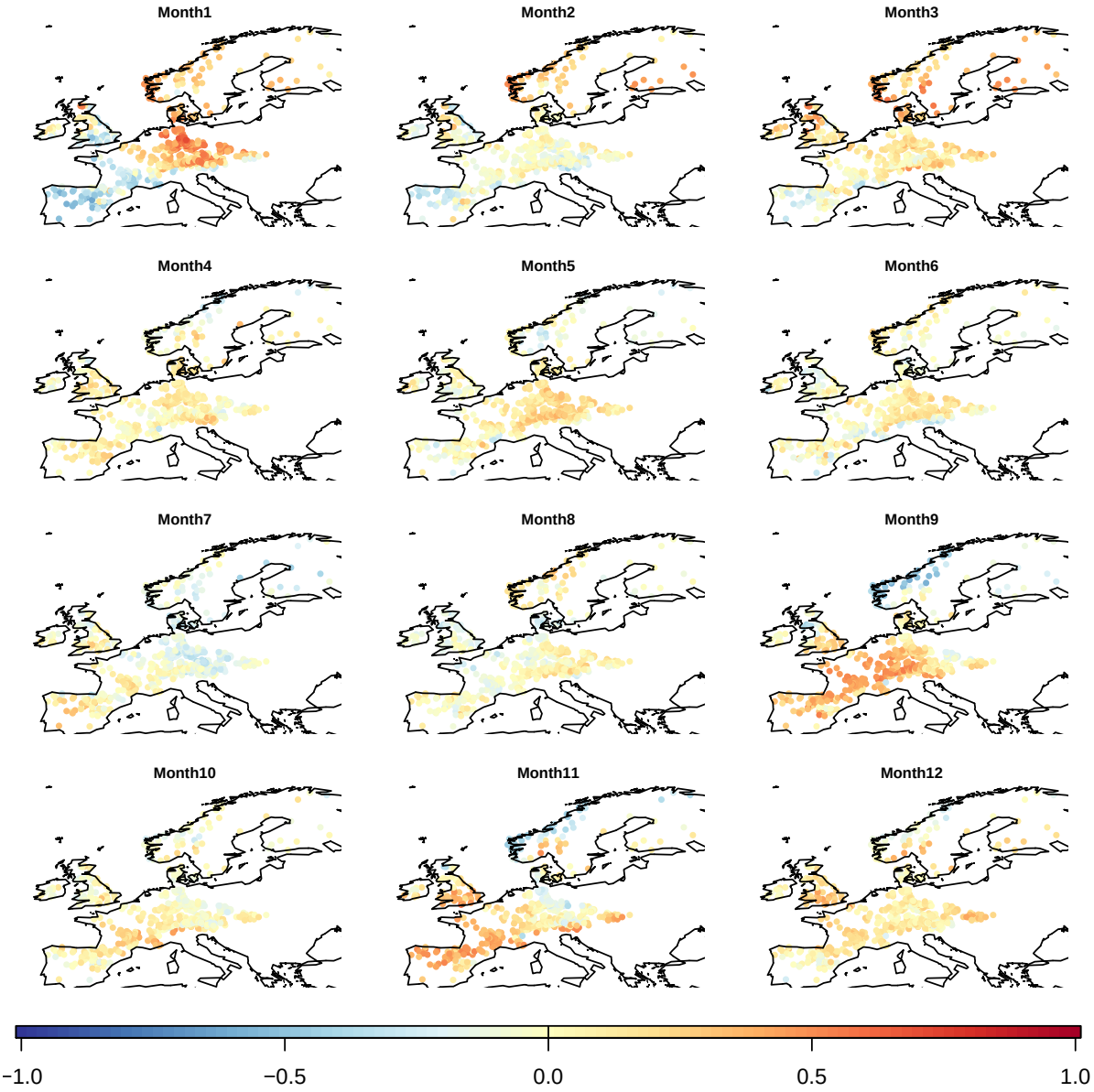

Figure A.10.: Monthly correlations CT2 - Scandinavian Pattern

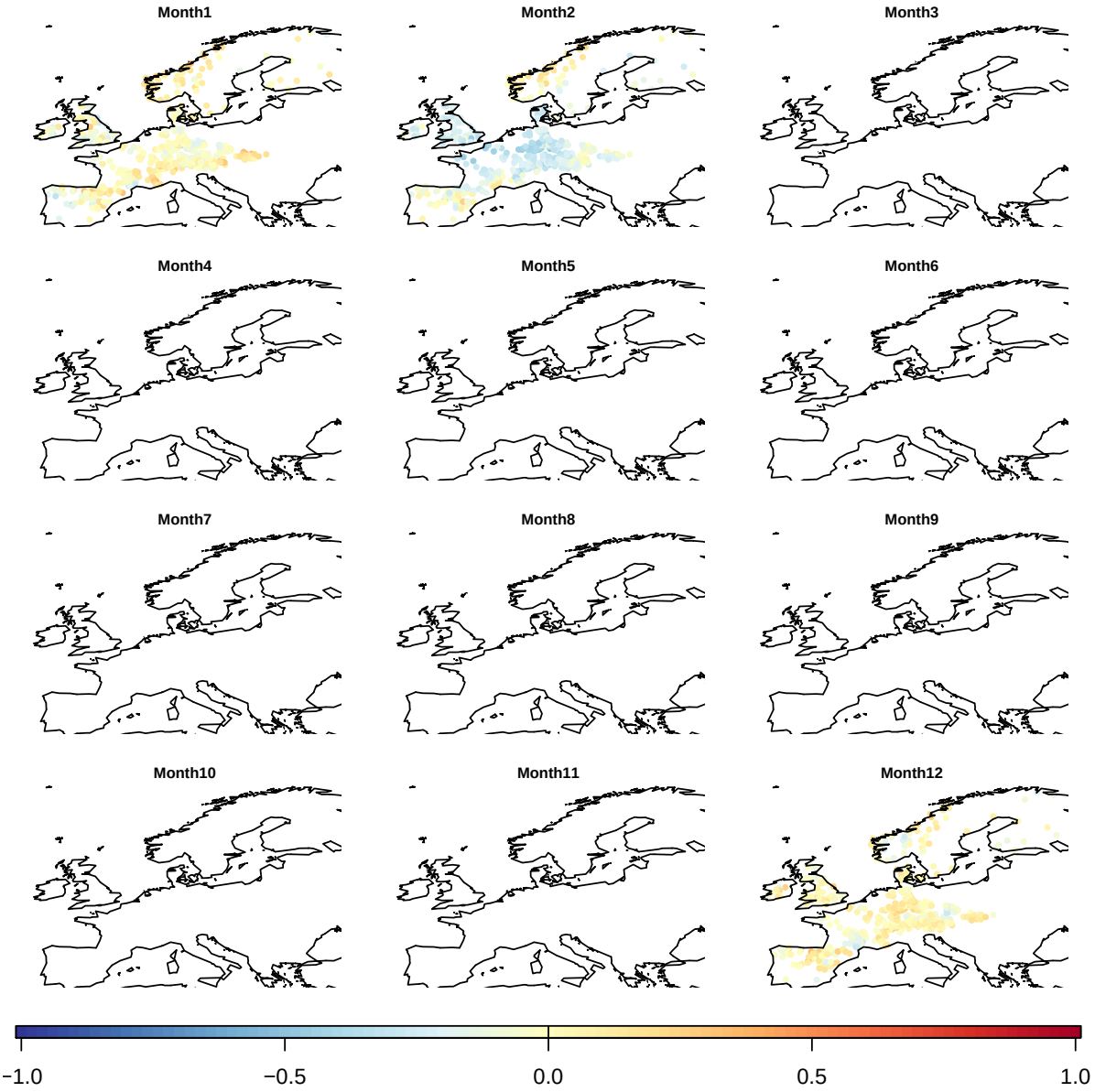

Figure A.11.: Monthly correlations CT2 - Tropical/Northern Hemisphere

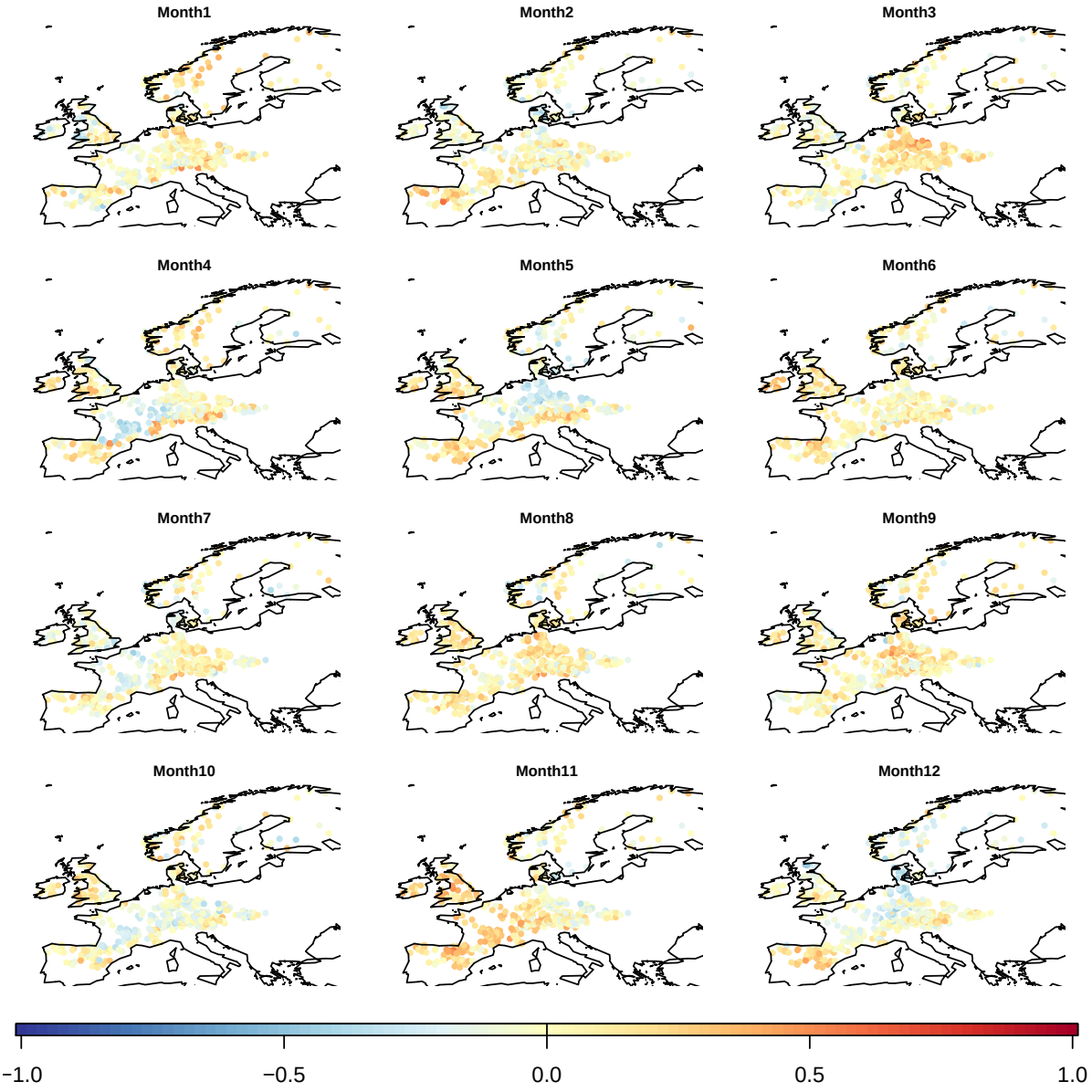

Figure A.12.: Monthly correlations Max91 - East Atlantic

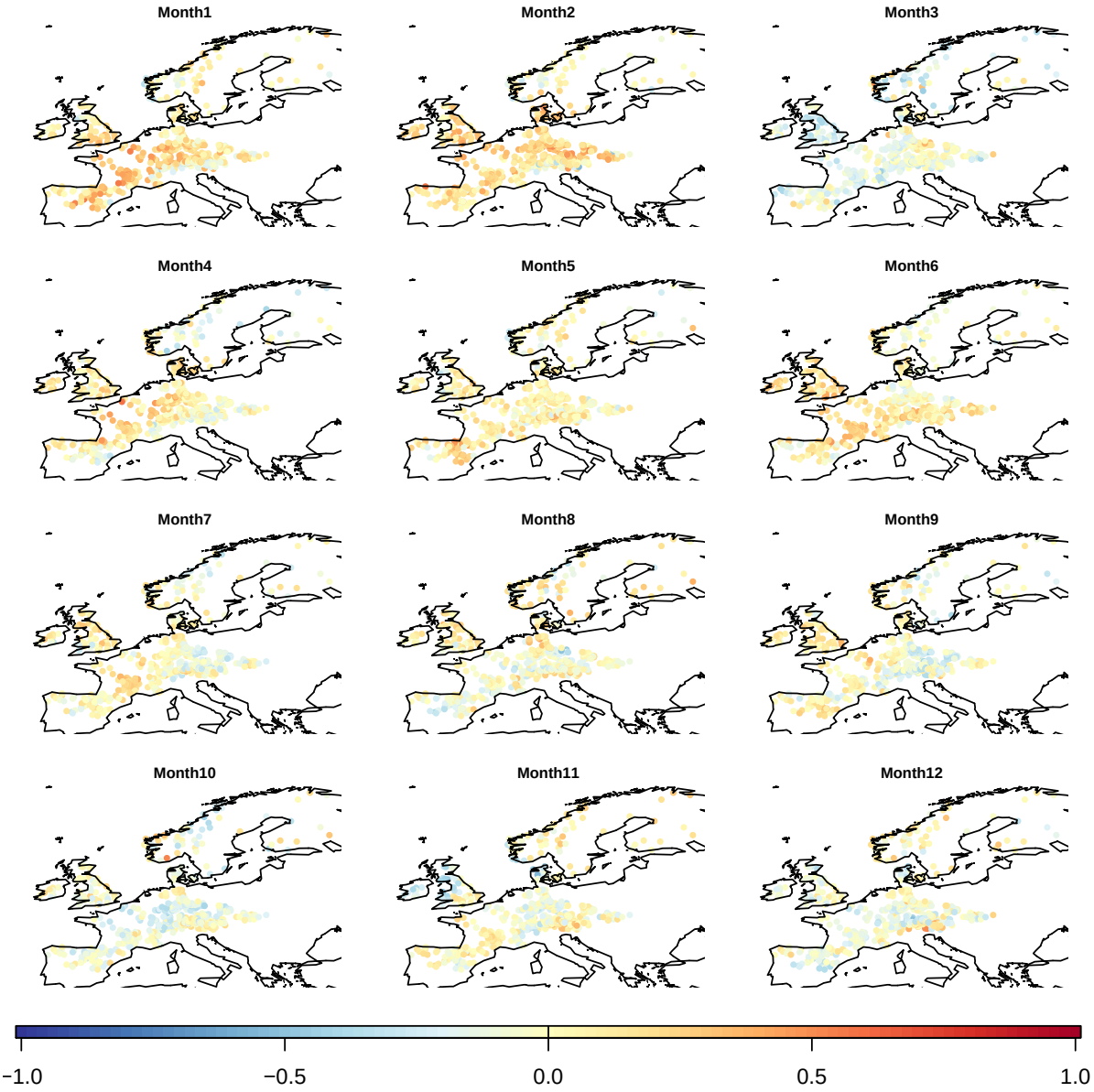

Figure A.13.: Monthly correlations Max91 - East Atlantic/Western Russia

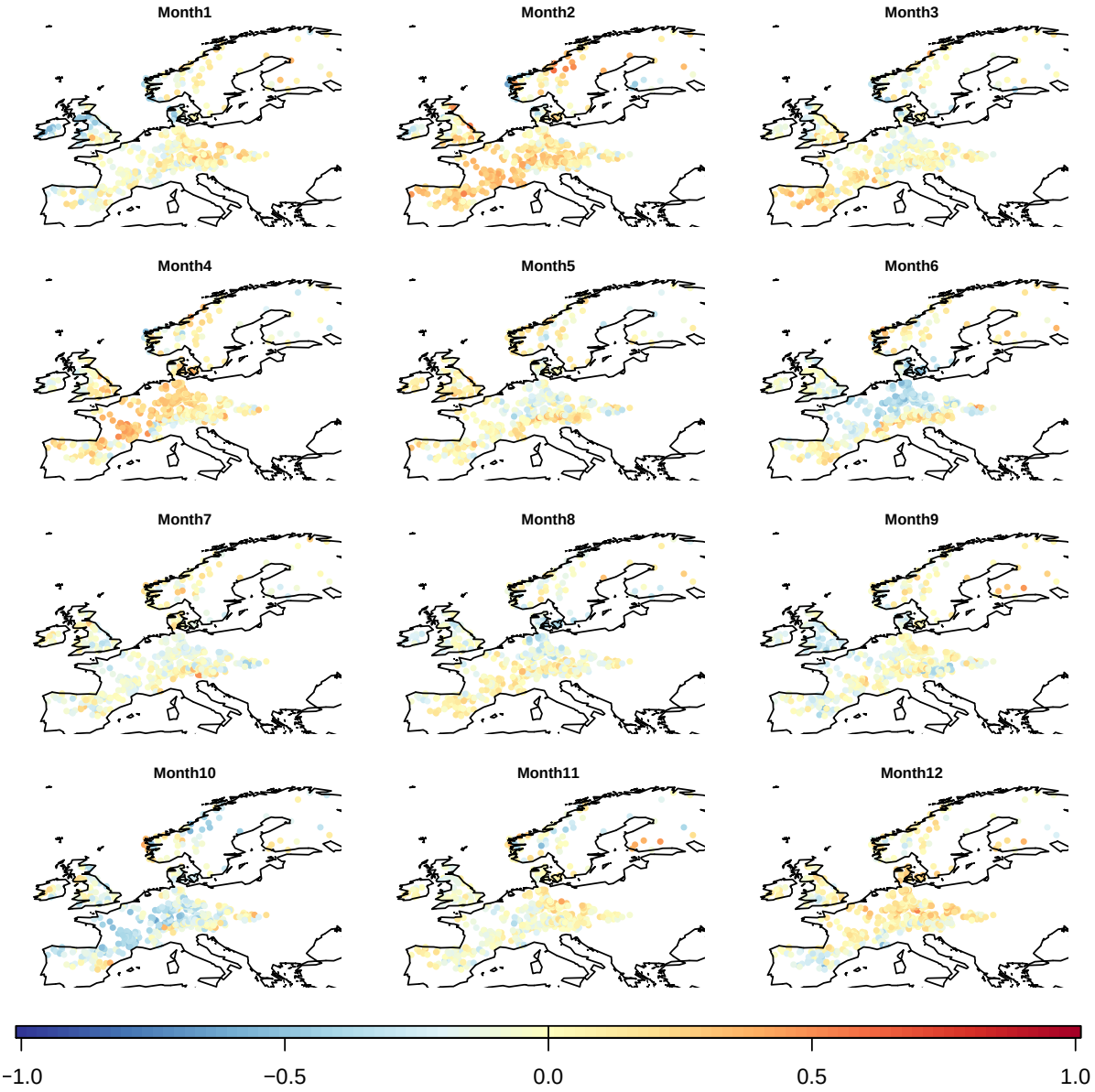

Figure A.14.: Monthly correlations Max91 - North Atlantic Oscillation

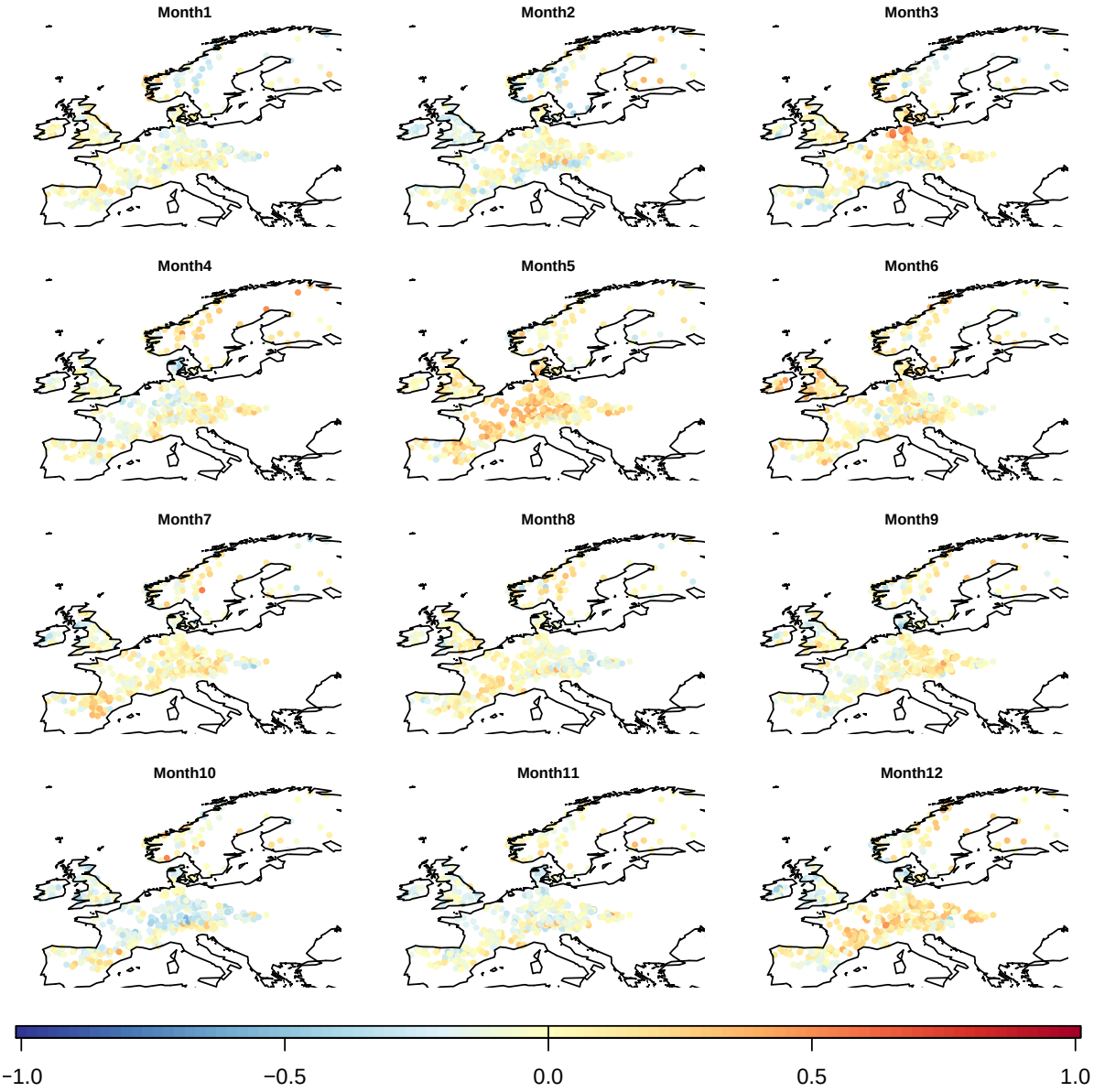

Figure A.15.: Monthly correlations Max91 - Polar/Eurasia

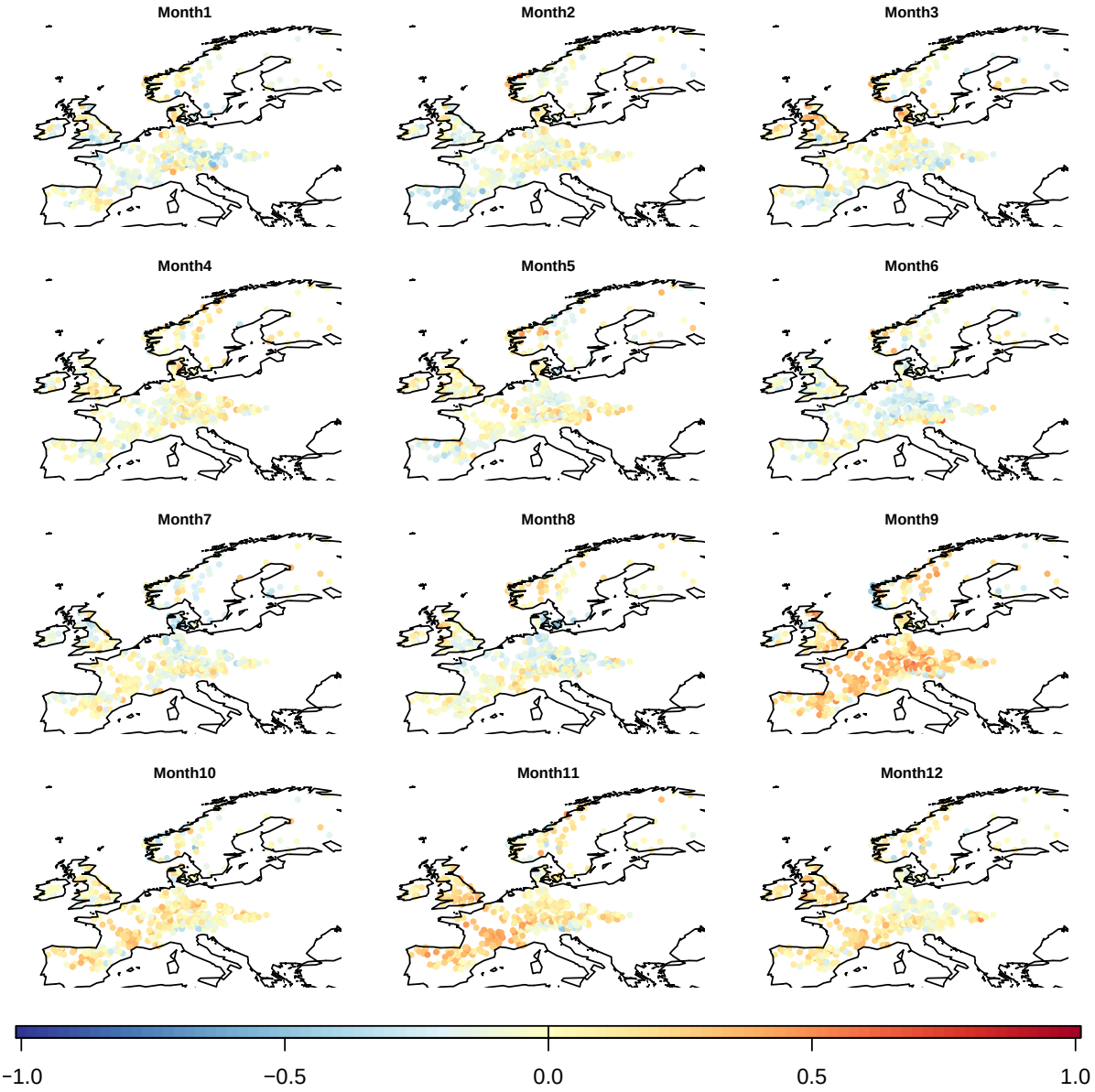

Figure A.16.: Monthly correlations Max91 - Scandinavian Pattern

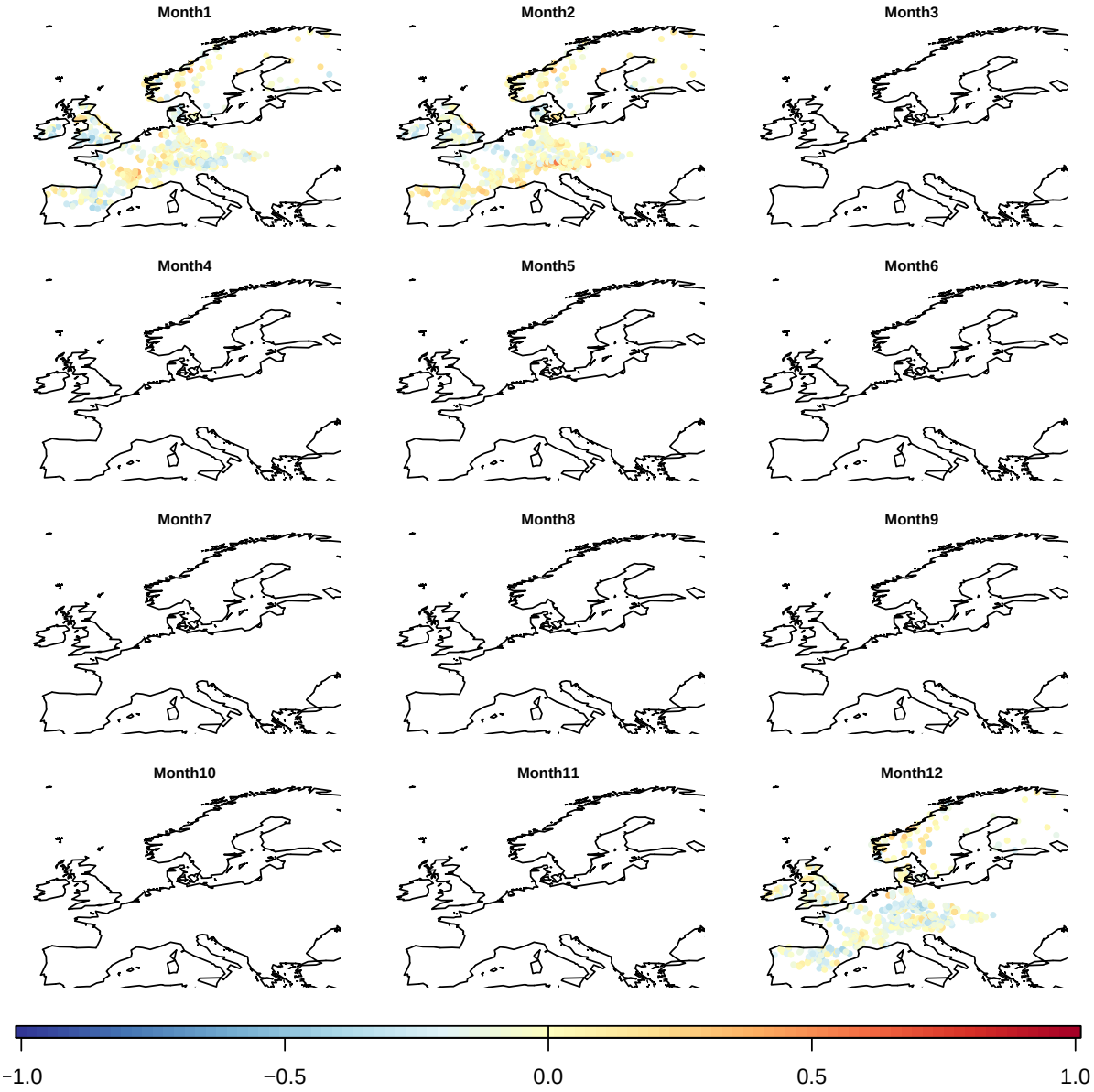

Figure A.17.: Monthly correlations Max91 - Tropical/Northern Hemisphere

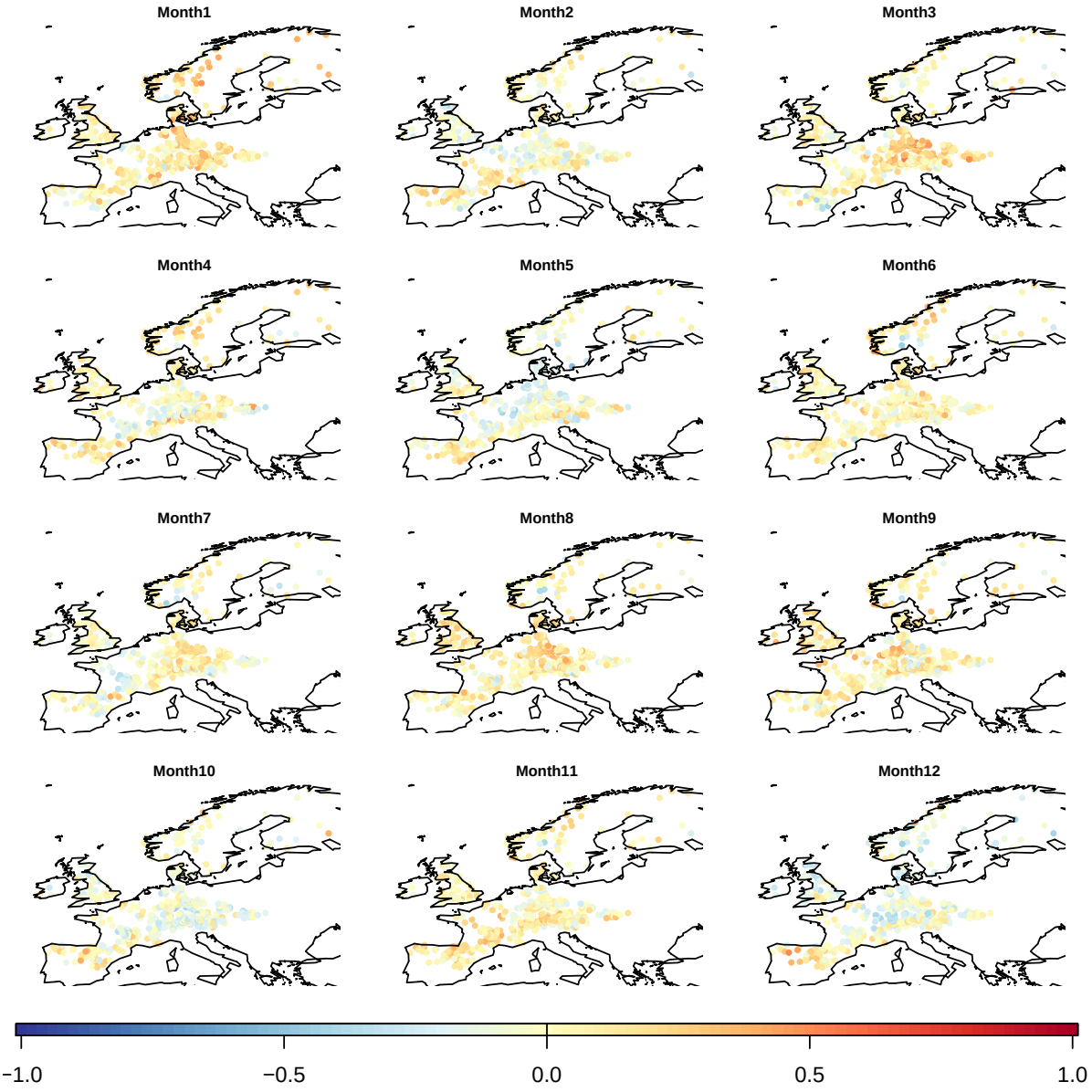

Figure A.18.: Monthly correlations Max181 - East Atlantic

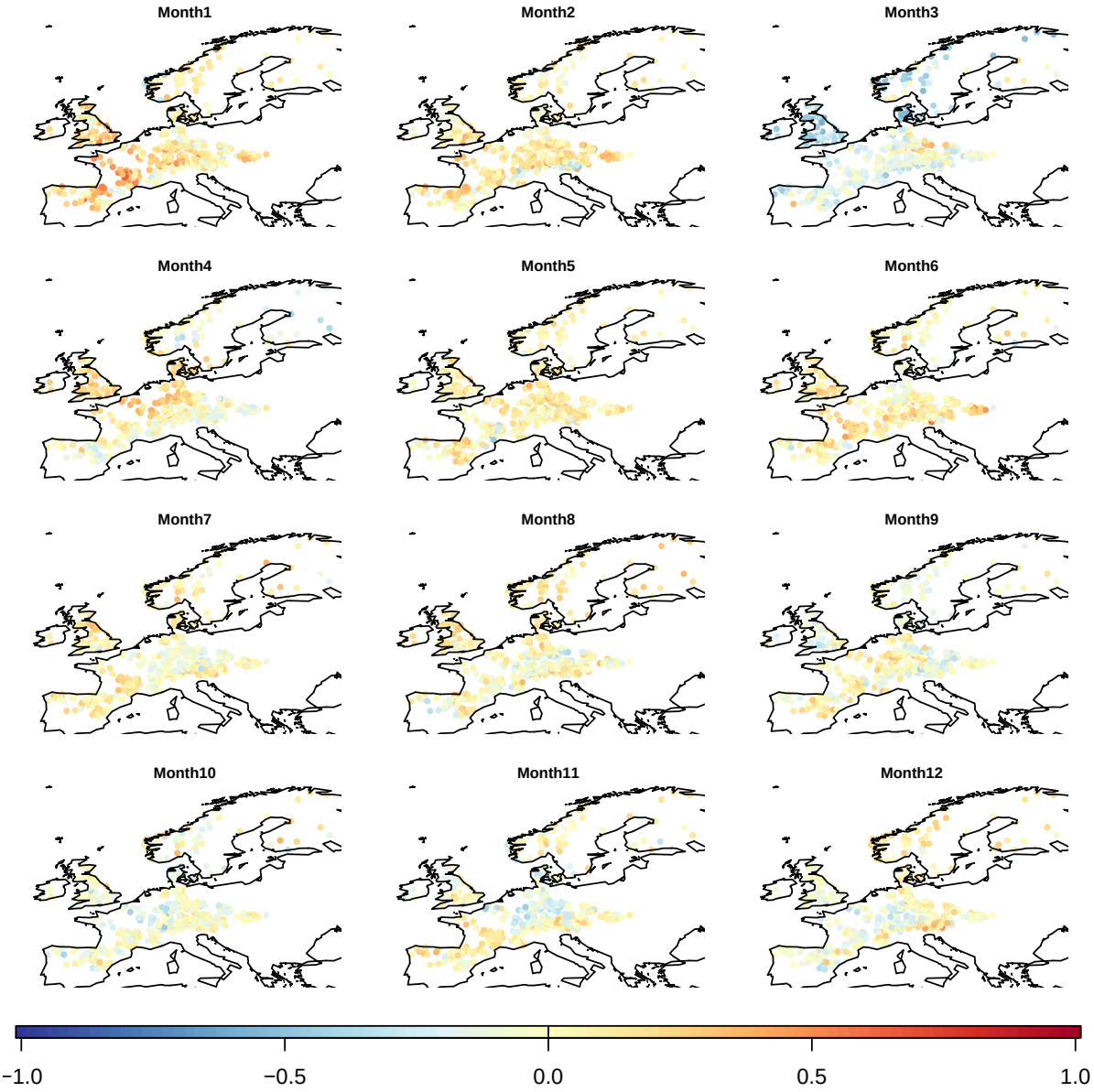

Figure A.19.: Monthly correlations Max181 - East Atlantic/Western Russia

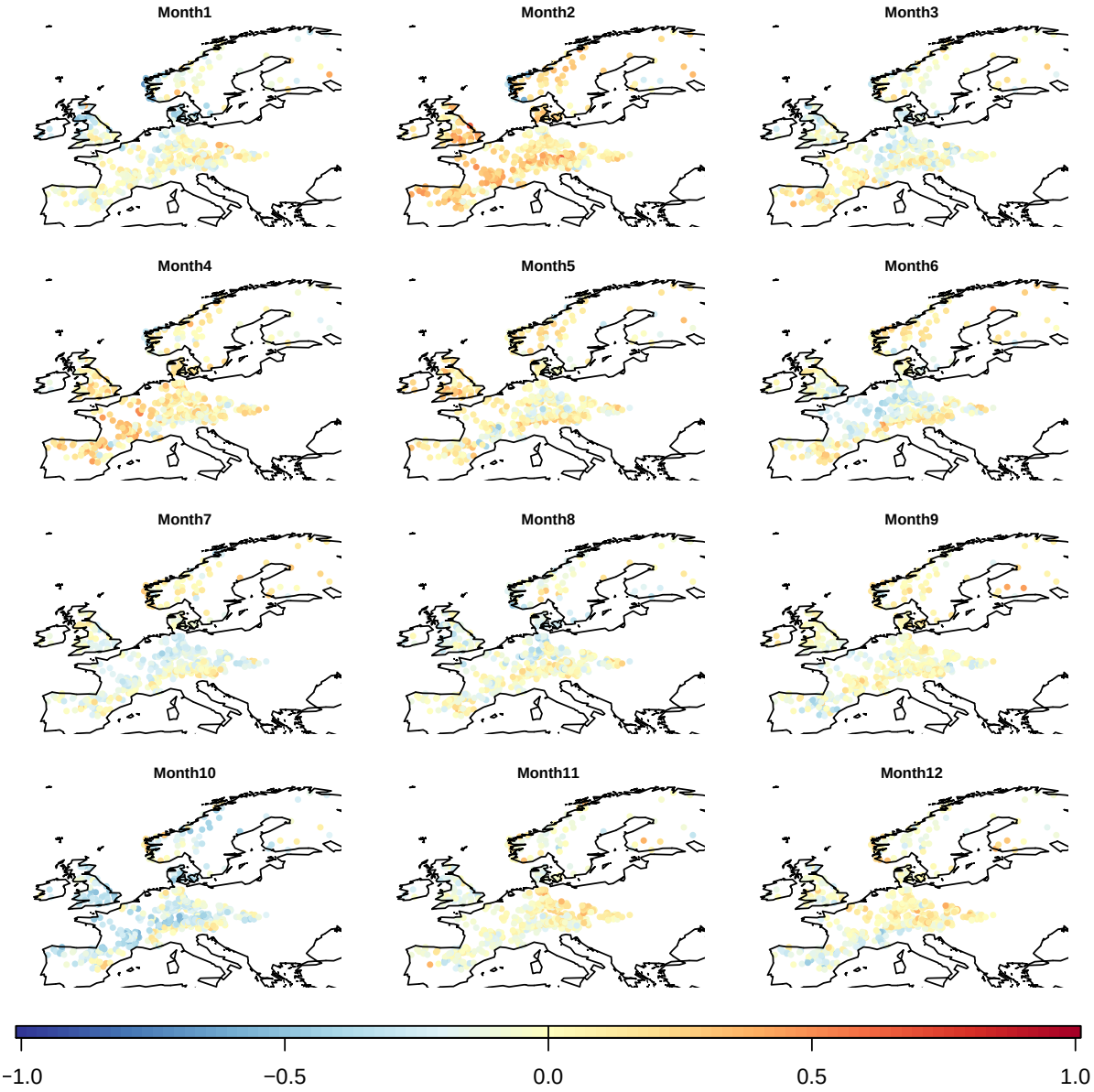

Figure A.20.: Monthly correlations Max181 - North Atlantic Oscillation

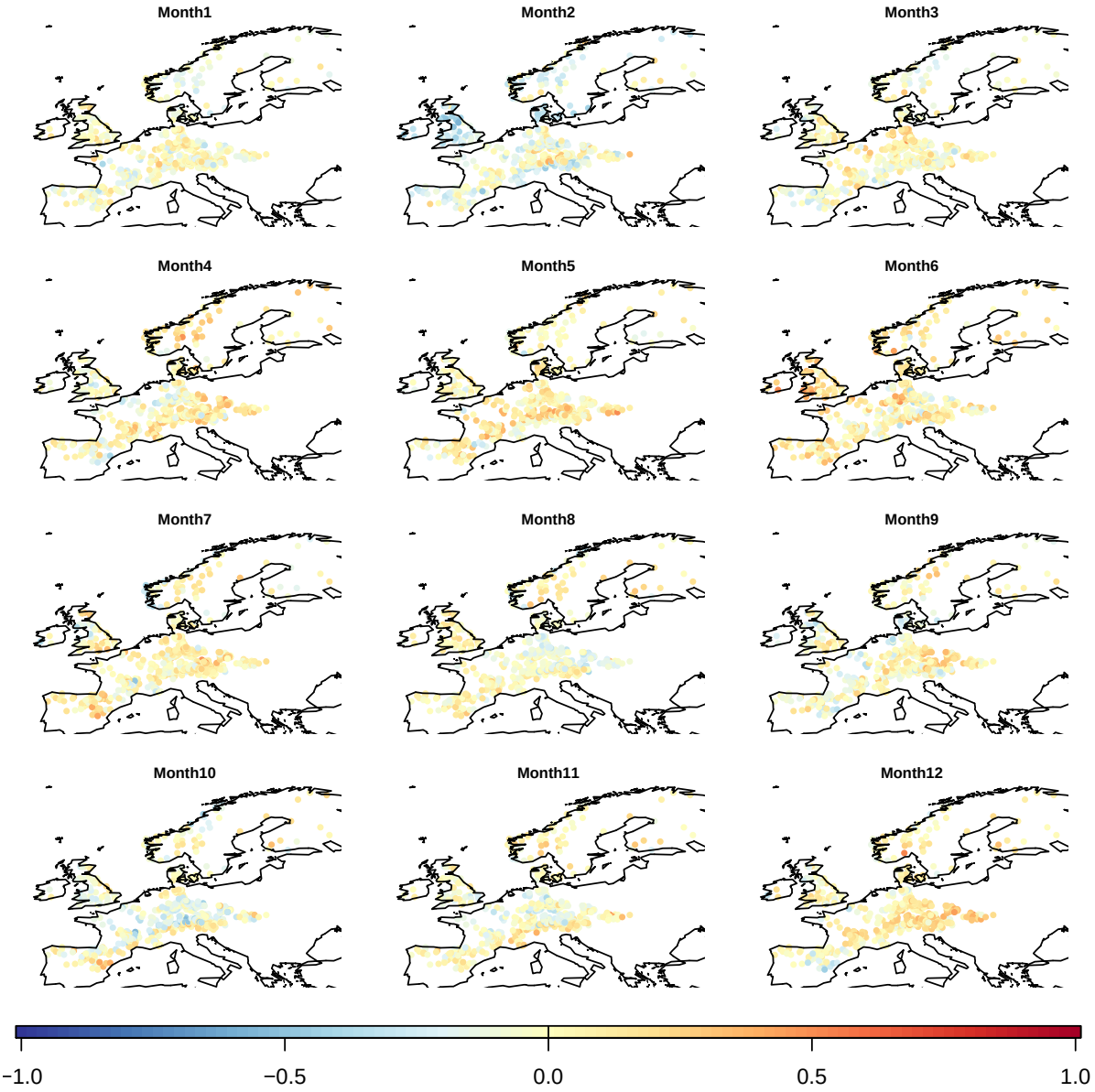

Figure A.21.: Monthly correlations Max181 - Polar/Eurasia

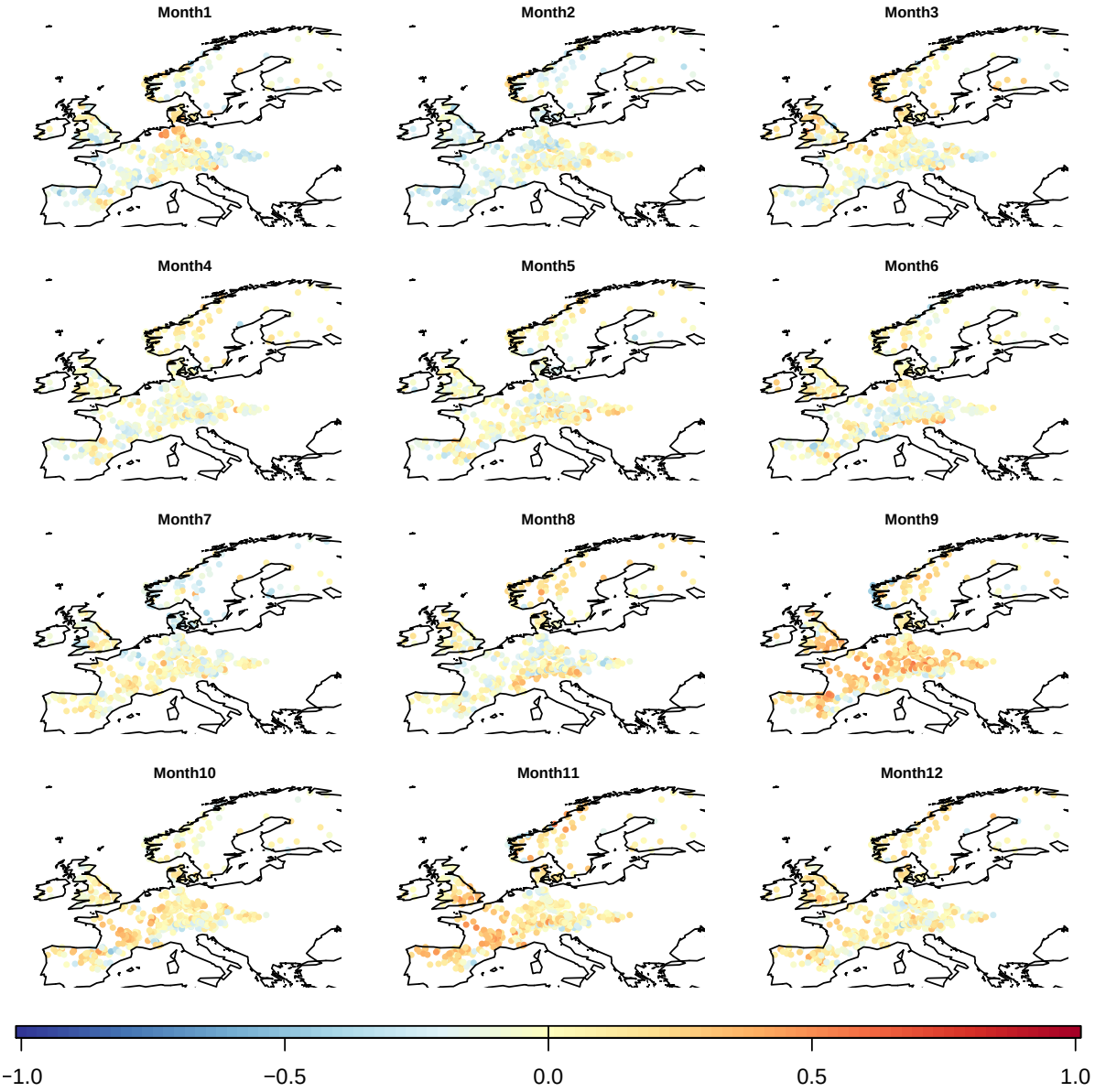

Figure A.22.: Monthly correlations Max181 - Scandinavian Pattern

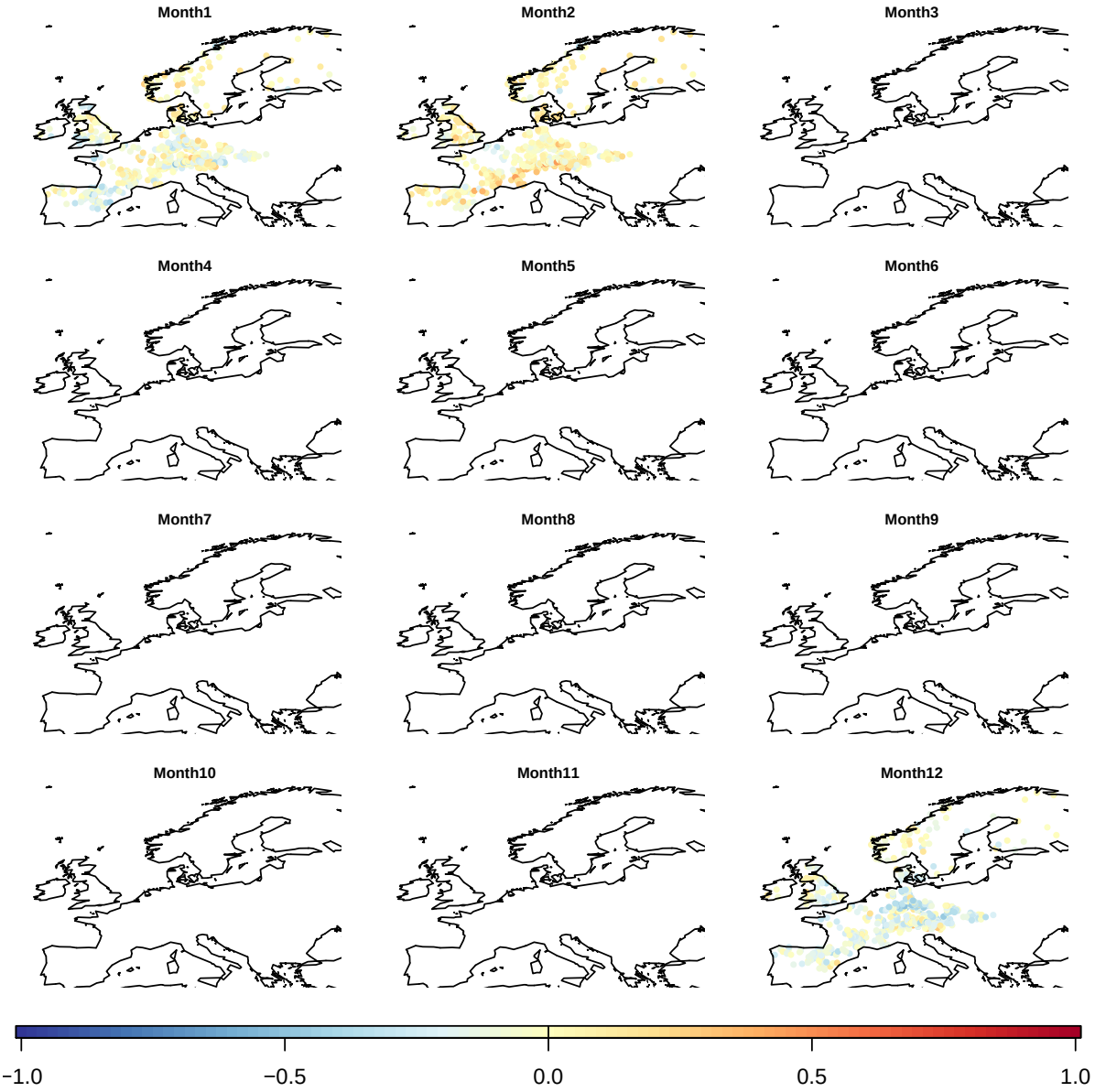

Figure A.23.: Monthly correlations Max181 - Tropical/Northern Hemisphere

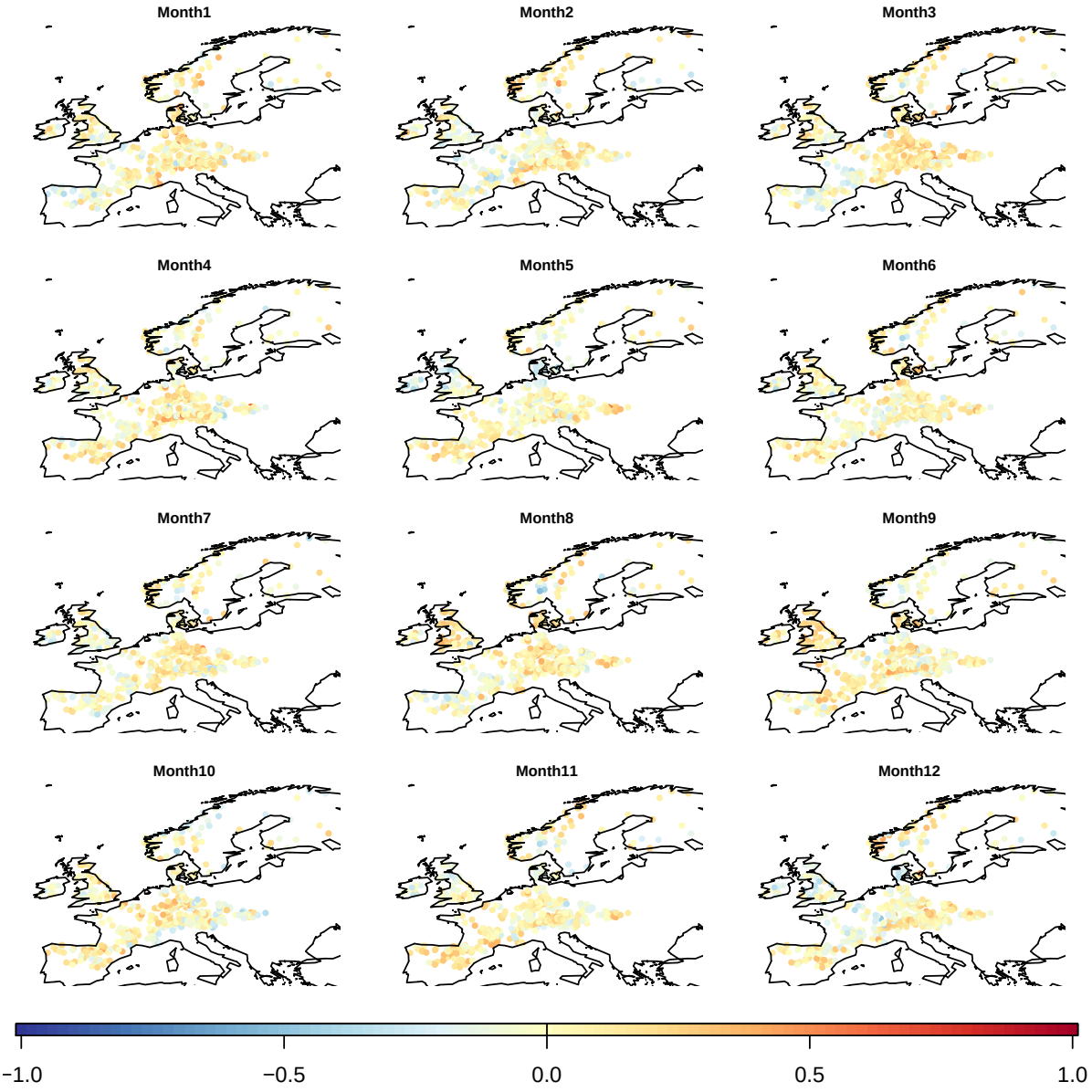

Figure A.24.: Monthly correlations Min91 - East Atlantic

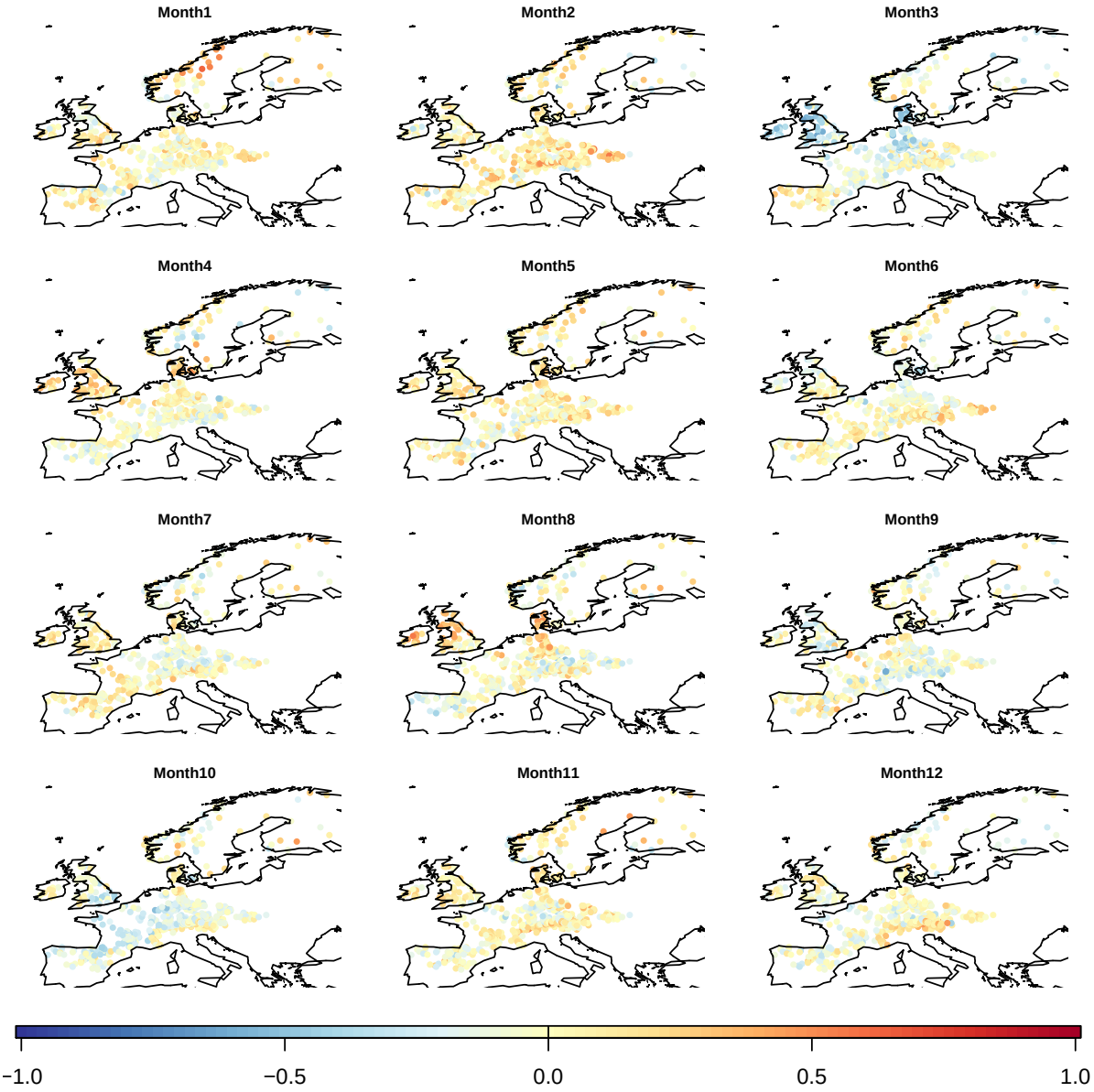

Figure A.25.: Monthly correlations Min91 - East Atlantic/Western Russia

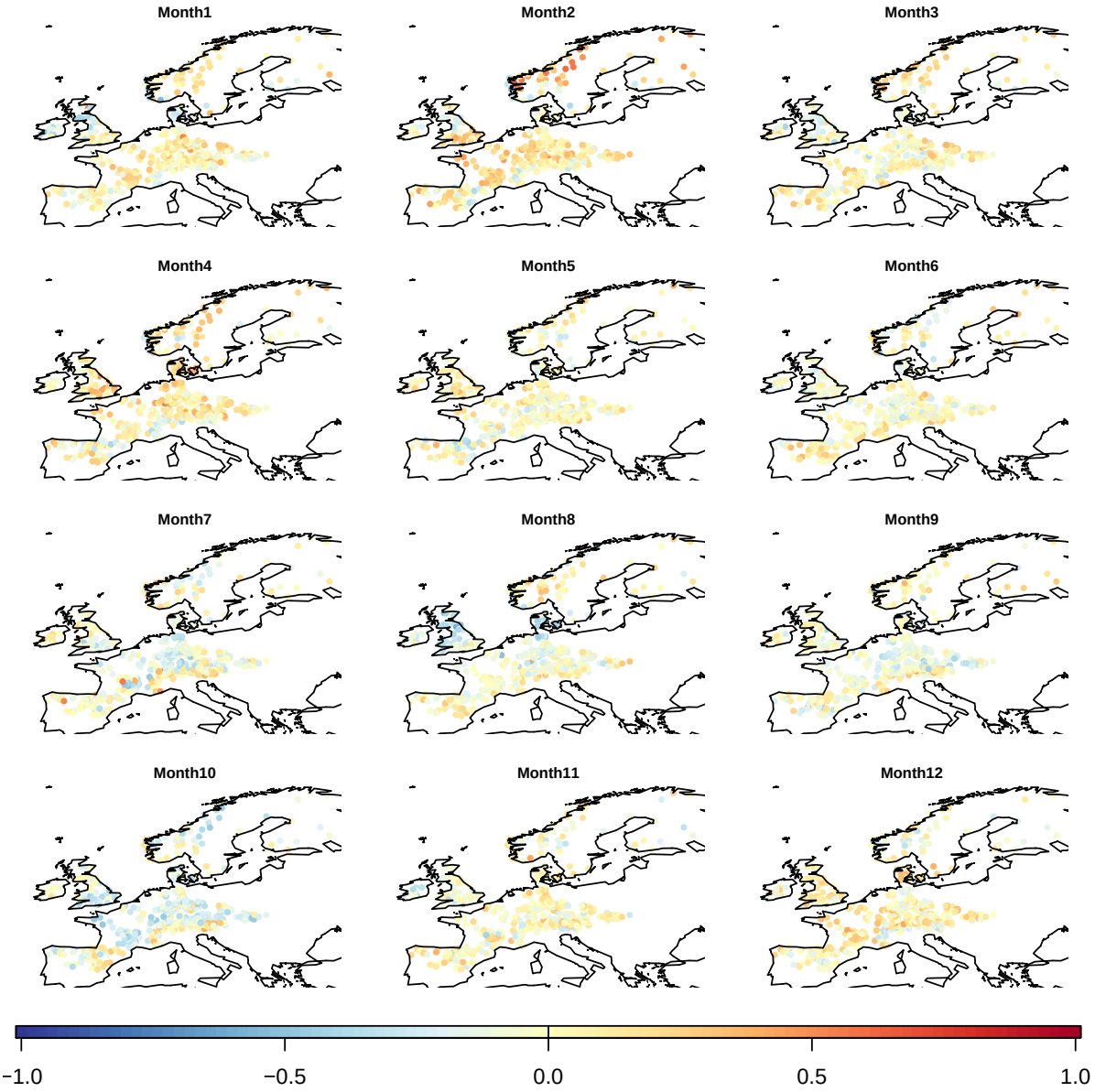

Figure A.26.: Monthly correlations Min91 - North Atlantic Oscillation

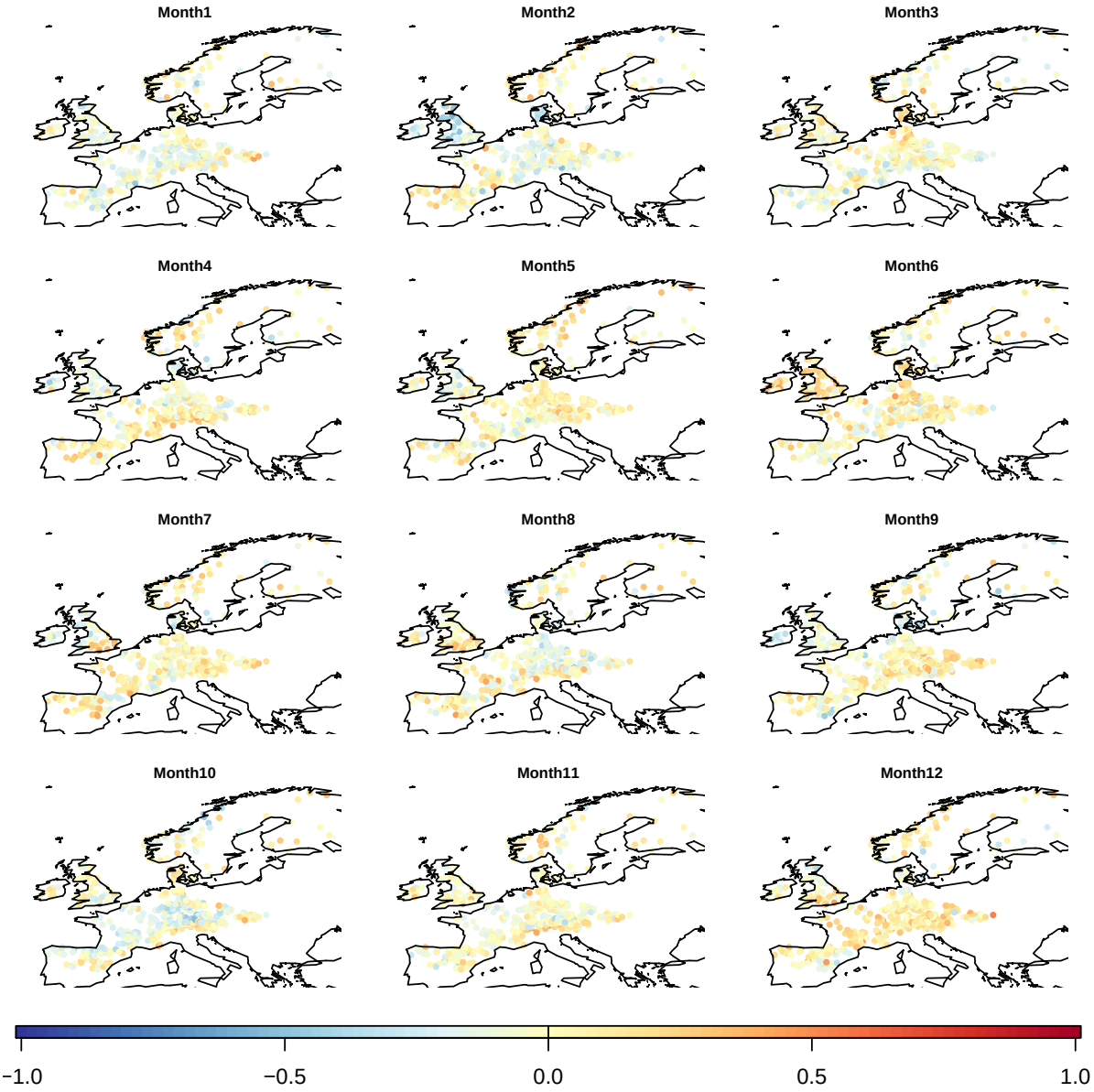

Figure A.27.: Monthly correlations Min91 - Polar/Eurasia

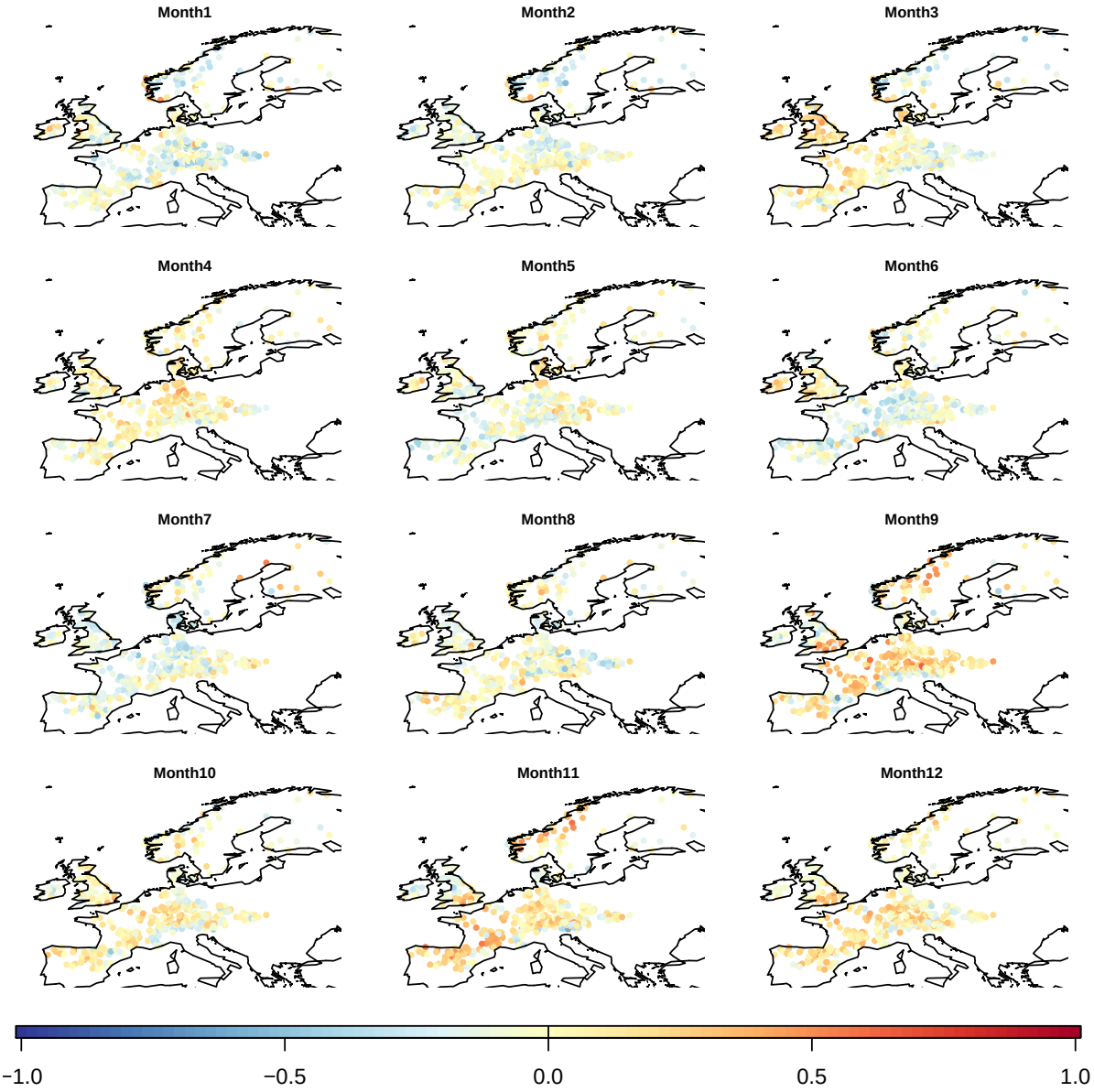

Figure A.28.: Monthly correlations Min91 - Scandinavian Pattern

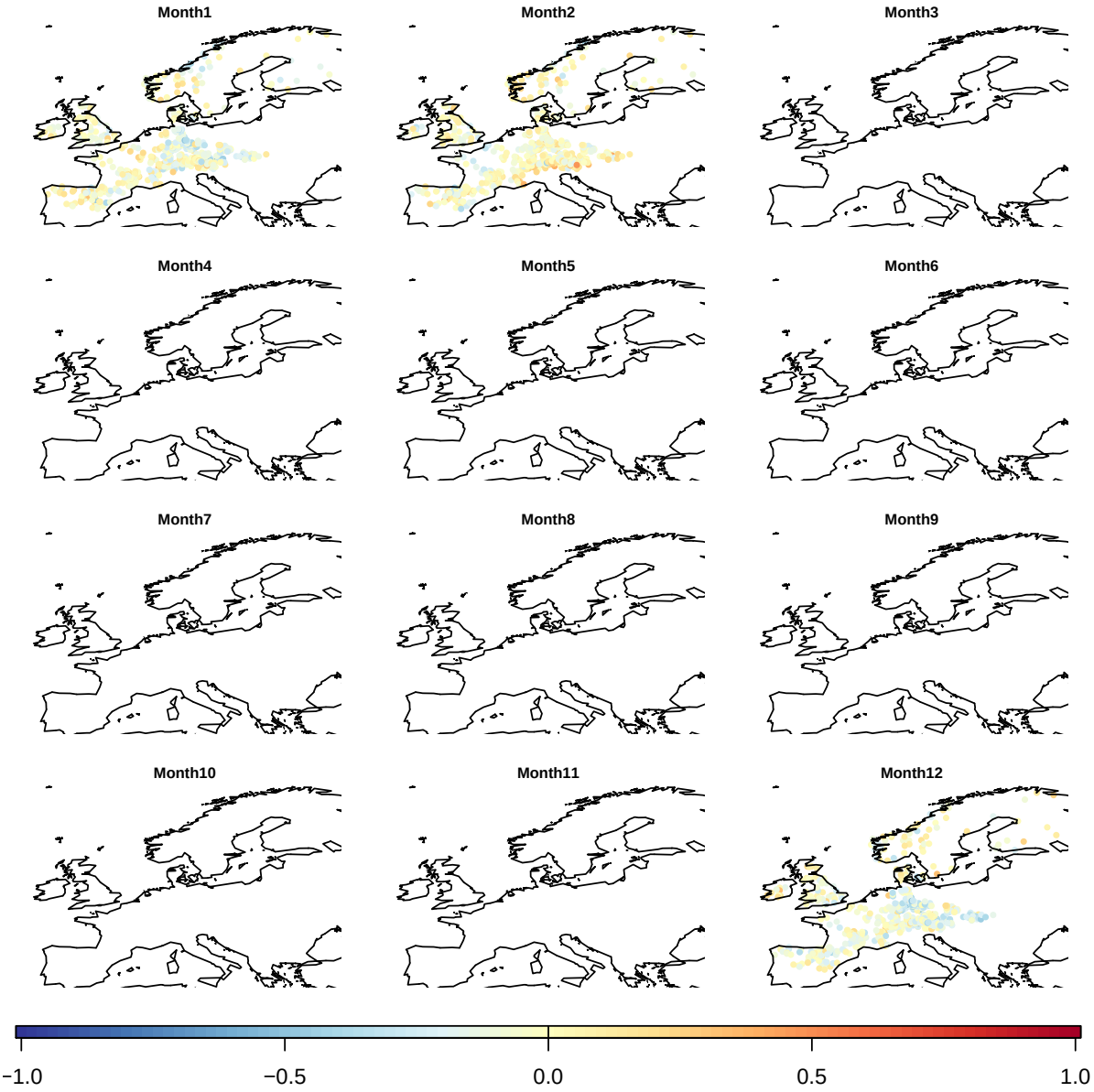

Figure A.29.: Monthly correlations Min91 - Tropical/Northern Hemisphere

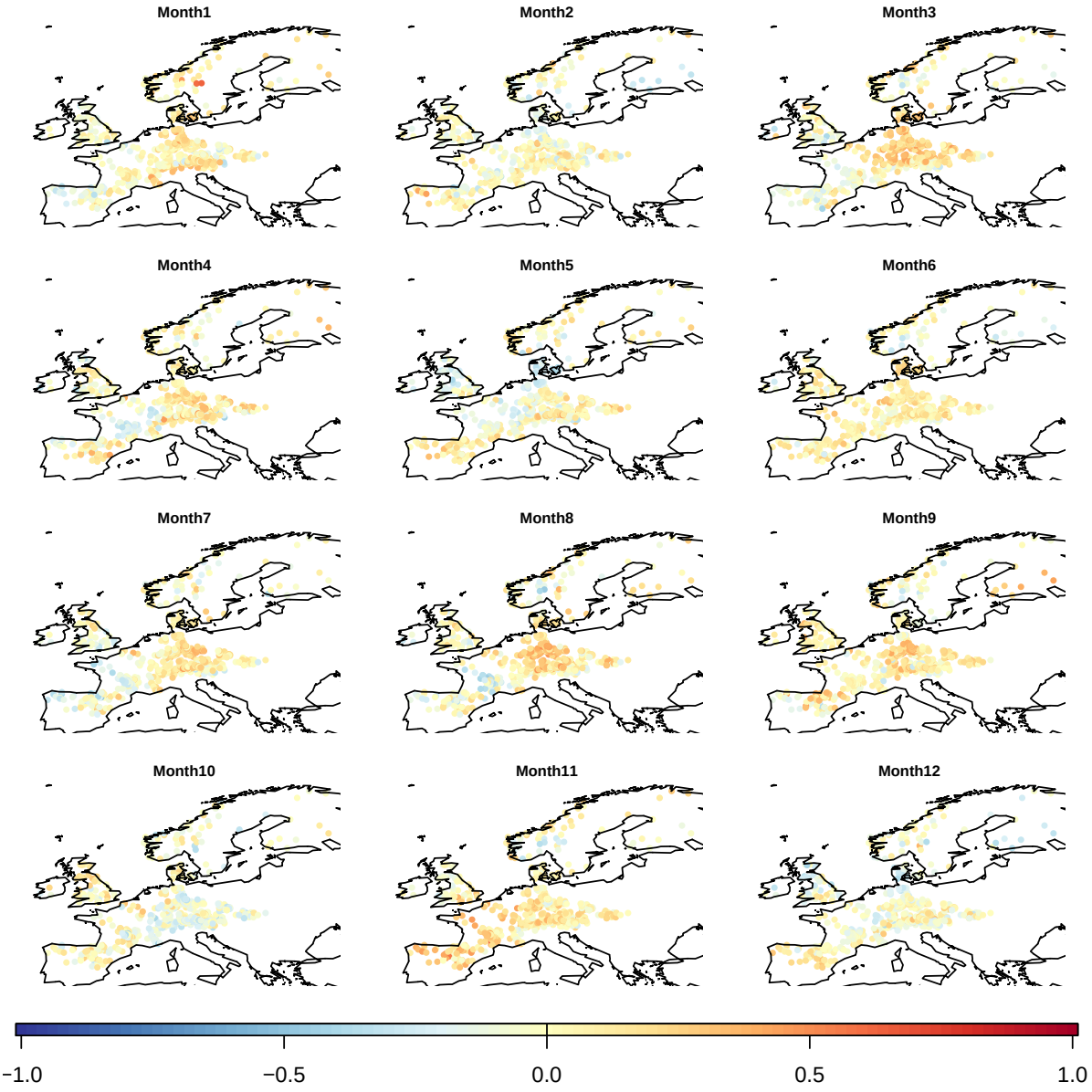

Figure A.30.: Monthly correlations Min181 - East Atlantic

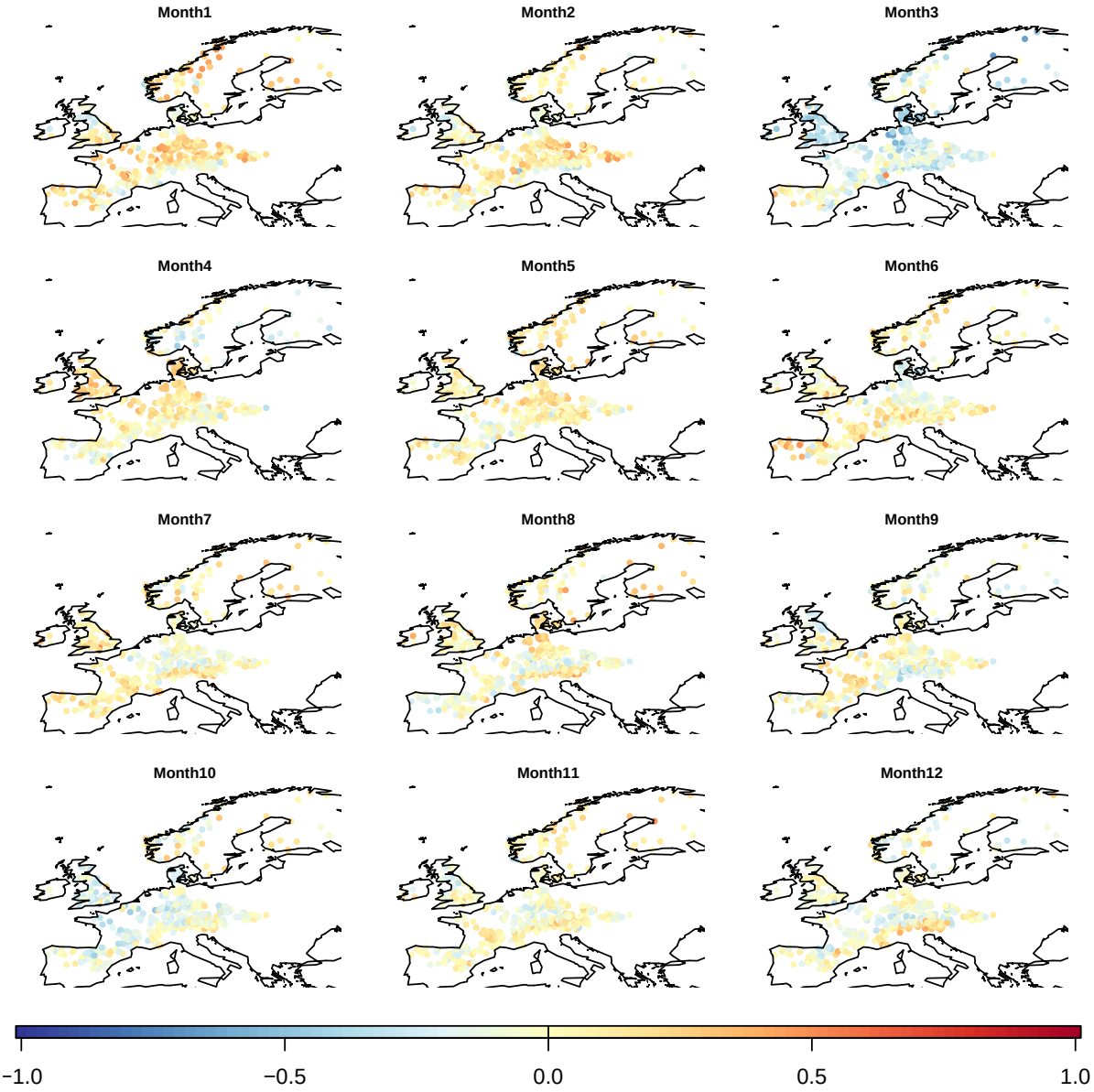

Figure A.31.: Monthly correlations Min181 - East Atlantic/Western Russia

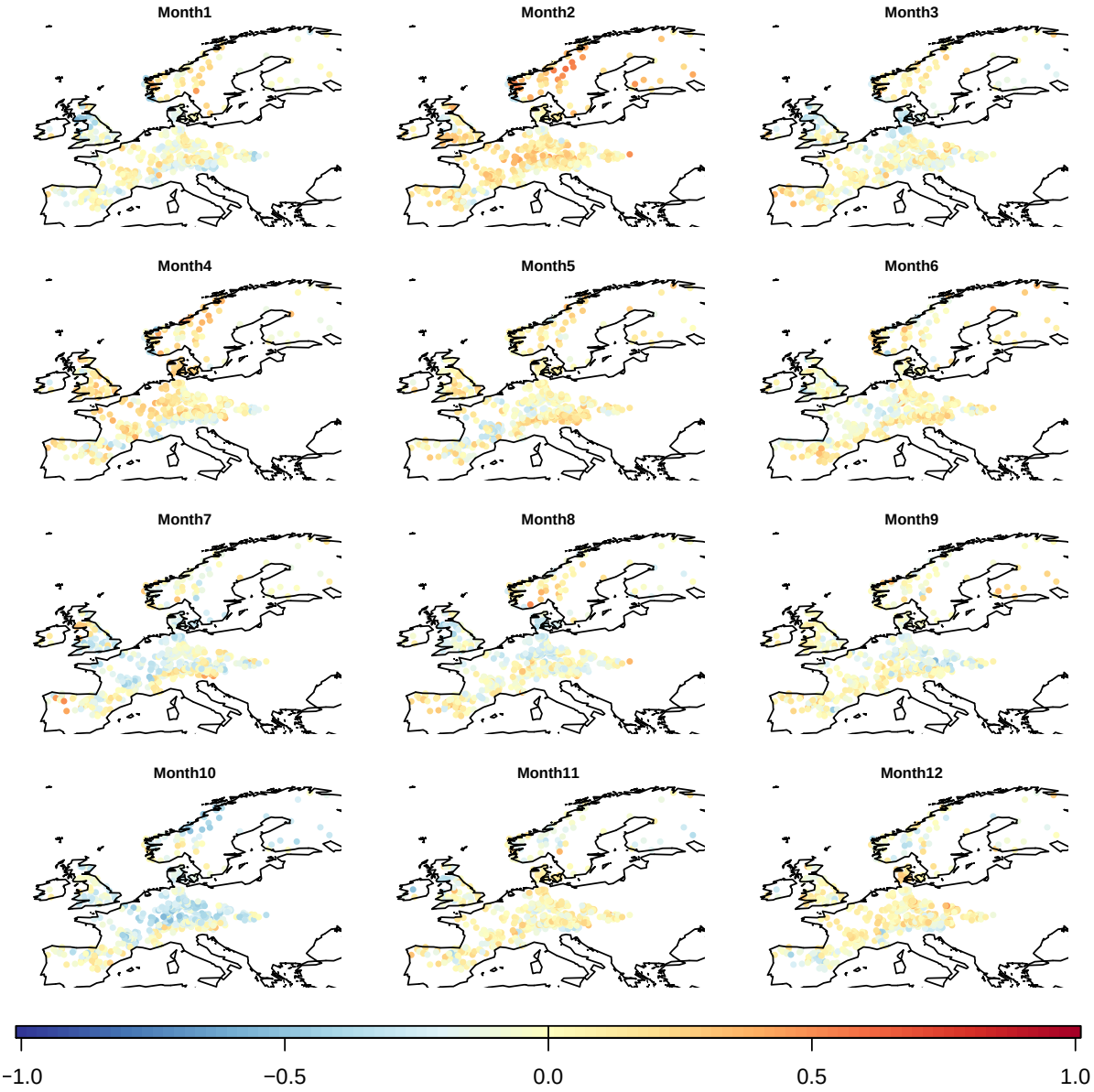

Figure A.32.: Monthly correlations Min181 - North Atlantic Oscillation

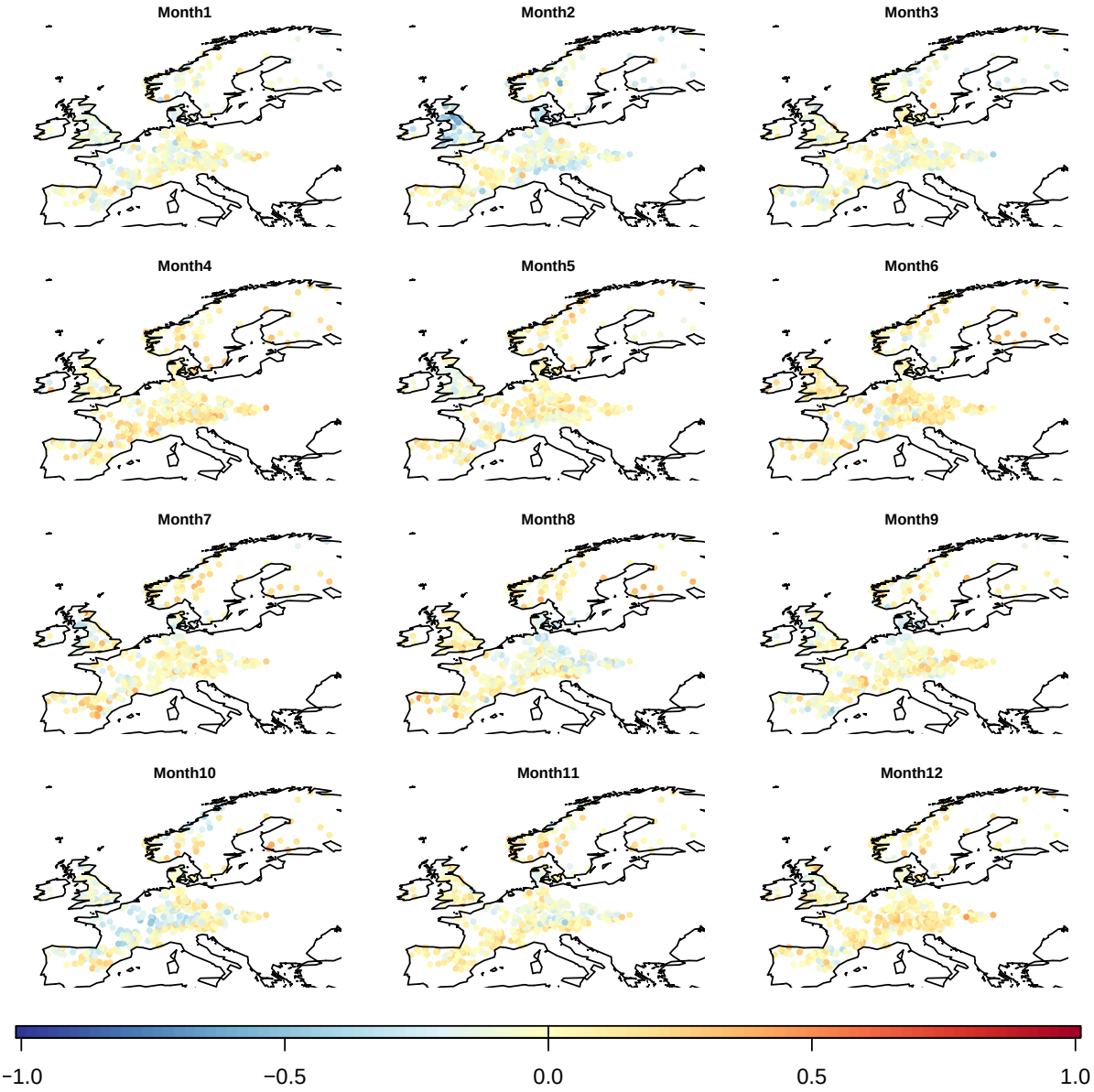

Figure A.33.: Monthly correlations Min181 - Polar/Eurasia

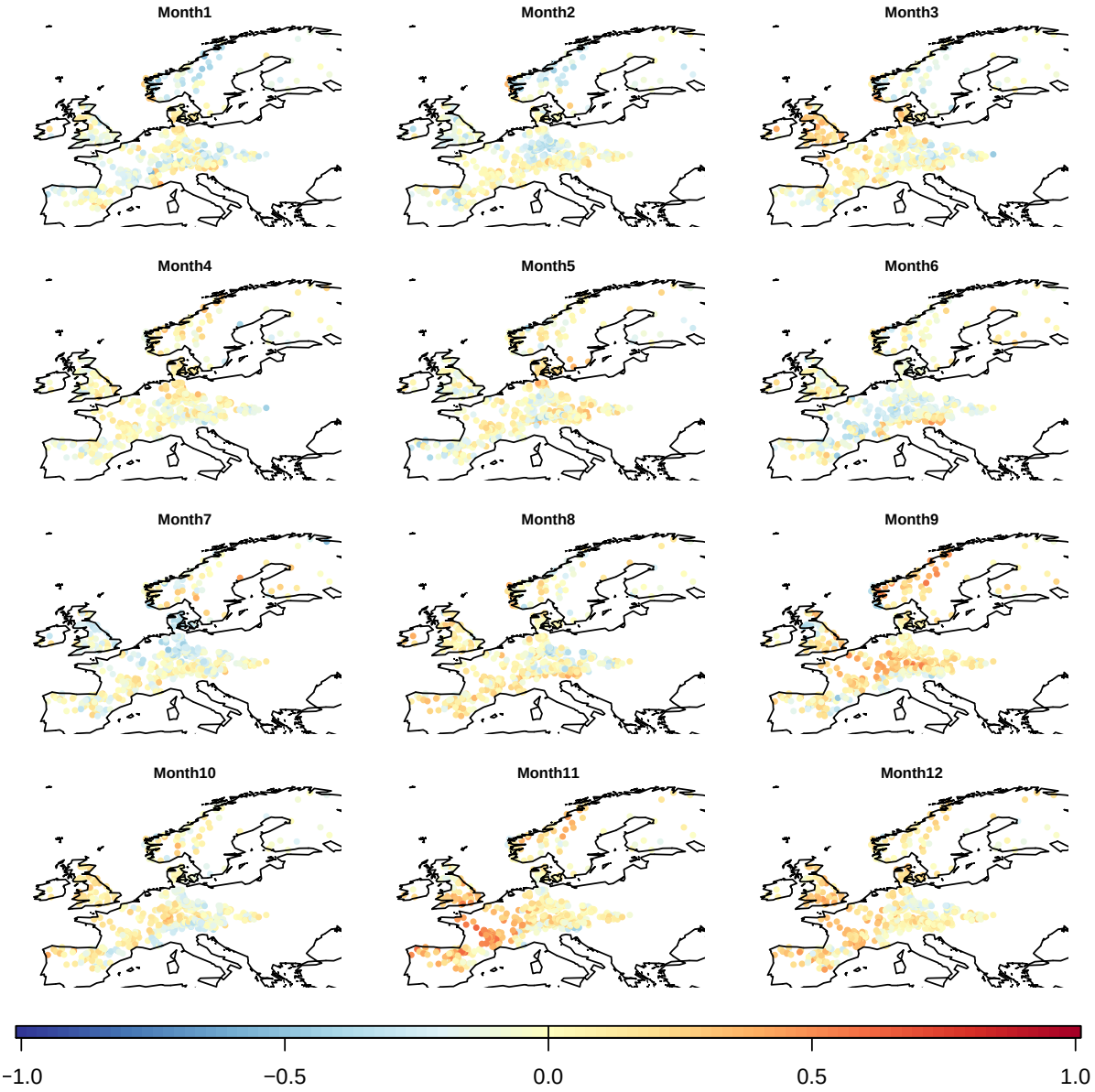

Figure A.34.: Monthly correlations Min181 - Scandinavian Pattern

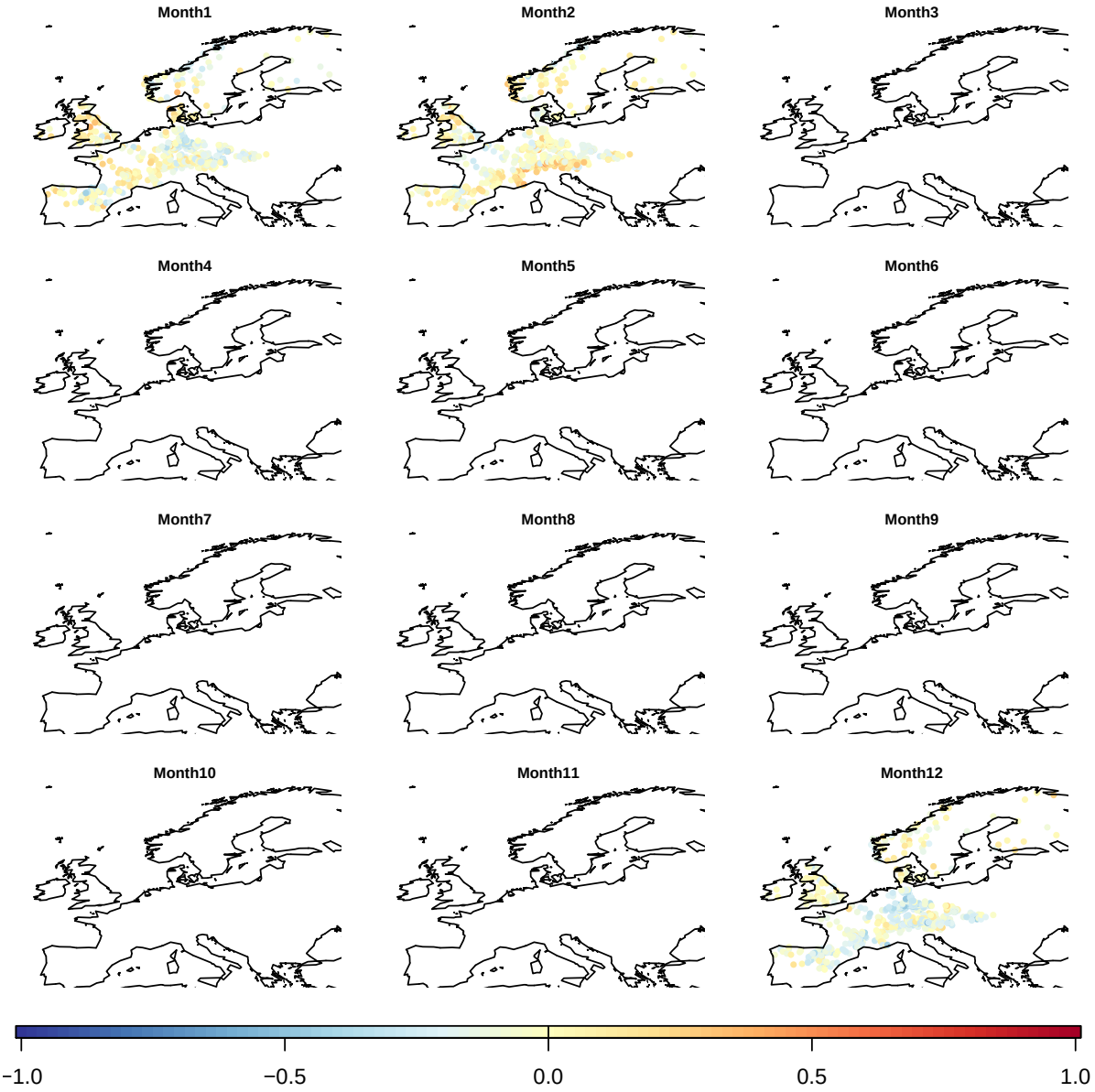

Figure A.35.: Monthly correlations Min181 - Tropical/Northern Hemisphere